

Washington University in St. Louis

Washington University Open Scholarship

Arts & Sciences Electronic Theses and
Dissertations

Arts & Sciences

4-26-2023

An Investigation of Second-Site Non-Complementation among Motile Cilia Genes in *Chlamydomonas reinhardtii*

Gervette M. Penny

Washington University in St. Louis

Follow this and additional works at: https://openscholarship.wustl.edu/art_sci_etds



Part of the [Genetics Commons](#)

Recommended Citation

Penny, Gervette M., "An Investigation of Second-Site Non-Complementation among Motile Cilia Genes in *Chlamydomonas reinhardtii*" (2023). *Arts & Sciences Electronic Theses and Dissertations*. 3228.
https://openscholarship.wustl.edu/art_sci_etds/3228

This Dissertation is brought to you for free and open access by the Arts & Sciences at Washington University Open Scholarship. It has been accepted for inclusion in Arts & Sciences Electronic Theses and Dissertations by an authorized administrator of Washington University Open Scholarship. For more information, please contact digital@wumail.wustl.edu.

WASHINGTON UNIVERSITY IN ST. LOUIS

Division of Biology and Biomedical Sciences
Molecular Genetics and Genomics

Dissertation Examination Committee:

Susan K. Dutcher, Chair

Steven Brody

Douglas Chalker

Sheng Chih Jin

Timothy Schedl

Jennifer Wang

An Investigation of Second-Site Non-Complementation among Motile Cilia Genes
in *Chlamydomonas reinhardtii*

by

Gervette M. Penny

A dissertation presented to
Washington University in St. Louis
in partial fulfillment of the
requirements for the degree
of Doctor of Philosophy

May 2023

St. Louis, Missouri

© 2023, Gervette M. Penny

Table of Contents

List of Figures	v
List of Tables	vii
Acknowledgments.....	viii
Astract.....	xv
Chapter 1: Introduction.....	1
1.1 What Are Motile Cilia?.....	1
1.2 In Humans, Motile Cilia Defects Cause Primary Ciliary Dyskinesia.....	3
1.3 Motile Cilia Consist of Many Protein Complexes That Cooperate to Generate Motility ...	5
1.4 DI/SSNC Can Manifest in Different Forms.....	6
1.5 <i>Chlamydomonas reinhardtii</i> – A Model Organism For Motile Cilia Studies	8
1.6 Mated <i>Chlamydomonas</i> haploid strains can be selected for diploids	11
Chapter 2: A Second-Site Non-Complementation Screen Identifies Novel Motile Cilia Gene Relationships in <i>Chlamydomonas reinhardtii</i>	14
2.1 Abstract	14
2.2 Introduction.....	15
2.2.1 Motile Cilia Are Complex Organelles	15
2.2.2 Motile Cilia Defects Cause Primary Ciliary Dyskinesia (PCD)	16
2.2.3 The Mechanism of DI/SSNC	17
2.2.4 Motile Cilia Structure, Genes & Mutants in <i>Chlamydomonas reinhardtii</i>	20
2.2.5 Diploid Generation in <i>Chlamydomonas</i>	22
2.3 Results.....	23
2.3.1 Characterization of Haploid <i>Chlamydomonas</i> Wild-Type And Mutant Strains	23
2.3.2 Generation And Assessment of <i>Chlamydomonas</i> Diploid Strains.....	27
2.3.3 Diploids Regenerate Faster Than Haploids After Deciliation	31
2.3.4 Diploids Heterozygous for Mutations in DNAAFs Show SSNC in Deciliation Screen.....	33
2.3.5 Generation and Screening of Null <i>pf23</i> Alleles	35
2.3.6 A Null <i>pf23</i> Mutant Completely Lacks All ODAs and IDAs in the Cilia	38
2.3.7 Cilia Length Phenotypes Due to SSNC is Restricted to a Subset of Assembly Factors	40
2.3.8 PF23 Protein Exhibits a Dosage-Dependent Reduction in Heterozygous Diploids.....	42
2.4 Discussion	44

2.4.1	<i>Chlamydomonas</i> Diploid Strains Have a Larger Ciliary Protein Pool.....	44
2.4.2	Challenges With Modeling SSNC in <i>Chlamydomonas</i>	45
2.4.3	The <i>pf23</i> Null Mutants Provide New Insights Into ODA and IDA Assembly in <i>Chlamydomonas</i> 46	
2.4.4	Assembly Factors PF23 and WDR92 Have a Unique Role in IC138 Assembly or Modification 48	
2.4.5	SSNC Among Assembly Factors in <i>Chlamydomonas</i>	49
2.4.6	PF23 Protein Demonstrates a Combined Haploinsufficiency SSNC Model	50
2.4.7	Second-site Non-Complementation as an Inheritance Model in PCD.....	51
2.5	Materials and Methods.....	52
2.5.1	Strains and Diploid Generation.....	52
2.5.2	Deciliation and Regeneration.....	52
2.5.3	Imaging and Cilia Length Measurement.....	53
2.5.4	Genome Editing	54
2.5.5	Axoneme Isolation and Mass Spectrometry	54
2.5.6	Immunoblotting.....	57
2.5.7	RNA and cDNA Isolation and Analysis	58
2.5.8	Statistical Analysis.....	58
2.5.9	Whole Genome Sequencing and Analysis	58
2.6	Supplemental Tables	59
Chapter 3: A Gap-Free Genome Assembly of <i>Chlamydomonas reinhardtii</i> and Detection of Translocations Induced by CRISPR-Mediated Mutagenesis.....		61
3.1	Abstract	61
3.2	Introduction.....	62
3.3	Results.....	65
3.3.1	Assembly of the CC-5816 Genome Using PacBio HiFi and Nanopore Reads.....	65
3.3.2	CC-5816 Haplotypes, Repeat Content, Cytosine Methylation, and Gene Content.....	72
3.3.3	Organellar Sequences Are Present Throughout The Nuclear Genome of CC-5816.....	78
3.3.4	Ribosomal DNA Arrays.....	82
3.3.5	Gene Editing of The <i>PF23</i> Gene by CRISPR/Cas9.....	84
3.3.6	Meiotic Analysis of <i>pf23</i> null CRISPR-Generated Strains	87
3.3.7	Behavior of Other CRISPR-Generated Strains in Meiosis	92
3.4	Discussion	93

Chapter 4: A closer look at dynein assembly and maturation factors in <i>Chlamydomonas reinhardtii</i>	99
4.1 Introduction.....	99
4.1.1 ODA8 is an ODA Maturation Factor	99
4.1.2 An Overview of Dynein Arm Assembly Factor PF23 in <i>Chlamydomonas reinhardtii</i>	100
4.2 Results.....	101
4.2.1 ODA8 Localizes to the Cytoplasm, Basal Body Regions, and Cilia of <i>Chlamydomonas</i>	101
4.2.2 Dynein Assembly Factor PF23 Colocalizes With ODA Intermediate Chain IC69	107
4.3 Discussion.....	108
4.4 Materials and Methods.....	109
4.4.1 Strains and Reagents	109
4.4.2 Transformation and Screening	109
4.4.3 Swimming Velocity and Cilia Length Measurements	110
4.4.4 Arp 2/3 Inhibitor Experimental Protocol	110
Chapter 5: Summary, Discussion, and Conclusion.....	112
5.1 Summary of findings.....	112
5.1.1 SSNC in <i>Chlamydomonas</i>	112
5.1.2 Null Alleles of the PF23 gene in <i>Chlamydomonas reinhardtii</i> contain translocations	113
5.1.3 DyNAPs in <i>Chlamydomonas</i>	113
5.2 Discussion of Findings and Future work	114
5.2.1 Models of SSNC in <i>Chlamydomonas reinhardtii</i>	114
5.2.2 SSNC among the <i>Chlamydomonas</i> mutants selected is gene-specific.....	116
5.2.3 The Mechanism Behind Short Cilia Phenotypes in <i>Chlamydomonas</i>	117
5.2.4 A Consideration of DyNAPs in <i>Chlamydomonas</i>	119
5.3 Conclusions.....	120
References.....	122
Appendix: BioRender Publication Licenses for Figures Used in This Dissertation.....	149

List of Figures

Chapter 2

- Figure 1: SSNC between mutants in intraflagellar transport machinery in IFTB (anterograde) and IFTA (retrograde) in *Chlamydomonas reinhardtii* diploids... 19
- Figure 2: Whole Genome Sequencing analysis of the *pf13-1* strain, and *oda4-1* strain.....25
- Figure 3: A phenotypic summary of the motile cilia mutants used in this study.....26
- Figure 4: Generation and genotyping of *Chlamydomonas reinhardtii* wild-type diploid Strains.....27
- Figure 5: A comparison of haploid and diploid *Chlamydomonas reinhardtii* strains.....29
- Figure 6: A subset of single and double heterozygous diploids show normal steady-state Phenotypes.....30
- Figure 7: Cycloheximide restricts cilia regeneration after deciliation in haploid and diploid cells.....32
- Figure 8: A Matrix of diploid cilia lengths following regeneration in cycloheximide.....34
- Figure 9: Isolation and analysis of wild-type strains transformed with *aphvii* targeted to exon 1 of the *PF23* gene.....36
- Figure 10: Characterization of null *pf23* alleles generated by CRISPR/Cas9 site-directed insertional mutagenesis.....37
- Figure 11: Cilia length of gametic diploids after 180 minute regeneration.....40
- Figure 12: PF23 dynein arm assembly factor shows a dosage-dependent phenotype in heterozygous strains.....42

Chapter 3

- Figure 1: Hifiasm assembly generates highly contiguous assembly using PacBio HiFi Data.....67

Figure 2:	Telomere-to-telomere assembly of CC-5816.....	74
Figure 3:	Characterization of organellar sequences in the nuclear genome.....	78
Figure 4:	NUPTs and NUMTs originate from specific sequences and are located near specific elements within the nuclear genome.....	80
Figure 5:	Ribosomal DNA arrays.....	83
Figure 6:	Characterization of null <i>pf23</i> CRISPR-generated alleles.....	85
Figure 7:	Translocations in <i>pf23-2</i> and <i>pf23-3</i> were induced by site-directed CRISPR/Cas9 mutagenesis.....	89

Chapter 4

Figure 1:	Screening and analysis of <i>oda8</i> ; <i>ODA8::HA-TG</i> transgenic strains.....	102
Figure 2:	Assessment of ODA8 localization in <i>Chlamydomonas</i>	103
Figure 3:	Analysis of ODA8-HA localization and abundance in dynein structural and DNAAF mutants.....	104
Figure 4:	Actin cytoskeleton disruption affects cilia length but not ODA8 localization or abundance.....	106
Figure 5:	Localization dynamics of <i>pf23-1</i> ; <i>PF23::HA-TG</i>	107

List of Tables

Chapter 2

Table 1:	Chlamydomonas mutant strains used to generate diploids for SSNC screen.....	24
Table 2:	Mass spectrometry analysis of axonemes of wild-type strain WT 4-2P and <i>pf23-4; cnk11-3</i>	39
Table S1:	PCR primers designed to genotype strains used in this work.....	59

Acknowledgments

First, I give thanks to God for His leading and guidance in bringing me to Washington University in Saint Louis. He has opened so many doors and provided countless opportunities to me beyond the things that I could have imagined for my own life. I thank Him for giving me the strength to make it through those arduously difficult first two semesters as I battled the unknowns of graduate school far away from my family and friends. I am so very grateful to Him for blessing me with the opportunity to grow as a scientist and as an individual, for making a way for me through every circumstance that seemed impossible, for taking me over every mountain, and for bringing me to the end of this chapter of my life even when it seemed that there was no light at the end of the tunnel. I thank Him for giving me a family who loves and supports me in everything I do, and for providing me with an extended family here in St. Louis at Jubilee Church. I am also grateful for the other friends that I have made here both at graduate school and through other activities during my time here. I express my thanks to Him for keeping me through every challenge these past seven years and blessing me with the success that I have today as a result.

Next, I want to thank my PhD supervisor, Dr. Susan Dutcher, for the opportunity to train and learn in your laboratory as a graduate student. You have provided an unwavering example of discipline, exemplary work ethic, and attention to detail. I am thankful to you for the training opportunities that you allowed me to participate in, even when they were not directly related to my thesis projects. I appreciate your support for my involvement in other professional development activities outside of the lab as these have helped to shape the trajectory I wish to follow as a scientist in the future. I am constantly amazed at how knowledgeable you are, your sharp thinking and reasoning, your phenomenal memory, and your continued passion for science. I someday aspire to be as well-traveled, broadly experienced, and productive in life as you are.

A special thanks to my thesis committee for guiding me through graduate school by providing constructive criticism, helpful comments, and lots of encouragement. Thank you for helping me to find direction when I floundered and teaching me to appreciate the progress that I made, however small. Thank you for being patient with me for the times that I missed deadlines while scrambling to obtain data to present at my thesis updates. Finally, thank you for making my time with you engaging, intellectually stimulating, and thought provoking. Thank you, Dr. Douglas Chalker, for being an amazing committee chair. My last interview at WashU was a Skype call with you, and I vividly remember our one and a half hour conversation on the very intriguing genetics of *Tetrahymena*. You led my committee with a firm, but warm, hand, and I am thankful for the support that you provided. A special thanks to Dr. Tim Schedl whose office is just a few feet away from my lab. I am grateful for the advice on my experiments, helping me to see new ways to think about my data, and for being a voice of reason when I was being too hard on myself when things did not work the way that I anticipated. I enjoyed your sense of humor, witty banter, and conversations, and it was always great to know that you were just down the hall when I needed a break and wanted to chat. Dr. Steven Brody – I admire your unquenchable curiosity and thirst for knowledge. I am always in awe of how you think about your own science and how you thoughtfully engage in the work of others. To Dr. Winfield Sale – though your time on my thesis committee was brief, I am so thankful that you agreed to join my committee. Your positive outlook, constant encouragement, and optimism helped me to push through a very rough phase of my thesis project. Finally, to Dr. Peter Jin and Dr. Jenn Wang, I am thankful for your willingness to join my committee at a moment's notice. It was a pleasure to have you participate in my thesis defense, and I truly appreciate all your kind words, helpful feedback, and great advice.

Thank you to Monsanto/Bayer for the three years of stipend funding that I received through The Bayer Excellence Fund for Graduate Fellowships in Life Sciences, and thanks to NIH and other federal funding sources for the financial support that enabled me to do the research necessary to earn this doctoral degree.

Thank you to my past lab mates Huawen Lin, Peipei Sun, Maureen Wirschell, Komal Sharma, Mihaela Stoyanova, Manishi Pandey, Kara Jones, Emily Hunter, and Mathieu Bottier. You each brought something unique to my experience of graduate school in the lab, and I learned so much from each of you as you brought your experience and expertise to the lab. I enjoyed our conversation times together in the lab talking about science, making jokes, and eating together. Thank you for bringing all your fun personalities and skills to the lab during the time that you were here. I am very thankful for the time that we got to spend outside of lab, to have fun, decompress from a long day, and talk about all things non-science.

Thanks to the MGG program directors Jim Skeath, John Edwards, and Tim Schedl for making our time through this program an amazing experience. Thank you, Melanie Relich, my program coordinator, for answering my endless questions and providing necessary clarification. Thanks, Cherie Moore, for your continued support and interest in my life as a graduate student. I know that you work tirelessly behind the scenes to keep things running smoothly. Thanks for your warm smiles, cute face masks, and for checking in on me ever so often when you visited the department. It has not gone unnoticed!

To my dear family – the Penny Five – none of this would have been possible without your love, support, and encouragement. You have been my rock, my pillow, my shoulders to cry on, and I could not have made it through the past 7 years without you. I am eternally grateful to my mother, Yvette, who spent countless nights awake (or asleep) with me while I worked to finish an

assignment, study for a test, troubleshoot a problem, or listen to me when I was discouraged. You left your own work in Grenada to help me move here to St. Louis to settle away from home for the first time. You prayed for me, made me laugh, listened to my complaints, sympathized with me, and encouraged me. I am so, so, so thankful to have you with me through this journey. To my father, Derrick, thank you for the world of wisdom that you have to offer, the crazy jokes you make and all the love you constantly send me. I am blessed to have you around to see me achieve the dream that I have had since the age of 10. To my siblings Kerrick and Valeska, thank you for reminding me that I will never stop being your big sister no matter how old we get or how far away we are from each other. I am so very grateful for our love and care for each other, and that we are there to celebrate each other's successes, encourage each other through our failures, and to walk through life together knowing that no matter what happens, that we have each other's backs. Thank you for always sending me jokes and making me laugh! It really is good medicine when the sting of failure really can seem like too much to bear.

Thanks to my home church Faith Deliverance Tabernacle for praying for me, supporting me, and cheering me on. Thanks to my dear friends in Grenada Natasha Joseph and Nakitha Noel – I am grateful for the bond that we share, despite the distance between us. Thanks to all my other friends in Grenada who constantly ask after my well-being and wish me success.

Thank you to my undergraduate mentor Dr. Kotelnikova for introducing me to genetics. I would not be here if I had not enrolled in your class and fallen in love with genetics after my first project on Tay-Sach's disease. Thank you to my undergraduate professors Dr. Clare Morrall and Dr. Antonia MacDonald for their mentorship, friendship, and guidance during my senior undergraduate years. You helped to mold me professionally and prepare me for my first job. You challenged me intellectually and pushed me outside of my comfort zone. Thank you for seeing my

potential and nudging me in the direction of success. A special thanks to Dr. Andrew Sobering and Dr. Kathryn Gibson for giving me the opportunity to participate in research projects on the SGU campus, and for trusting me with responsibilities that helped me to grow as a young science enthusiast aiming to go to graduate school. I must say a big thank you to Dr. Peter Slinger. You were my first boss, and I grew from a young, freshly-minted undergraduate into a confident professional under your care and guidance. Your friendship, mentorship, compassion, kindness, and ability to see my potential for success has always stayed with me, and I feel very blessed to have shared 5 ½ years of my life working with you as a colleague. You have supported all my academic and professional pursuits, challenged me to grow even when I wanted to stay in the comfort of what I grew into, and always made work fun! Thank you to my SL colleagues Atom, Elias, Marsha, Beth, and Lisa for making the SL department an amazing place to work and for supporting me in my decision to apply for graduate school. It was not easy to leave such a warm, friendly environment, but I am grateful that I got to spend this time with you. To my other DES colleagues, thank you for your contributions to my professional growth, and for being my work family during my time at SGU.

Finally, I must say thanks to all the people in St. Louis who have made my time here a bit less daunting and a lot more enjoyable. Thanks to Nigel who welcomed me and my mom as complete strangers to St. Louis, and for ensuring that we had a smooth transition from Grenada. Thanks to Geralle, Liza and Tomas who have been my graduate school friends from the very beginning. It was a pleasure going through graduate school with you. To my fellow international graduate school friend Alejandro, thank you for so many wonderful adventures in St. Louis together. I loved all the time that we were able to spend outdoors kayaking, skiing, watching eclipses, biking, and soaking up the sun. I am so blessed to have found Jubilee Church during my

time in graduate school. Larry and Vicky Mowrey, and Blessing and Ben Ojie, you are no longer friends, but family. Thank you for welcoming me into your homes and into your hearts, and for extending compassion and grace to me when I was frustrated or wanted to give up. Thank you for allowing me to be a part of your families when mine was so far away. To my other friends Renee, Sylvia, Sherell, Lauren, Ayana, Ashley and so many others who are still here in St. Louis or who have moved on to other areas and pursuits, I am so grateful to call you all my friends. You have poured into my life in ways that I did not even know I needed, and I am truly grateful.

To everyone else who has contributed to my life in one way or another up to this point, I extend my thanks to you. If I were to continue writing thanks to all the people who have brought me to where I am, there would be no space left to write my dissertation!

Gervette M. Penny

Washington University in St. Louis

May 2023

*Dedicated to my parents Derrick and Yvette,
my brother Kerrick,
and,
my sister Valeska*

*It is because of you that my dream of
earning a PhD was made possible.*

ABSTRACT OF THE DISSERTATION

An Investigation of Second-Site Non-Complementation among Motile Cilia Genes

in *Chlamydomonas reinhardtii*

by

Gervette M. Penny

Doctor of Philosophy in Biology and Biomedical Sciences

Molecular Genetics and Genomics

Washington University in St. Louis, 2023

Professor Susan K. Dutcher, Chair

Motile cilia are complex microtubule-based organelles used by eukaryotic cells for locomotion or directing fluid flow. In humans, motile cilia defects cause primary ciliary dyskinesia (PCD), characterized by neonatal respiratory distress, recurrent lung infections, bronchiectasis, infertility, and low nitric oxide. Situs inversus and/or male infertility are present in about 50% of cases. PCD inheritance is recessive; both copies (alleles) of a single gene have a deleterious variant, known as homozygosity. The result is loss-of-function and disease. In recessive inheritance, a variant in one allele, or heterozygosity, is insufficient to cause a disease phenotype. Despite identification of over 50 PCD genes, approximately 30% of clinically diagnosed patients have unknown genetic etiology using exome sequencing. Explanations for this finding are: 1) causative PCD genes remain undiscovered, 2) patient variants may be non-coding, or 3) an alternative inheritance mechanism exists. One alternative is digenic inheritance (DI) or second-site non-complementation (SSNC). Co-occurring heterozygous mutations in two recessive genes often produce a normal phenotype; they complement. Abnormal phenotypes are absent because each gene has one functional copy

that provides sufficient gene product. In rare instances, double heterozygosity in two genes causes a mutant phenotype and disease; this is the definition of DI/SSNC. In SSNC, the gene products often interact. Motile cilia proteins are organized into interacting structures or complexes and are good candidates for SSNC studies. *Chlamydomonas reinhardtii* is a haploid algal cell with two motile cilia; most human motile cilia proteins are conserved. I assessed whether SSNC can occur among motile cilia genes in *Chlamydomonas* diploids. I screened 231 strains with mutations in dynein arm structural proteins, dynein adapters, dynein maturation factors, dynein assembly proteins, and a radial spoke protein. Initial assessment revealed no obvious phenotypes and indicated that these genes are recessive. In a sensitized screen, double heterozygous diploids show a cilia regeneration phenotype under stress conditions. *Chlamydomonas* cilia were removed using pH shock and allowed to regenerate in medium with cycloheximide, a protein synthesis inhibitor that requires the cells to use the existing pool of ciliary proteins. A subset of double heterozygous diploids shows SSNC and regenerate shorter cilia than the wild-type control; each of these diploids contains at least one mutation in a dynein arm assembly factor gene. To assess whether assembly factors show gene dosage effects, I generated a null strain of dynein assembly factor PF23 (pf23-4) using CRISPR/Cas9 targeted insertional mutagenesis. Mass spectrometry analysis shows a more severe loss of dynein arm components in the cilia than the pf23-1 in-frame deletion strain with a shorter PF23 protein. Immunoblot analysis of steady-state pf23-4/PF23; wdr92/WDR92 and pf23-4/PF23; oda8/ODA8 diploids shows that PF23 protein is reduced compared to wild-type controls. In the pf23/PF23 single heterozygous strain, PF23 protein is also reduced. I suggest that PF23 shows a dosage-dependent phenotype. When heterozygous with other dynein assembly factors, the proteins in the dynein assembly pathway may be reduced below a critical functional threshold during stress. Analysis of patients for SSNC is an important novel approach for the future.

Chapter 1: Introduction

1.1 What Are Motile Cilia?

Motile cilia are small, microtubule-based organelles that are used for cell motility and the generation of fluid flow. Anthony van Leeuwenhoek, known as the Father of Microbiology, was the first to describe these organelles. He set upon the task to study rainwater that he gathered outside his house; observation of this water under his microscope revealed the presence of tiny ‘animalcula’ of several types that moved around with ‘little feet’.¹ Later, J.E. Purkinje and G.G. Valentin reported that vertebral oviduct walls possessed ciliated epithelium.² Extensive analyses of the gills of *Mytilus edulis* (Blue mussel) showed that its motile cilia beat back and forth with an effective stroke that propelled fluid (forward) and a recovery stroke (backward).³ Gray then developed a camera apparatus and used stroboscopic analysis to further describe the ciliary waveform by capturing the entire beat cycle of a single cilium in this organism.⁴ Using a new fixation method in electron microscopy, Afzelius provided the earliest insights about the 9+2 arrangement of the ‘filaments’ (microtubule doublets) of sea urchin spermatozoa and the triplet arrangement of the basal body, as well as a sheath/membrane surrounding the 9+2 structure. His cross-sectional analysis provided rudimentary descriptions of spoke-like structures, ‘arms’ and central pair.⁵ Gibbons and Grimstone utilized epoxy-resin fixation and heavy metal staining to generate early high-contrast EM sections of the cilia of protists *Trichonympha*, *Pseudotriconympha*, and *Holomastigotoides*, and another fresh-water mussel species *Anodonta cataracta*. In this work, they provided the first detailed description of ciliary structure. They proposed that the ‘figure-of-8’ structure seen in the 9 filaments are composed of two sub-fibers,

which they named A and B. These are now known as the A and B tubules. Other structures were mentioned in greater detail, including the ‘arms’ that Afzelius described. These arms existed along the length of the cilium with a remarkably reproducible periodicity.^{6,7} In 1965, Gibbons and Rowe isolated 14S and 30S globular proteins with rod-like structures from *Tetrahymena pyriformis*. They demonstrated that these proteins contained ATPase activity, showed periodicity that corresponded with the ‘arms’ described in earlier work, and could exist in monomeric and dimeric forms. They coined the term ‘dynein’ to represent these structures.⁸ In sea urchin sperm, these dynein motors could be activated by the addition of ATP, which resulted in the sliding of trypsin-digested microtubule doublets that were adjacent to each other.⁹ Additionally, these dyneins were shown to be directly responsible for the rate at which this sliding occurred. A decrease in dyneins bound to the axoneme resulted in a proportional decrease in sliding speed.¹⁰ These early studies provided the groundwork for our current knowledge of motile cilia structure and function. Since this early work, many other model organisms have been developed for cilia studies, each with their own advantages¹¹. Vertebrate models include mice,^{12,13} zebrafish,^{14,15} *Xenopus*,^{16,17} and medaka fish.^{18,19} An invertebrate *Schmidtea mediterranea* has proven useful in some motile cilia studies.^{20,21} In addition to the protists mentioned earlier, *Trypanosoma*,^{22–24} *Paramecium*,^{25,26} and *Tetrahymena*^{27–29} are also popular in the cilia research community. *Volvox*^{30,31} and *Chlamydomonas*³² are green algal species also used for a wide range of motile cilia studies. In the work described in this dissertation, I use the single-celled alga *Chlamydomonas reinhardtii* as the model organism for studies of motile cilia genes. The next section describes *Chlamydomonas* in more detail.

1.2 In Humans, Motile Cilia Defects Cause Primary Ciliary Dyskinesia

Motile cilia are complex, diverse organelles found in many different areas of the body. When motile cilia malfunction, this causes primary ciliary dyskinesia (PCD). In 1904, PCD was first described as a syndrome in patients that exhibited situs inversus, nasal polyps and bronchiectasis.³³ The name Kartagener syndrome was introduced after a physician observed many patients with situs abnormalities (left-right asymmetry abnormalities), bronchiectasis (damage to the airways), and chronic sinus and lung infections.³⁴ Later, these symptoms were associated with immotile cilia in patients.³⁵ This name was subsequently changed to dyskinetic cilia syndrome after other patients who presented similar symptoms were found to have cilia with abnormal motility.³⁶ About 50% of patients also present with situs inversus totalis (total reversal of left-right asymmetry)^{37,38} or in some cases, situs inversus ambiguus / heterotaxy (partial reversal sometimes accompanied by congenital heart defects)³⁹⁻⁴¹. Situs abnormalities are due to defective nodal cilia. During development, nodal cilia are found within the embryonic node. The nodal cilia have a non-canonical 9+0 axoneme arrangement because they lack the central apparatus. This arrangement causes nodal cilia to beat in a circular pattern and to generate leftward fluid flow that determines left-right asymmetry. This mechanism is conserved across many different organisms.^{42,43} Cilia with a 9+2 arrangement on human sperm provides cell motility during fertilization. Cilia are also present in the oviducts of females. As a result, a portion of males and females with PCD experience subfertility or infertility.⁴⁴ Recurrent lung infections, sinusitis, and bronchiectasis results from abnormal function of cilia in the respiratory system. Persistent ear

infections (otitis media) are also observed in patients. Many infants experience neonatal respiratory distress.⁴⁵⁻⁴⁸

The prevalence of PCD is roughly 1:10,000 to 1:20,000 people, although this number may be higher⁴⁹. A recent study suggests that PCD may occur as frequently as 1 in 7,500 people.⁵⁰ There are now at least 50 genes associated with PCD in humans. These genes fall into structural groups and cause a diverse range of effects on cilia structure and function. Some genes are necessary for cilia formation (*CCNO*⁵¹⁻⁵⁴, *MCIDAS*⁵⁵, *NEK10*⁵⁶, and *FOXJ1*^{57,58}). Mutations in *CCDC39* and *CCDC40* produce the most severe phenotypic effects; the cilia structure is extremely compromised, and several complexes are missing.⁵⁹⁻⁶¹ Variants in other genes like dynein assembly factors *LRRC50*⁶²⁻⁶⁴, *DNAAF4 (DYX1CI)*⁶⁵, and *SPAG1*⁶⁶, among others, cause loss of both the outer dynein arms on cilia needed to generate force, and inner dynein arms that regulate ciliary waveform. Another gene, *DNAH11*, has a normal structure when observed using transmission electron microscopy^{37,67,68} *DNAH11* belongs to a class of proteins that code for dynein motors. These include *DNAH5*, *DNAH9*, *DNAH11*, *DNAI1*, and *DNAI2*.^{45,48,49} PCD is usually diagnosed by the presence of clinical features in combination with other testing methods like analysis of cilia from cell cultures of affected patients, gene panel testing, nitric oxide measurements, transmission electron microscopy, immunofluorescence analysis, and more recently, whole exome and genome sequencing^{46,69-72}. However, roughly 30% of patients with a clinical diagnosis have unknown genetic etiology despite genetic testing, exome, or rarely genome sequencing. Several explanations may account for the lack of disease-associated genotypes in these individuals. First, a patient may harbor variants in genes that have not yet been associated with PCD, or sequencing may produce variants of unknown significance.⁴⁶ Second, variants may be non-coding or large structural variants that are difficult to identify by panels or exome

sequencing.⁶² Alternatively, another inheritance mechanism of PCD, digenic inheritance (DI) or second-site non-complementation (SSNC) may exist. This will be discussed more in chapter 2.

1.3 Motile Cilia Consist of Many Protein Complexes That Cooperate to Generate Motility

Motile cilia are microtubule-based organelles that are used by cells to generate fluid flow or facilitate motility.⁷³ They are comprised of >1000 different proteins organized into structural and functional groups.⁷⁴⁻⁷⁶ The cytoskeleton, or axoneme, of most motile cilia is composed of nine outer microtubule doublets (MTDs) and two inner microtubule singlets known as the central apparatus. This is referred to as a '9+2' arrangement.⁷⁷ A special type of motile cilia called nodal cilia is only present during development in higher eukaryotes in a transient structure called the embryonic node. These cilia generate fluid flow that directs body axis formation and left-right asymmetry. They lack the central apparatus and have a '9+0' microtubule doublet arrangement.⁴² The axoneme skeleton is built from repeating rows of alpha- and beta-tubulin heterodimers arranged into a lattice. Each doublet is comprised of an A-tubule with 13 protofilaments and an incomplete B-tubule with 10 protofilaments. The interior of each doublet is occupied by various microtubule inner proteins (MIPS).⁷⁸ The outer dynein arms (ODAs) are motors that attach to the A-tubule and contact the neighboring B-tubule. They generate the force that leads to ciliary bending through sliding and determine the beat frequency of the cilia.^{10,79} Inner dynein arm motors (IDAs) are also attached on the A-tubule. They regulate the ciliary waveform.^{80,81} There are several other complexes that connect the central apparatus and the outer doublets that are important in regulation of motility. These include the nexin-dynein regulatory complex (N-DRC), radial spokes (RS) and calmodulin spoke complex (CSC), outer and inner dynein linkers (OIDL), and

MIA (modifier of inner arms). Other factors important in the assembly, maturation and transport of dynein arms include dynein arm assembly factors (DNAAFs), ODA and IDA maturation factors, and ODA and IDA adapters, respectively.^{77,82–85}

1.4 DI/SSNC Can Manifest in Different Forms

When a gene follows a recessive inheritance pattern, both copies of that gene must carry a deleterious mutation/variant to manifest a mutant phenotype.⁸⁶ The complementation test is based on the premise that two recessive mutant alleles belong to different genes if they produce a wild-type phenotype when each allele is in *trans* (on different parental chromosomes). If the two heterozygous mutant alleles produce a mutant phenotype when in *trans*, they exhibit failure to complement and are presumed to belong to the same gene. However, failure to complement can also occur when the alleles are in different genes. This is also known as Second-Site Non-Complementation (SSNC).⁸⁷ Early records of SSNC are found in studies of *am* mutants in the NADP synthesis pathway of *Neurospora*^{88–91} and *ad₂* mutants involved in adenine synthesis in Yeast and was termed ‘negative complementation’.⁹²

This concept has been considered regarding PCD, when individuals are reported as heterozygous for a single allele, although there are no recorded cases thus far.^{93–95} Interestingly, a few examples are reported with other syndromes. One study identified individuals with heterotaxy, a PCD-associated phenotype, with one variant in *DNAH6*, an IDA heavy chain gene, and another variant in *DNAIL1*, an ODA intermediate chain gene. Other individuals in the study had additional heterozygous combinations with *DNAIL1* (ODA intermediate chain).⁴¹ DI has been reported for another ciliopathy, short-rib polydactyly syndrome type Majewski with variants in *NEK1* (a serine/threonine kinase with roles in ciliogenesis) and *DYNC2H1* (cytoplasmic dynein 2 heavy

chain 1).⁹⁶ In retinitis pigmentosa, another cilia-related disease, two genes, *ROM-1* (retinal outer segment membrane protein) and *Peripherin* (retinal outer segment protein) displayed a DI pattern.^{97,98}

SSNC is observed in many model organisms. In type I SSNC (poison model), mutant gene products from two different loci interact to form a complex that is detrimental to the cell or organism. This is the rarest type of SSNC, and usually implies a specific protein-protein interaction. One well-known example involves a cold-sensitive α -tubulin (*tub1-1*) mutation that fails to complement a mutation in β -tubulin (*tub2*) in yeast.⁹⁹ Type II SSNC (sequestration) occurs when mutant protein binds and sequesters wild-type protein into an inactive complex. This occurred between α - and β -tubulin non-complementing mutations in *Drosophila*.¹⁰⁰ Type III SSNC (combined haplo-insufficiency) manifests when a reduction in the normal levels of two protein products generate a phenotype that is absent when the levels of only one protein product is lowered.⁸⁷ In mice, the *hoxb-5* and *hoxb-6* genes involved in body segmentation also exhibit SSNC; the double heterozygous mice show skeletal abnormality phenotypes seen in either homozygote.¹⁰¹ One group tested several combinations of *hoxd-11*, *hoxd-12* and *hoxd-13* and found that the trans-heterozygotes showed skeletal abnormalities that were reduced or absent in animals heterozygous for only one mutation.¹⁰² Interestingly, a human patient with a missense mutation in *HOXD13* and a polyalanine tract expansion in *HOXA13* had more severe skeletal defects than her parents, who were heterozygous carriers of either single mutation.¹⁰³ Despite familial segregation, this finding has not been confirmed in model organisms.

In *C. elegans*, non-allelic non-complementation was shown between the genes that encode synaptic proteins UNC-13 and syntaxin/UNC-64.¹⁰⁴ One example of SSNC was shown among strains with temperature-sensitive mutations in genes involved in intraflagellar transport (IFT), the

complex that transports cargo in and out of the cilia. IFT is divided into two complexes. In the combinations tested, several *Chlamydomonas* mutants within each complex failed to complement each other in diploids and have short cilia. Additionally, IFTB mutant *ift172* fails to complement IFTA mutants *ift139*, *ift144* and *dhc2* (Figure 1).¹⁰⁵

SSNC can also emerge in the form of “dominant enhancement”, although this is not a true form of complementation. This occurs when a dominant mutation at a second locus enhances the phenotype of a semi-dominant or weak antimorphic mutation at a primary locus. Genetic analysis of *pf10*, a *Chlamydomonas reinhardtii* mutant with impaired flagellar beating and aberrant swimming provided several examples of this. In the *pf10* background, most diploids heterozygous for paired suppressor mutations in *lis1* and *lis2* and some *lis2* and *bop1* failed to complement, resulting in a wild-type swimming phenotype¹⁰⁶ Screens for second site dominant enhancers are more likely to identify physical protein interactors or members of the same pathway than SSNC, because they begin with weak dominant mutations.^{87,104}

It is possible to discover all three types of SSNC interactions, albeit with different frequencies. However, many cases of DI have insufficient levels of evidence to be deemed truly causative. Therefore, there is a need to systematically demonstrate the feasibility of SSNC. In the case of ciliopathies, the expanse of the ciliary proteome, the inter-dependency of ciliary functional modules, and the large number of proteins which work together to form individual complexes make this group of diseases an excellent candidate for modeling SSNC.

1.5 *Chlamydomonas reinhardtii* – A Model Organism For Motile Cilia Studies

Chlamydomonas reinhardtii is a haploid, single-celled, photosynthetic motile alga that uses two cilia for motility. It was isolated from a potato field in Amherst, Massachusetts.³² *Chlamydomonas* is eukaryotic. It generates energy using mitochondria and a chloroplast. There is a special organelle within the chloroplast called the eyespot. This is used by *Chlamydomonas* to orient its swimming in response to changes in light.¹⁰⁷⁻¹⁰⁹ The cytoplasm also contains a nucleus, the pyrenoid that collects carbon dioxide, which is converted to starch, contractile vacuoles, the endoplasmic reticulum, Golgi bodies, and centrioles that are converted to basal bodies that form the base of the cilia.^{110,111} The cilia of *Chlamydomonas* are about 10-12 microns long with a diameter of approximately 250 nanometers.^{112,113} The *Chlamydomonas* genome is fully sequenced, and there are now several annotated versions available as a resource for the community.¹¹⁴⁻¹¹⁷ Recently, the first gapless telomere-to-telomere *Chlamydomonas* genome was published using a combination of Nanopore and HiFi long range sequencing, and various genome assembly tools.¹¹⁸

Chlamydomonas reinhardtii has been used extensively in motile cilia research due to its ease of performing genetic, biochemical, and microscopic analysis.¹¹⁹ To test whether motile cilia structural and assembly genes exhibit SSNC, and to learn more about the relationships between these genes, we utilized available strains from the *Chlamydomonas* Resource Center.^{120,121} A subset of these strains originated from a large UV mutagenesis screen that produced a variety of slow-swimming or paralyzed mutants with defects in the outer arms and/or inner arms in *Chlamydomonas*.¹²² Each strain discussed below contains a mutation in a previously characterized motile cilia structural or functional gene. The gene products of selected mutants are ODA motor components, ODA docking complex proteins, ODA maturation proteins, cytoplasmic dynein arm assembly factors (DNAAFs), and ODA and IDA intraflagellar transport adapters. A mutant affecting radial spoke was included as an outgroup.

ODAs in *Chlamydomonas* contain three heavy chains, α -, β - and γ -HCs. A mutant in the α -HC, *oda11*¹²³, lacks only the α - heavy chain, while β - and γ - heavy chain mutants, *oda4-1*¹²² and *oda2-1*¹²⁴, respectively, lack all three heavy chains. An allele of *oda4-1*, *sup-pf1-1*^{125,126}, contains an in-frame deletion that shortens the microtubule-binding domain (stalk) of the β -HC. Intermediate and light chains connect the ODA heavy chains to the axoneme along with the ODA docking complex. We obtained mutants in the two ODA heterodimer-forming intermediate chains IC69 and IC78, *oda6-95*¹²⁷ and *oda9*^{122,128}, respectively, and a mutant, *oda12-2*¹²⁹ of one of the 11 ODA-associated light chains, LC2.

Although the assembled ODA heavy, intermediate, and light chain complex can bind to the axoneme, the ODA docking complex (ODA-DC) is needed to stabilize this interaction.^{130,131} Mutants in two ODA-DC complex components, *oda1*¹³² and *oda3-1*¹³³ completely lack ODAs, while a mutant in the third component, *oda14-F28*,¹³⁴ partially lacks dynein arms. Dynein arms are assembled in the cytoplasm by DNAAFs before they are transported into the axoneme. Mutations in *DNAAF* genes affect the assembly of both ODAs and IDAs to varying degrees. In *Chlamydomonas*, this failure of motor assembly results in ciliary paralysis and short cilia, and includes mutants *pf22-1*¹³⁵, *pf23-1*^{65,136}, *pf13-1*¹⁸ and *wdr92*^{137,138}.

Another DNAAF, ODA7, differs in that it only affects assembly of ODAs. It primarily localizes to the cytoplasm but is also found in the cilia where it interacts with both ODAs and IDAs to form a link between them.^{63,139} The *oda7-1* mutant, in contrast to other *DNAAF* mutants, is motile. Following cytoplasmic assembly, dyneins are made binding-competent or 'matured' by maturation complex factors. ODA5 and ODA10 interact directly with each other and localize to the cytoplasm and proximal axoneme.

ODA8 is reported to localize to the cytoplasm and interact with IFT proteins.²⁴ The *oda5*,^{140,141} *oda10*,^{141,142} and *oda8*¹⁴³ mutants were collected for use in our screen. Mature ODAs and IDAs are transported into the cilia by IFT, with the aid of IFT adapters ODA16 and IDA3. Mutants *oda16-2*^{144,145} and *ida3*¹⁴⁶ were also used. The radial spoke (RS) connects the central pair and outer doublets. It is comprised of approximately 23 proteins.¹⁴⁷ The *PF14* gene encodes the RSP3 subunit, and the *pfl4*¹⁴⁸ mutant lacks the radial spoke head. Given that many of the previously mentioned proteins have physical or functional interactions, we hypothesized that they would be good candidates for an investigation of SSNC in *Chlamydomonas*. However, SSNC requires the presence of two alleles *in trans* in a diploid organism. Since *Chlamydomonas* is haploid, it was necessary to generate diploids to conduct this study.

1.6 Mated *Chlamydomonas* haploid strains can be selected for diploids

Haploid *Chlamydomonas* strains of mating-type plus and mating-type minus can be mated to produce diploid zygotes that undergo meiosis. This results in haploid progeny. Mating creates intermediary quadriflagellate zygotes (with separate nuclei) called dikaryons that mature into diploid cells that undergo meiosis to form four haploid tetrads. Structural and biochemical analysis is easily performed on isolated flagella and basal bodies^{119,149,150} which allows the study of cytoplasmic and nuclear contributions to attached flagella or flagellar assembly after resection. David Starling and John Randall were the first to show that the flagella of a paralyzed mutant (*pfl6*) could regain motility after being mated with a wild-type strain of *Chlamydomonas*.¹⁵¹ The inability of dikaryons to rescue a mutant phenotype has also provided insightful information about

basal body and transition zone function, as well as dynein outer arm assembly.¹⁵² A small percentage of dikaryons fail to enter meiosis, and instead become mitotically stable diploids that can be selected using auxotrophic markers.^{152,153} Diploid cells are heterozygous for the mating type plus (*mt+*) and mating type minus (*mt-*) genes but mate as *mt-*.^{153,154} Unlike yeast, *Chlamydomonas* diploids cannot naturally enter meiosis. Treatment of matings between diploid and haploid *Chlamydomonas* cells with colchicine, a microtubule destabilizing drug, allows the diploid to enter meiosis.¹⁵⁵

A small percentage of mated cells undergo mitotic division and form stable, vegetative diploids.¹⁵³ Diploids can be generated using several methods in *Chlamydomonas*. The first was described by Wetherell and Krauss¹⁵⁶ who explored the ability of colchicine to inhibit nuclear fusion and induce polyploidy (and diploidy) in *Chlamydomonas*. This method was used to study the cytoplasmic contribution of mating-type functions to nuclear fusion.¹⁵⁵ Ebersold used two haploid strains containing different auxotrophic mutations in arginine genes, *arg-1*, and *arg-2* (now called *arg7-1* and *arg7-4* respectively). Using this method, strains were mated and then plated onto medium lacking arginine; only diploid cells grow, as the two heterozygous arginine mutations complement¹⁵³. Arginine and other auxotrophic strains have been used by others to generate diploids.¹⁵⁷⁻¹⁵⁹ Diploids can also be generated through somatic fusion of cells treated with polyethylene glycol after their cell walls have been removed.^{160,161} Complementing arginine auxotrophs were used in other work.^{153,155-158}

In this thesis, I utilize *Chlamydomonas* motile cilia mutants in diploids to investigate the occurrence of SSNC. I find that PF23, an assembly factor shows SSNC phenotypes with another dynein assembly factor WDR92. This finding suggests that SSNC is a model to be considered

when looking at human patients who may have an unknown genetic etiology with a clinical PCD diagnosis.

Chapter 2: A Second-Site Non-Complementation Screen Identifies Novel Motile Cilia Gene Relationships in *Chlamydomonas reinhardtii*

Gervette M. Penny and Susan K. Dutcher

From:

Penny, G.M., & Dutcher, S.K. (2023) A second-site non-complementation screen identifies novel motile cilia gene relationships in *Chlamydomonas reinhardtii*. Manuscript in preparation

2.1 Abstract

Motile cilia are complex organelles comprised of >1000 proteins. Mutations in many of the genes encoding these proteins cause primary ciliary dyskinesia (PCD) in humans. Despite the prevalence of exome sequencing among PCD patients, roughly 30% of clinically diagnosed individuals have unknown genetic etiology.⁴⁵ To date, inheritance of all known PCD genes is recessive, except for FOXP1 (dominant, pLI = 0.97) and PIH1D3 and OFD1 (X-linked). This missing heritability could be due to difficulty in identifying variants in known genes using exome sequencing, variants in novel PCD genes, or an alternative inheritance mechanism. One possible mechanism is called digenic inheritance in humans, or second-site non-complementation (SSNC) in model organisms. Here, we utilize the single-celled green alga *Chlamydomonas reinhardtii* to ask whether SSNC exists among various functional groups of motile cilia genes. To accomplish this, haploid strains with mutations in different motile cilia genes were used to create either single

or double heterozygous diploids. Our results show that these diploids are phenotypically recessive under steady-state conditions. Double heterozygous diploids with both mutations in cytoplasmic dynein arm assembly factors (DNAAFs) regrow cilia that are shorter than wild-type diploids when subjected to deciliation and regeneration in the presence of cycloheximide. Cilia from a null *pf23* strain, *pf23-4*, completely lacks outer dynein arms (ODAs) and inner dynein arms (IDAs), suggesting that the PF23 DYX domain has an important role in IDA assembly, while the TPR and CS domains may play a greater role in ODA assembly. Immunoblot analysis of cytoplasmic extracts from the *pf23-4/PF23* heterozygous diploids shows a reduction of PF23 protein levels. PF23 protein is reduced further in the double heterozygous diploid of *pf23-4/PF23; wdr92/WDR92*, but not in the *oda8/ODA8; pf23/PF23* or *oda8/ODA8; wdr92/WDR92* double heterozygotes or the corresponding single heterozygous parents. These results suggest that PF23 expression is dosage dependent. Additionally, *PF23* and *WDR92* exhibit SSNC in steady-state cells in the form of combined haploinsufficiency. Finally, the I1/f intermediate chain protein IC138 shows an altered band pattern by immunoblot in DNAAF mutants *pf23* and *wdr92*, but not in other assembly factor mutants. This reveals a unique role for PF23 and WDR92 in IC138 assembly and provides the first example of SSNC among dynein arm assembly factors.

2.2 Introduction

2.2.1 Motile Cilia Are Complex Organelles

Motile cilia are microtubule-based organelles that are used by cells to generate fluid flow or facilitate motility.⁷³ They are comprised of >1000 different proteins organized into structural and functional groups.⁷⁴⁻⁷⁶ The cytoskeleton, or axoneme, of most motile cilia is composed of nine outer microtubule doublets (MTDs) and two inner microtubule singlets known as the central

apparatus. This is referred to as a '9+2' arrangement.⁷⁷ A special type of motile cilia called nodal cilia is only present during development in higher eukaryotes in a transient structure called the embryonic node. These cilia generate fluid flow that directs body axis formation and left-right asymmetry. They lack the central apparatus and have a '9 + 0' microtubule doublet arrangement.⁴² The axoneme skeleton is built from repeating rows of α - and β -tubulin heterodimers arranged into a lattice. Each doublet is comprised of an A-tubule with 13 protofilaments and an incomplete B-tubule with 10 protofilaments. The interior of each doublet is occupied by various microtubule inner proteins (MIPS).⁷⁸ The ODAs are motors that attach to the A-tubule and contact the neighboring B-tubule. They generate the force that leads to ciliary bending through sliding and determine the beat frequency of the cilia.^{10,79} IDAs are also attached to the A-tubule. They regulate the ciliary waveform.^{80,81} There are several other complexes that connect the central apparatus and the outer doublets that are important in regulation of motility. These include the nexin-dynein regulatory complex (N-DRC), radial spokes (RS) and calmodulin spoke complex (CSC), outer and inner dynein linkers (OIDL), and MIA (Modifier of inner arms complex). Other factors important in the assembly, maturation and transport of dynein arms include DNAAFs, ODA and IDA maturation factors, and ODA and IDA adapters, respectively.^{77,82-85}

2.2.2 Motile Cilia Defects Cause Primary Ciliary Dyskinesia (PCD)

In humans, defects in motile cilia cause a rare, recessive ciliopathy disease known as Primary Ciliary Dyskinesia (PCD). It is characterized by neonatal respiratory distress, recurrent lung infections, bronchiectasis, and male infertility. Left-right asymmetry (*situs inversus totalis*) or heterotaxy (*situs ambiguus*) occurs in approximately 50% of patients because of defective nodal cilia function during development.^{35,45} PCD is usually diagnosed through analysis of cilia from

cell cultures of affected patients, gene panel testing, nitric oxide measurements, transmission electron microscopy, immunofluorescence analysis, and more recently, whole exome and genome sequencing.^{46,69-72} However, roughly 30% of patients with a clinical diagnosis have unknown genetic etiology despite genetic testing, exome, or rarely, genome sequencing.⁴⁵ Several explanations may account for the lack of disease-associated genotypes in these individuals. First, a patient may harbor variants in genes that have not yet been associated with PCD, or sequencing may produce variants of unknown significance.⁴⁶ Second, variants may be non-coding, or large structural variants that are difficult to identify by panels or exome sequencing.⁶² Alternatively, another inheritance mechanism of PCD, digenic inheritance (DI) or second-site non-complementation (SSNC) may exist.

2.2.3 The Mechanism of DI/SSNC

When a gene follows a recessive inheritance pattern, both copies of that gene must carry a deleterious mutation/variant to manifest a mutant phenotype.⁸⁶ The complementation test is based on the premise that two recessive mutant alleles belong to different genes if they produce a wild-type phenotype when each allele is in *trans* (on different parental chromosomes). If the two heterozygous mutant alleles produce a mutant phenotype when in *trans*, they exhibit failure to complement and are presumed to belong to the same gene. However, failure to complement can also occur when the alleles are in different genes (in a double heterozygote). This is known as Second-Site Non-Complementation (SSNC).⁸⁷ This concept has been considered regarding PCD, when individuals are reported as heterozygous for a single allele, although there are no recorded cases thus far.⁹³⁻⁹⁵ Interestingly, a few examples are reported with other syndromes. One study identified individuals with heterotaxy, a PCD-associated phenotype, with one variant in *DNAH6*,

an IDA heavy chain gene, and another variant in *DNAIL1*, an ODA intermediate chain gene. Other individuals in the study had additional heterozygous combinations with *DNAIL1* (ODA intermediate chain).⁴¹ DI has been reported for another ciliopathy, short-rib polydactyly syndrome type Majewski with variants in *NEK1* (a serine/threonine kinase with roles in ciliogenesis) and *DYNC2H1* (cytoplasmic dynein 2 heavy chain 1).⁹⁶ In retinitis pigmentosa, another cilia-related disease, two genes, *ROM1* (retinal outer segment membrane protein) and *Peripherin* (retinal outer segment protein) displayed a DI pattern.^{97,98}

SSNC is observed in many model organisms. In type I SSNC (poison model), mutant gene products from two different loci interact to form a complex that is detrimental to the cell or organism. This is the rarest type of SSNC, and usually implies a specific protein-protein interaction. One well-known example involves a cold-sensitive α -tubulin (*tub1-1*) mutation that fails to complement a mutation in β -tubulin (*tub2*) in yeast.⁹⁹ Type II SSNC (sequestration) occurs when mutant protein binds and sequesters wild-type protein into an inactive complex. This is observed between α - and β -tubulin non-complementing mutations in *Drosophila*.¹⁰⁰ Type III SSNC (combined haploinsufficiency) manifests when a reduction in the normal levels of two protein products generate a phenotype that is absent when the levels of only one protein product is lowered.⁸⁷ In mice, the *hoxb-5* and *hoxb-6* genes involved in body segmentation also exhibit SSNC; the double heterozygous mutant mice show skeletal abnormality phenotypes not seen in either homozygote.¹⁰¹ In *C. elegans*, non-allelic non-complementation (another name for SSNC) was shown between the genes that encode synaptic proteins UNC-13 and syntaxin/UNC-64.¹⁰⁴ SSNC has also been observed in *Chlamydomonas reinhardtii*, a haploid, single-celled, bi-ciliated, photosynthetic alga. SSNC was found between alleles that fail to suppress a mutant, *pf10*, with aberrant motility that was exacerbated in low or absent light. One group of suppressors termed

‘bypass of paralysis’ (*bop*) reverses the *pf10* phenotype in low light, while another group, ‘light influenced suppressors’ (*lis*), requires light for *pf10* suppression.¹⁰⁶ A second instance of SSNC was shown among strains with temperature-sensitive mutations in genes involved in intraflagellar transport (IFT), the complex that transports cargo in and out of the cilia. IFT is divided into two complexes (IFT-A and IFT-B). Work by Iomini et. al.¹⁰⁵ found that IFT mutants *ift39* and *ift44* fail to complement at both permissive (21°), and non-permissive (32°) temperatures. The double heterozygotes completely lack cilia. In other combinations tested, several *Chlamydomonas* mutants within each complex failed to complement each other in double heterozygous diploids and are aciliate. Additionally, IFTB mutant *ift172* fails to complement IFTA mutants *ift139*, *ift144* and *dhc2* (Figure 1).

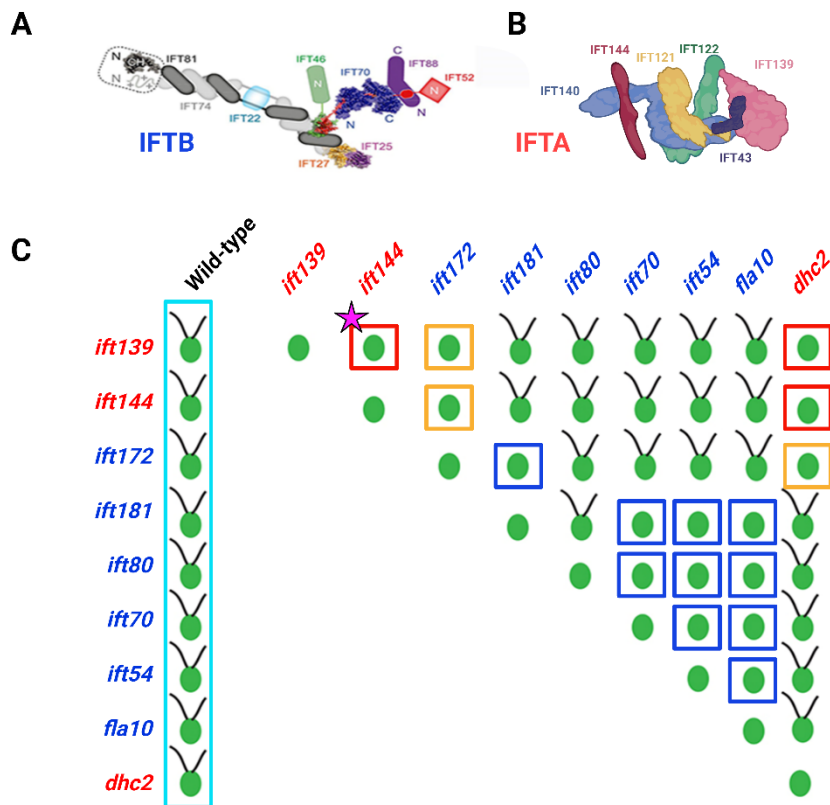


Figure 1: SSNC between mutants in intraflagellar transport machinery in IFTB (anterograde) and IFTA (retrograde) in *Chlamydomonas reinhardtii* diploids. (A) A schematic of the IFTB complex.¹⁶² (B) A schematic of the IFTA complex.¹⁶³ (C) The *ift* mutants shown above are temperature-sensitive. At the permissive temperature (21°C), these mutant strains assemble cilia and swim. After 12 hrs at the restrictive temperature (32°C), the strains are

aciliate. The mutations are recessive, since in their heterozygous state they assemble cilia at the restrictive temperature (cyan rectangle). Several members of the same complex fail to complement each other as double heterozygotes (red squares represent IFTA, blue squares are IFTB). Interestingly, IFT172 complements other components of the IFTB complex, but fails to complement mutants of IFTA (yellow squares). The data was generated using methods described in Iomini et. al.¹⁰⁵ The original published SSNC combination of mutants *ift44* and *ift139* is highlighted by a pink star. Created with BioRender.com.

It is evident that SSNC occurs among genes involved in motility in *Chlamydomonas*. To test whether DI/SSNC could be an alternative inheritance mechanism in PCD patients, we performed a systematic screen in *Chlamydomonas* diploids to ask whether DI/SSNC occurs among motile cilia genes. We focused on genes known to cause PCD in humans.

2.2.4 Motile Cilia Structure, Genes & Mutants in *Chlamydomonas reinhardtii*

Chlamydomonas reinhardtii has been used extensively in motile cilia research due to its ease of performing genetic, biochemical, and microscopic analysis.¹¹⁹ To test whether motile cilia structural and assembly genes exhibit SSNC, and to learn more about the relationships between these genes, we utilized available strains from the *Chlamydomonas* Resource Center.^{120,121} A subset of these strains originate from a large UV mutagenesis screen that produced a variety of slow-swimming or paralyzed mutants with defects in the ODAs and/or IDAs in *Chlamydomonas*.¹²² Each strain discussed below contains a mutation in a previously characterized motile cilia structural or functional gene. The gene products of selected mutants are ODA motor components, ODA docking complex proteins, ODA maturation proteins, DNAAFs, and ODA and IDA intraflagellar transport adapters. A mutant affecting the radial spoke was included as an outgroup.

ODAs in *Chlamydomonas* contain three heavy chains, α -, β - and γ -HCs. A mutant in the α -HC, *oda11*,¹²³ lacks only the α - heavy chain, while β - and γ - heavy chain mutants, *oda4-1*¹²² and *oda2-1*,¹²⁴ respectively, lack all three heavy chains. An allele of *oda4-1*, *sup-pf1-1*,^{125,126} contains

an in-frame deletion that shortens the microtubule-binding domain (stalk) of the β -HC. Intermediate and light chains connect the ODA heavy chains to the axoneme along with the ODA docking complex. We obtained mutants in the two heterodimer-forming ODA intermediate chains IC69 and IC78, *oda6-95*¹²⁷ and *oda9*,^{122,128} respectively, and a mutant, *oda12-2*¹²⁹ of one of the 11 ODA-associated light chains, LC2.

Although the assembled ODA heavy, intermediate, and light chain complex can bind to the axoneme, the ODA docking complex (ODA-DC) is needed to stabilize this interaction.^{130,131} Mutants in two ODA-DC complex components, *oda1*¹³² and *oda3-1*,¹³³ completely lack ODAs, while a mutant in the third component, *oda14-F28*,¹³⁴ partially lacks dynein arms. Dynein arms are assembled in the cytoplasm by DNAAFs before they are transported into the axoneme. Mutations in *DNAAF* genes affect the assembly of both ODAs and IDAs to varying degrees. In *Chlamydomonas*, this results in ciliary paralysis and short cilia, and includes mutants *pf22-1*,¹³⁵ *pf23-1*,^{65,136} *pf13-1*,¹⁸ and *wdr92*.^{137,138} Another DNAAF, ODA7, differs in that it only affects assembly of ODAs. It primarily localizes to the cytoplasm but is also found in the cilia where it interacts with both ODAs and IDAs to form a link between them.^{63,139} The *oda7-1* mutant, in contrast to other *DNAAF* mutants, is motile. Following cytoplasmic assembly, dyneins are made binding-competent or 'matured' by maturation complex factors. ODA5 and ODA10 interact directly with each other and localize to the cytoplasm and proximal axoneme. ODA8 is reported to localize to the cytoplasm and interact with IFT proteins.²⁴ The *oda5*,^{140,141} *oda10*,^{141,142} and *oda8*¹⁴³ mutants were used. Mature ODAs and IDAs are transported into the cilia by IFT, with the aid of IFT adapters ODA16 and IDA3. Mutants *oda16-2*^{144,145} and *ida3*¹⁴⁶ were also used. The radial spoke (RS) connects the central pair and outer doublets. It is comprised of approximately 23 proteins.¹⁴⁷ The *PF14* gene encodes the RSP3 (radial spoke protein 3) subunit, and the *pf14*¹⁴⁸

mutant lacks the radial spoke head. Given that many of the previously mentioned proteins have physical or functional interactions, we hypothesized that they would be good candidates for an investigation of SSNC in *Chlamydomonas*. However, SSNC requires the presence of two alleles *in trans* in a diploid organism. Since *Chlamydomonas* is haploid, it was necessary to generate diploids to conduct this study.

2.2.5 Diploid Generation in *Chlamydomonas*

Haploid *Chlamydomonas* strains of mating-type plus and mating-type minus can be mated to produce diploid zygotes that undergo meiosis. This results in haploid progeny. However, a small percentage of mated cells undergo mitotic division and form stable, vegetative diploids.¹⁵³ Diploids can be generated using several methods in *Chlamydomonas*. Complementing arginine auxotrophs were used in other work.^{153,155–158} We generated diploids using an acetate auxotroph (*ac17*) and the drug resistance marker paromomycin (*aphviii*). In this work, we show that diploids heterozygous for the mutations tested behave recessively under steady-state conditions. Following deciliation and regeneration in cycloheximide, diploids heterozygous for *DNAAF* mutations show a cilia length regeneration phenotype. Immunoblot analysis of steady-state/vegetative cells suggests that one DNAAF, PF23, is reduced by half in a single heterozygous strain *pf23-4/PF23* and shows SSNC when heterozygous with DNAAF WDR92. Additionally, PF23 and WDR92 both affect IDA component IC138, the I1/f intermediate chain.

2.3 Results

2.3.1 Characterization of Haploid *Chlamydomonas* Wild-Type And Mutant Strains

The strains were originally obtained by either UV mutagenesis or insertional mutagenesis. The causative genes were generally identified by rescue and some of the causative mutations were identified by sequencing. Many of the genes used in this study are associated with PCD (Table 1). Because SSNC mechanisms are often related to the type of allele present in mutant strains, we wanted to identify the mutations present in *pf13-1*, *oda3-1*, *oda4-1*, *oda9*, and *oda11-1*. We used whole genome short-read sequencing with SNP analysis.¹⁶⁴ We identified the mutations in strains *oda3-1*, *oda9*, and *oda11-1* (Table 1, Figure 2). The SnpEff analysis did not reveal any candidate mutations in *oda4* and *pf13-1*. Therefore, the sequenced reads were manually examined at the *ODA4* locus, *DHC14*. We found a 5 base-pair deletion in the *oda4* mutant that changes the reading frame. After manual curation of *pf13-1* sequence, we found an approximately 49 kb deletion that includes the *PF13* gene and 7 other adjacent genes (Table 1, Figure 2). Primers were generated to genotype the mutant strains by PCR (Table S1).

The strains we selected are divided into functional groups (Figure 3A-3E). To verify the phenotypes of the strains, we looked at cilia length. We performed immunofluorescence using acetylated α -tubulin to stain the cilia and rootlet microtubules, and quantified swimming velocity and beat frequency (Figure 3F-I). Most of the *oda* strains possess full-length cilia; the *oda16*, *oda11* and the *sup-pf1-1* strains have shorter cilia than wild-type. The *oda3* cilia were also slightly shorter than wild-type strain CC-125 ($p = 0.0285$), which is significantly different. Strains with assembly factor mutations (*pf22-1*, *pf13-1*, *pf23-1*, and *wdr92-2*) have short, immotile cilia. One

Table 1: *Chlamydomonas* mutant strains used to generate diploids for SSNC screen

Category	Mutant	Human Ortholog	Known PCD gene	Variant	Type of allele	Ref.
Dynein arm assembly factor	<i>pf22-1</i>	<i>DNAAF3</i>	Yes	W79X	Null	135
	<i>oda7-1</i>	<i>DNAAF1/LRRC50</i>	Yes	Exon 1 insertion	Null	63
	<i>pf13-1*</i>	<i>DNAAF2/KTU</i>	Yes	49 kb deletion	Null	165
	<i>pf23-1</i>	<i>DNAAF4/DYX1C1</i>	Yes	In-frame exon 5 deletion	Altered**	65,136
	<i>pf23-4</i>	<i>DNAAF4/DYX1C1</i>	Yes	Insertion exon 1	Null	94
	<i>wdr92-2^x</i>	<i>WDR92</i>	No	Exon 5 deletion, insertion	Null	137
Accessory complex	<i>oda8</i>	<i>LRRC56/MOT37</i>	Yes	E36fs	PN	143 140,14
	<i>oda5</i>	<i>CCDC63</i>	No	V108X	Null	1
	<i>oda10</i>	<i>CCDC151</i>	Yes	Unknown	Unknown	141,14 2
ODA docking complex	<i>oda1</i>	<i>CCDC114</i>	Yes	E46X	Null	132
	<i>oda3-1*</i>	<i>CCDC151</i>	Yes	M279fs; 1bp deletion	Null	166
	<i>oda14-F28</i>	None	No	Exon 1 insertion	Null	167
ODA intermediate & light chain	<i>oda6-95*</i>	<i>DNAI2</i>	Yes	V54Gfs	Null	127,16 8
	<i>oda9*</i>	<i>DNAI1</i>	Yes	K225fs	Null	128,16 9
	<i>oda12-2</i>	<i>DYNLT2</i>	No	3'UTR insertion	Null	129
ODA heavy chain	<i>oda4-1*</i>	<i>DNAH9/11/17</i>	Yes	R2872fs; 5 bp deletion in exon 22	Null	169
	<i>sup-pf1-1</i>	<i>DNAH9/11/17</i>	Yes	In-frame deletion of 21 bps in Exon 25	Altered**	125
	<i>oda11-1*</i>	-	Yes	W778X	Null	170
	<i>oda2^x</i>	<i>DNAH5/8</i>	Yes	Exon 9 insertion	Unknown	171
ODA adapter	<i>oda16-1</i>	<i>WDR69</i>	No	Insertion unknown	Null	172
IDA adapter	<i>ida3</i>	None	No	W22X	Null	173
Radial spoke	<i>pf14</i>	<i>RSPH3</i>	Yes	Q21X	Altered**	148

Table 1: *Chlamydomonas* mutant strains used to generate diploids for SSNC screen. Each mutation is classed by structural or functional group according to the literature. *Chlamydomonas* mutant gene/strain is listed with the human orthologs. Dashes indicate no ortholog is found in humans. Variants of mutants that have been identified are listed in column along with the known or predicted consequences of those variants. Mutations are classed as null, predicted null or loss-of-function. *Sequenced in this work **Partial function: ^xCLiP strain

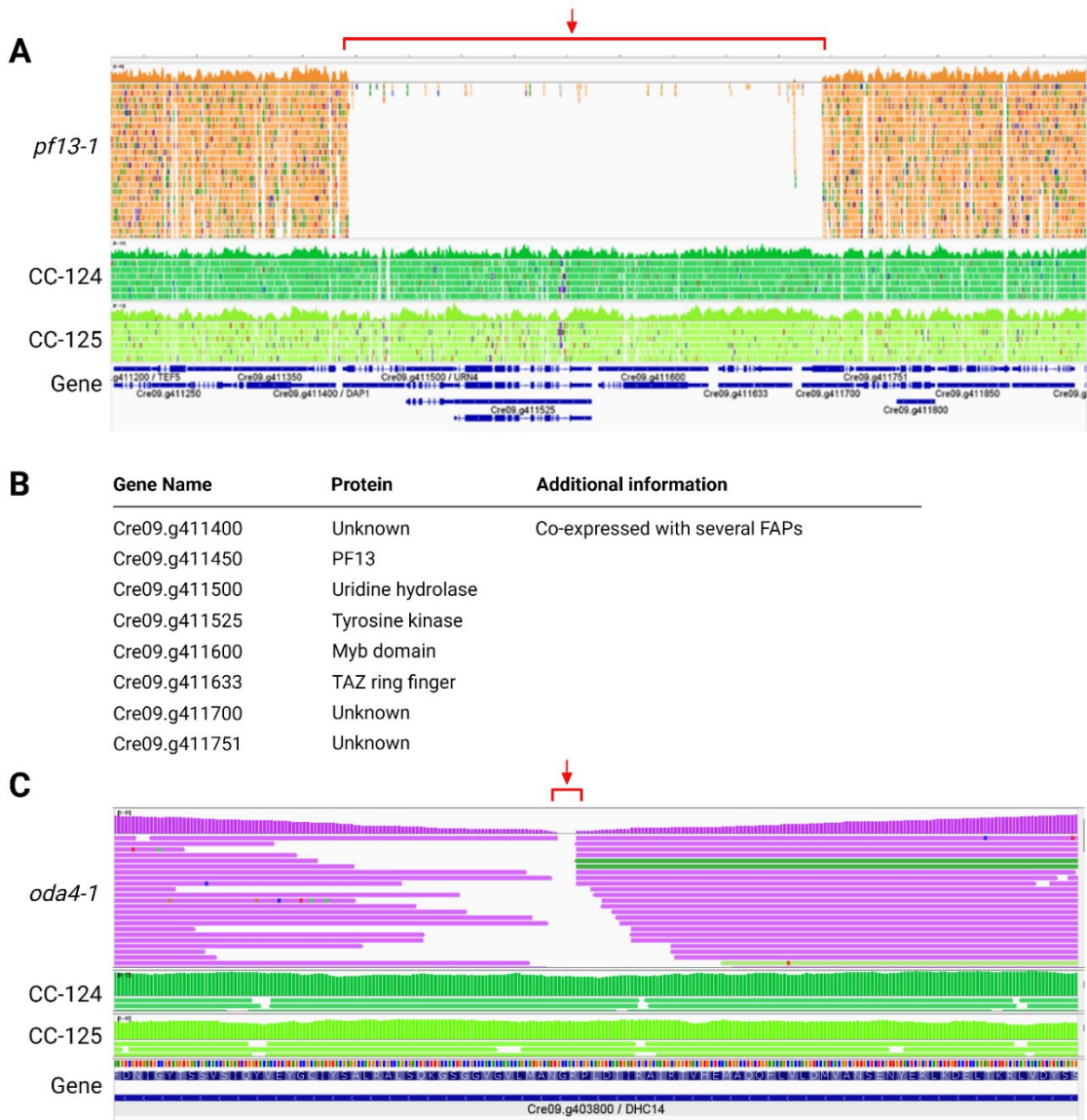


Figure 2: Whole Genome Sequencing analysis of the *pf13-1* strain and *oda4-1* strain (A) reads spanning the *PF13* locus (Cre09.g411450) from the *pf13-1* mutant show an approximately 49 kb region that is deleted in the mutant strain compared to wild-types CC-124 and CC-125. The IGV track at the bottom in blue shows the genes in that region. (B) Table showing the genes and corresponding protein products that are deleted in *pf13-1* strain. Only Cre09.g411400 may affect cilia based on the co-expression with known ciliary genes. (C) IGV snapshot of reads spanning the region of the *oda4-1* (Cre09.g403800) 5 bp deletion. Regions containing the deletions are indicated with a red arrow and bracket. Created with BioRender.com

known exception is the assembly factor mutant *oda7* that has full-length cilia and is motile (Figure 3F, 1G, 1H). The swimming phenotype resembles the slow, jerky movements characteristic of *oda* mutants.^{174–177}. Swimming velocities vary among strains. In general, *oda* strains swim at about

one-half the wild-type speed and have a reduced beat frequency.^{80,178} Most of the *oda16-1* cells were immotile, but approximately 10% of cells swam slowly. The *ida3* strain swims more slowly than wild-type but has a wild-type beat frequency (Figure 3G, 1H).^{146,179} Because the motile cilia

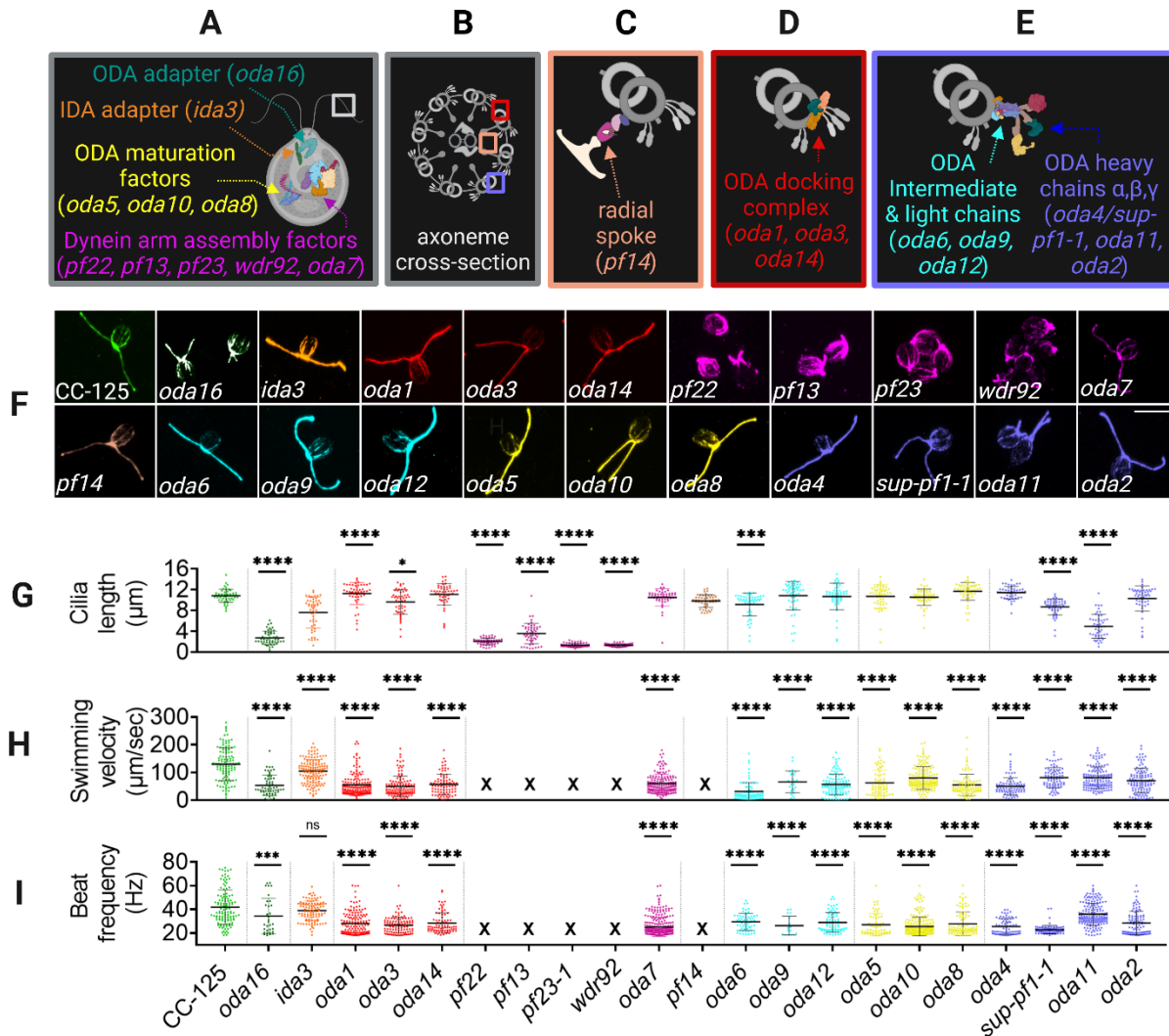


Figure 3. A phenotypic summary of the motile cilia mutants used in this study. (A-E) Motile cilia genes in *Chlamydomonas* are grouped according to their function or structure affected. The names of mutant strains in each group are listed in parentheses. (A) Dynein arm assembly factors (pink), ODA maturation factors (yellow), an ODA adapter (dark green) and an IDA adapter (orange). (B) A cross-section of the *Chlamydomonas* axoneme outlined by the white box in (A). The boxes highlight the locations of three structural groups respectively – the radial spoke (tan, inset in C) the ODA docking complex (red, inset in D), and the ODA intermediate and light chains (cyan, inset in E) and ODA heavy chains (purple, inset in E). (F) A wild-type *Chlamydomonas* strain and mutants from each functional group shown in A-E are stained with antibody against acetylated α -tubulin to show the cilia and rootlet microtubules. (G) Quantification of cilia lengths. Fifty individual cilia were measured for each strain. Statistical analysis was performed using a One-Way ANOVA with adjustments for multiple comparisons. Each strain is compared to wild-type strain CC-125. (H) Swimming velocity measurements for each strain in F. Strains *pf22*, *pf13*, *pf23-1*, *wdr92* and *pf14* are non-motile and are indicated by an 'X'. (I) Beat frequency measurements for each strain in F. Created with BioRender.com and GraphPad Prism.

mutants we selected have strong, easily discernable phenotypes, we hypothesized that we would be able to observe similar phenotypes in double heterozygous strains that show SSNC.

2.3.2 Generation And Assessment of *Chlamydomonas* Diploid Strains

To examine whether SSNC occurs with motile cilia genes in *Chlamydomonas*, we generated heterozygous diploid strains. One haploid strain with a mutation in gene 1 and wild-type for gene 2 was crossed with a second haploid strain with a mutation in gene 2 and wild-type for gene 1. Each strain contains a selectable genotype for acetate requirement (*ac17*) or paromomycin resistance (*aphviii*). The selectable genotypes are complementary in each haploid strain. The

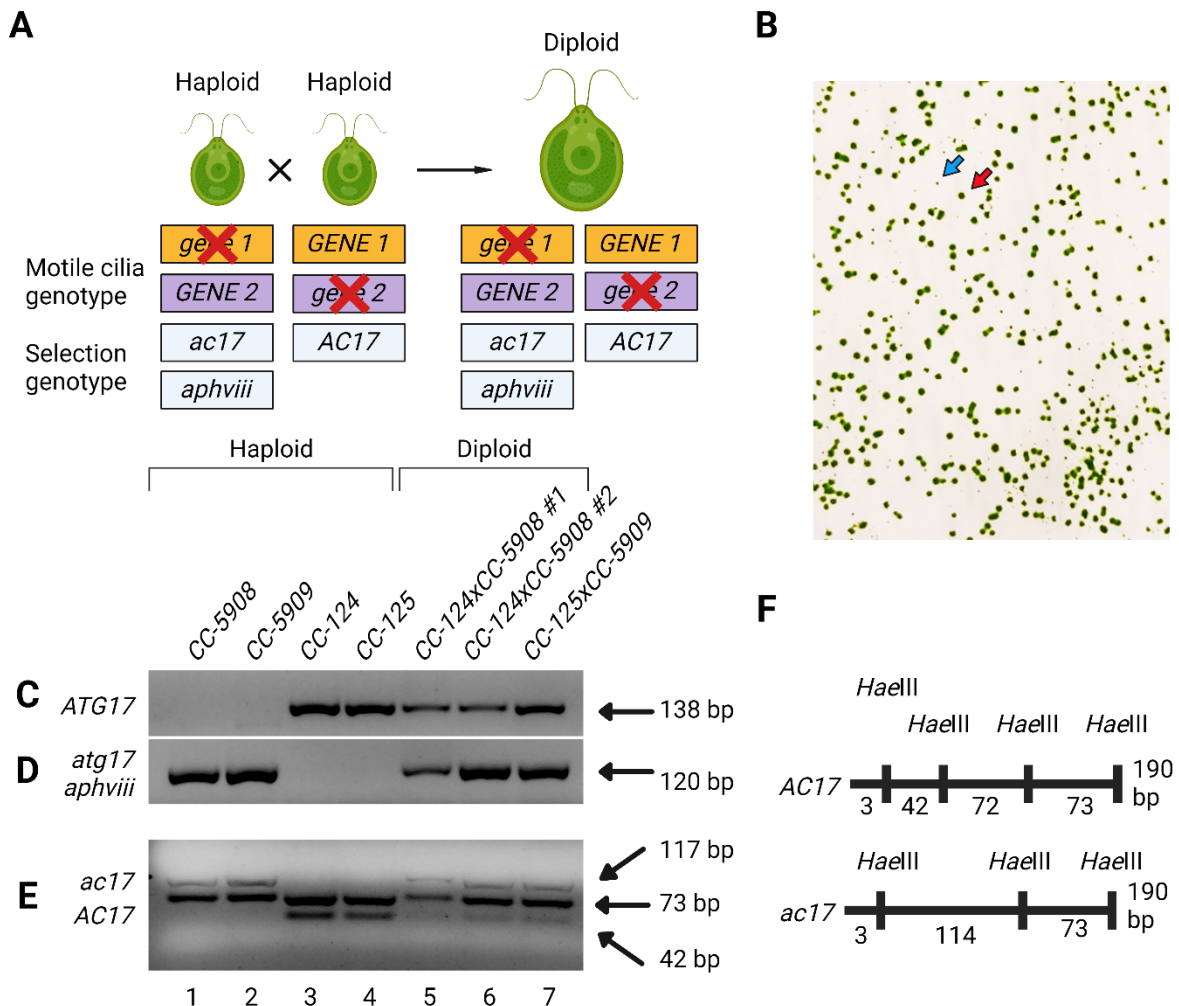


Figure 4: Generation and genotyping of *Chlamydomonas reinhardtii* wild-type diploid strains. (A) Diploids were selected after 3-5 days on medium lacking acetate and containing paromomycin. Haploid strains with the genotype *ac17*; *aphviii* die on plates that lack acetate although they are resistant to paromomycin. Haploid strains with the genotype *AC17* grow in the absence of acetate and die on medium with paromomycin. Only diploid cells survive on plates lacking acetate and containing paromomycin. The two sets of haploid cells each carry mutations in two different cilia genes (*gene1* and *gene2*). Mating these strains produces diploid cells that are heterozygous for both mutations. (B) Diploid colonies appear as bright green spots (red arrow) on a pale green background of haploid cells (blue arrow). (C) PCR markers were used to verify wild-type haploid and diploid strains generated in this study. Haploid strains CC-5908 and CC-5909 carry an insertion in the *ATG17* gene, and a mutation in *ac17*, but are wild-type swimmers. CC-124 and CC-125 are wild-type at both loci. The three wild-type diploid strains are heterozygous for the *atg17* and *ac17* mutations. PCR primers against the *ATG17* gene¹⁸⁰ were used to detect the wild-type copy of the gene in CC-124, CC-125 and three diploid wild types (lanes 3A-7A). No band is present in CC-5908 and CC-5909 (lanes 1 & 2), since the *aphviii* paromomycin resistance gene is inserted into the *atg17* gene. (D) PCR primers were designed to detect the junction between the *ATG17* gene and the *aphviii* insertion in the *ATG17* gene. This junction is present in the CC5908 and CC-5909 strains that carry the insertion (lanes 1B & 2B), as well as the heterozygous diploids (lanes 5B-7B). (E) PCR primers were designed to amplify across the region containing the mutation in the *AC17* gene.¹⁸¹ Digestion with *HaeIII* generates different sized products in the *ac17* containing strains (lanes 1C & 2C) compared to CC-124 and CC-125 wild-types (lanes 3C & 4C). The heterozygous diploid strains (5C-7C) generate both sets of digest products. (E) A map of the *AC17* PCR product digested with *HaeIII*. Created with BioRender.com

outcome of this cross is a double heterozygous diploid (Figure 4A). Diploids appear as bright green colonies on acetate(-) / paromomycin(+) selection plates (Figure 4B). When a wild-type haploid strain is crossed with a mutant haploid strain, the result is a single heterozygous diploid. The wild-type haploid and diploid strains were genotyped first using primers that differentiate the *ac17* and *aphviii* mutant genotypes from wild-type. Subsequently, they were genotyped using mating-type primers (Table S1, Figure 5).

We compared the haploid and diploid wild-type *Chlamydomonas* vegetative cells. Previous analyses of diploid cells reported differences in cell size, mating type, and DNA content compared to haploid cells.¹⁵³ Mating-type PCR analysis shows that diploid cells contain both mating-type plus and mating-type minus loci (Figure 5A).^{158,180} Diploid cells are larger and swim more slowly than haploid cells by phase microscopy observation. To quantitate the size of diploids, we performed immunofluorescence on haploid and diploid wild-type strains and found that diploid cell bodies are slightly longer (8.5 microns compared to 6.9 microns for haploids) (Figure 5B, 5G); This implies that diploids have a larger cell volume; this data agreed with Ebersold.¹⁵³ Diploid

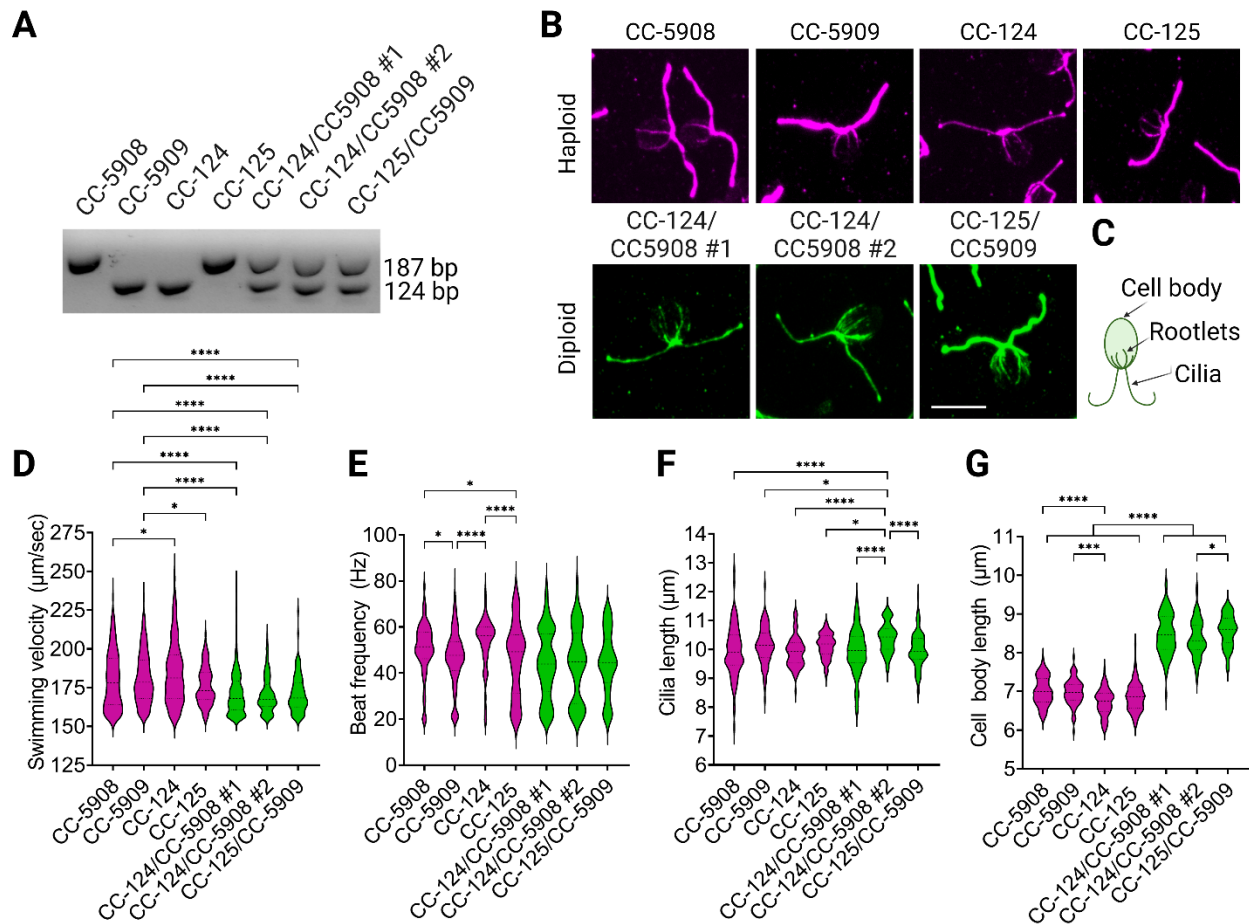


Figure 5: A comparison of haploid and diploid *Chlamydomonas reinhardtii* strains. (A) PCR products for the *MTD* gene (mating-type minus) and *MTA* gene (mating-type plus) differentiate haploid and diploid strains. The top band (187 bp) indicates the *MTA* genes, and the bottom band (124 bp) indicates the *MTD* gene. (B) Immunofluorescence of vegetative haploid strains with the genotype *ac17; aphviii* (CC-5908, CC-5909), CC-124 and CC-125 wild-type strains, and diploid strains generated by crosses between CC-5908 and CC-124 or CC-5909 and CC-125. Cells are stained using an antibody against acetylated α -tubulin. (C) An illustration of structures visualized is provided for reference (D) swimming velocity, (E) beat frequency, (F) cilia length and (G) cell body length measured from the apex of the cell to the base of the cilia, of strains illustrated in B. Diploid strains contain both mating-type plus and mating-type minus loci. Statistical analysis is a One-Way ANOVA using an all-by-all comparison. Created with BioRender.com and GraphPad Prism

strains have slightly slower average swimming velocities and beat frequencies than haploids (Figure 5D, 5E). The cilia of diploid cells are the same length as haploid cells (Figure 5F).

The strains in Table 1 were used to construct 1 wild-type, 21 single heterozygous, and 211 double heterozygous strains. None of the strains display parental phenotypes after initial observation (slow, jerky swimming for *oda* mutants, paralyzed (or short) cilia for assembly factors

and radial spoke mutants, or slow swimming for *ida* mutants. We quantified swimming velocity, cilia beat frequency, and cilia length of vegetative single and double heterozygous diploids using

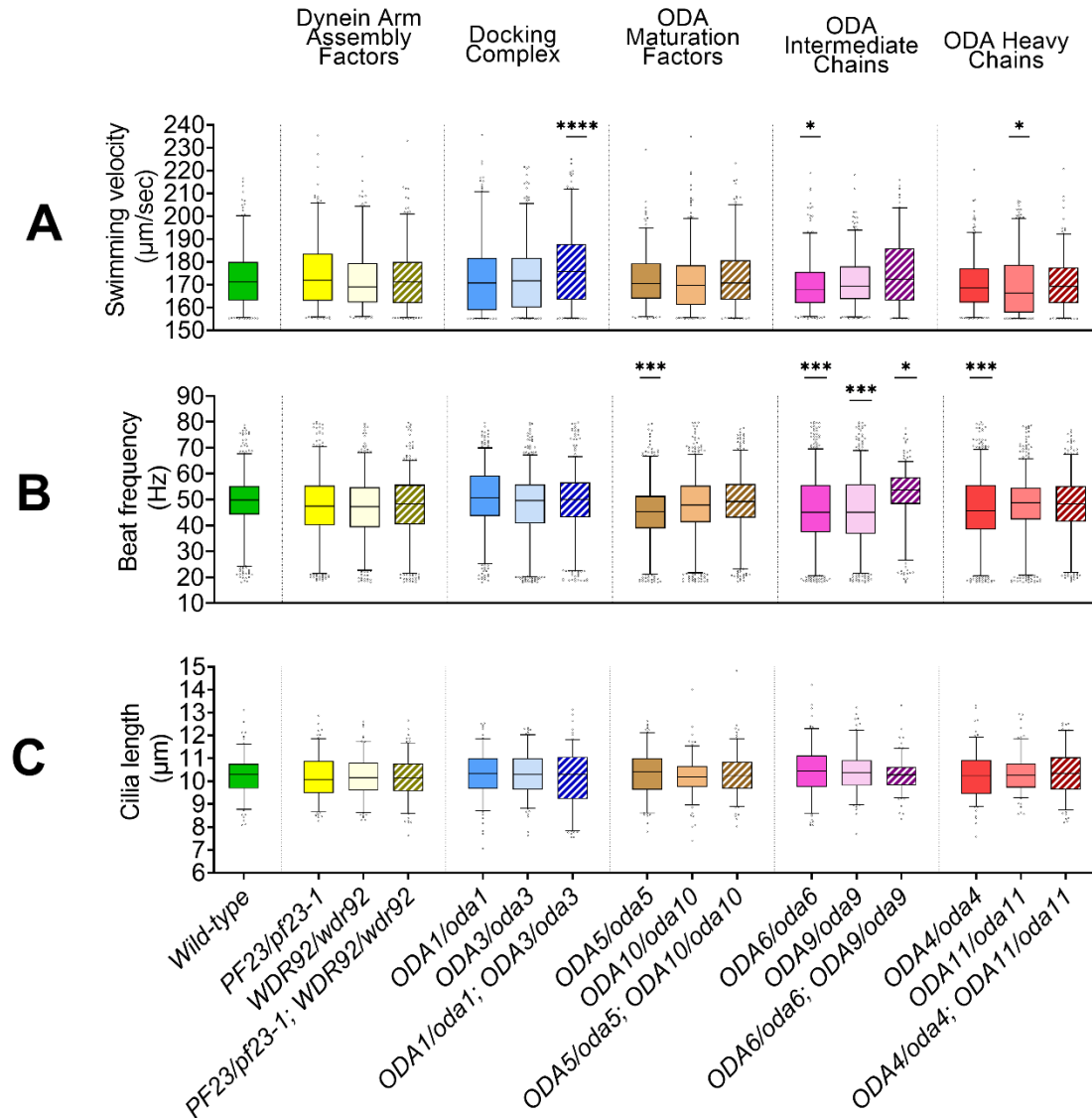


Figure 6: A subset of single and double heterozygous diploids show normal steady-state phenotypes. Previous analysis has demonstrated that a subset of proteins affected in our strains interact with each in yeast two-hybrid screens¹³⁸. These were used to examine the occurrence of SNNC (A) Swimming velocity, (B) Beat frequency, and (C) Cilia length for wild-type diploids and heterozygous diploids with mutations in different ODA assembly or structural genes. Pooled data for 3 biological replicates are shown for each strain. N= 50 cilia for each replicate. The individual data points shown are below and above the 10th and 90th percentile. Solid green fill indicates wild-type and single heterozygotes are represented by various other solid fill colors. Striped fill indicates double heterozygotes. Statistical analysis is a One-Way ANOVA. The cilia lengths of each strain are compared to the wild-type diploid.

strains with mutations in genes that have known genetic or biochemical interactions (Figure 6).^{131,132,138,141,182} A subset of single heterozygous strains showed a small, but statistically significant difference in swimming velocity (*oda1/ODA1*; *oda3/ODA3*, *oda6/ODA6*, and *oda11/ODA11*). Beat frequency differences were observed in single heterozygotes *oda5/ODA5*, *oda6/ODA6*, *oda9/ODA9* and *oda4/ODA4*, and the double heterozygote *oda6/ODA6*; *oda9/ODA9*) (Figure 6A,6B). There were no differences in cilia length between wild type and heterozygous diploids (Figure 6C). The changes in swimming velocity and beat frequency in these strains are small, and swimming behavior by phase microscopy appears wild-type. Additionally, there was no obvious pattern that we could detect in the data. These small changes would be difficult to interpret using a high-throughput screen.

2.3.3 Diploids Regenerate Faster Than Haploids After Deciliation

Because the single and double heterozygotes did not show any gross swimming or cilia length phenotypes under steady-state conditions, we hypothesized that phenotypes might be obtained if the cells were placed under stress conditions. Rosenbaum, Moulder & Ringo¹¹³ assessed the effect of cycloheximide on cilia assembly in haploid cells. They found that wild-type haploid cilia regenerate to approximately 5 to 6 microns in 10 µg/ml cycloheximide following deciliation. The cilia in a *pfl6-1* central apparatus mutant regrew less than 2 microns. These data suggest that the pool of proteins in wild-type cells is only sufficient to build half-length cilia and that the pool is further limited in the *pfl6* strain. We tested for a defect in cilia length regeneration, compared to wild-type, that could be observed in our heterozygous diploids if they were subjected to similar stress conditions.

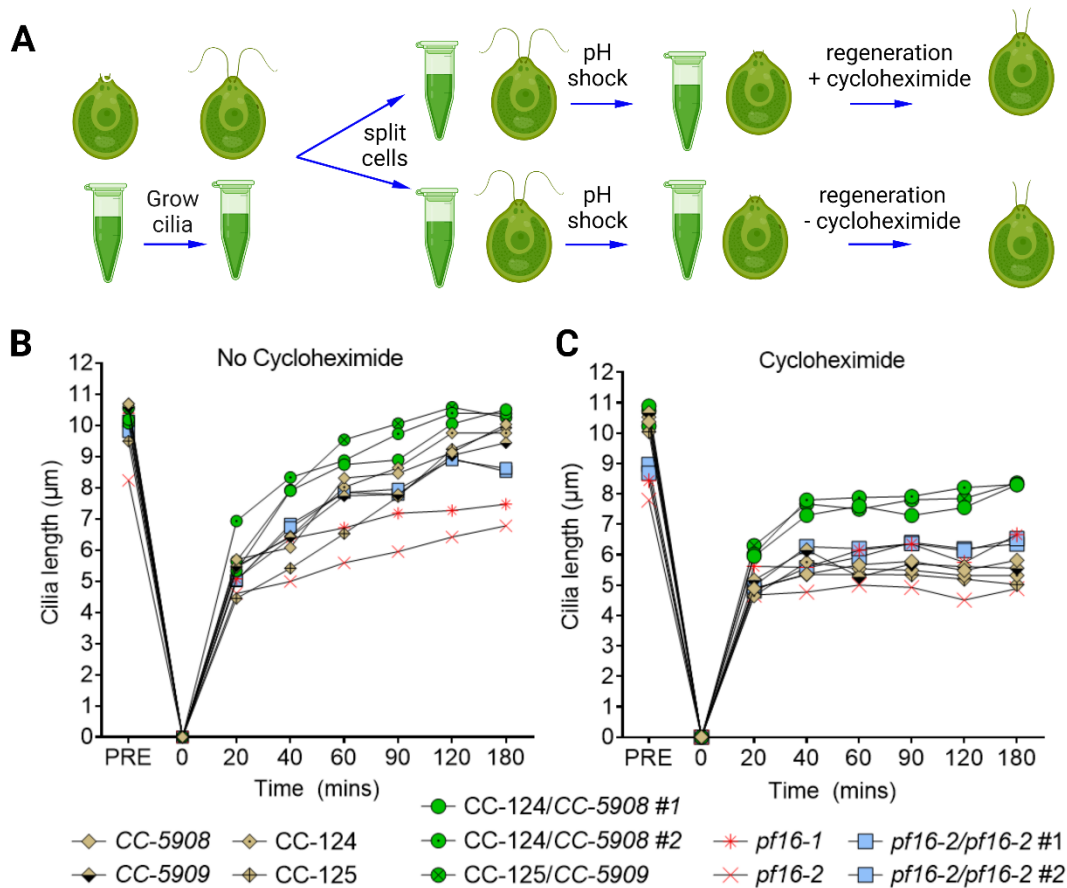


Figure 7. Cycloheximide restricts cilia regeneration after deciliation in haploid and diploid cells (A) Vegetative cells of the indicated genotypes were deciliated and allowed to regenerate for 180 minutes. Samples were collected for cilia length measurements at the timepoints shown. 100 individual cilia were measured for each strain and timepoint. (B) A parallel experiment to that shown in (A) was performed with 10 µg/ml cycloheximide added post-deciliation. Haploid wild-type strains are shown in brown, wild-type diploid cells are green, *pf16-1* and *pf16-2* haploid cells are red, and *pf16-2* homozygous diploid cells are blue. Created with BioRender.com and GraphPad Prism.

First, we assessed whether wild-type diploid *Chlamydomonas* cells regenerated similarly to haploid strains in the absence of cycloheximide. We included strains *pf16* and *pf16B* as controls. These are renamed *pf16-1* and *pf16-2*, respectively, to agree with the *Chlamydomonas* nomenclature. Haploid and diploid wild-type strains, and *pf16* strains, were deciliated and allowed to regenerate in the presence or absence of 10 µg/ml cycloheximide (Figure 7A). All wild-type haploid and diploid cells regenerate to their original pre-deciliation length in the absence of cycloheximide. The post-deciliation regeneration length of both *pf16* strains is shorter than pre-deciliation. Interestingly, diploid cells also regenerate more quickly than haploid cells under both

conditions. At 40 mins post-deciliation, diploid cilia are approximately 8, or 5, microns long in the absence (Figure 7A) or presence (Figure 7B) of cycloheximide respectively, while haploid cilia average 6 or 4 microns. The *pfl6* strains also differ in their regeneration capacities. Both strains fail to regenerate to their original length after deciliation; however, the defect in the *pfl6B* strain is more severe. Our data recapitulates that observed by Rosenbaum et. al.¹¹³ under cycloheximide treatment conditions. Diploid cilia are also longer than haploid cilia after 180 mins of regeneration (8.32 microns vs. 5.43 microns). The *pfl6B* diploids also regenerate longer cilia than the *pfl6B* haploid strains under both conditions (Figure 7B,7C). Our data suggests that the pool of proteins needed for building cilia is larger in diploid cells since they can generate cilia longer than half-length and regenerate more quickly. This behavior is maintained even when the *pfl6* mutation introduces a limiting factor that further reduces cilia length post-deciliation.

2.3.4 Diploids Heterozygous for Mutations in DNAAFs Show SSNC in

Deciliation Screen

Having established that diploid cells follow a similar regeneration pattern to that of haploid cells in the presence of cycloheximide, we asked if any of the single or double heterozygous strains show a cilia regeneration phenotype. Using the protocol outlined in Figure 7A, we deciliated the single and double heterozygous strains, and wild-type diploids, and allowed them to regenerate in cycloheximide for 40 mins.

As shown in the matrix in Figure 8 (rightmost column), all the mutations in the single heterozygous strains tested in this assay are recessive to the wild-type allele and support previous data from both human and model organism studies. The frequency of SSNC is low in our screen, but specific. Double heterozygous diploid strains with mutations in structural proteins (the radial

spoke gene *pf14*, the ODA heavy, intermediate, and light chains (*oda4*, *sup-pf1-1*, *oda11*, *oda2*, *oda6*, *oda9* and *oda12*), and ODA-DC (*oda1*, *oda3*, and *oda14*) all complement. The IFT adapters,

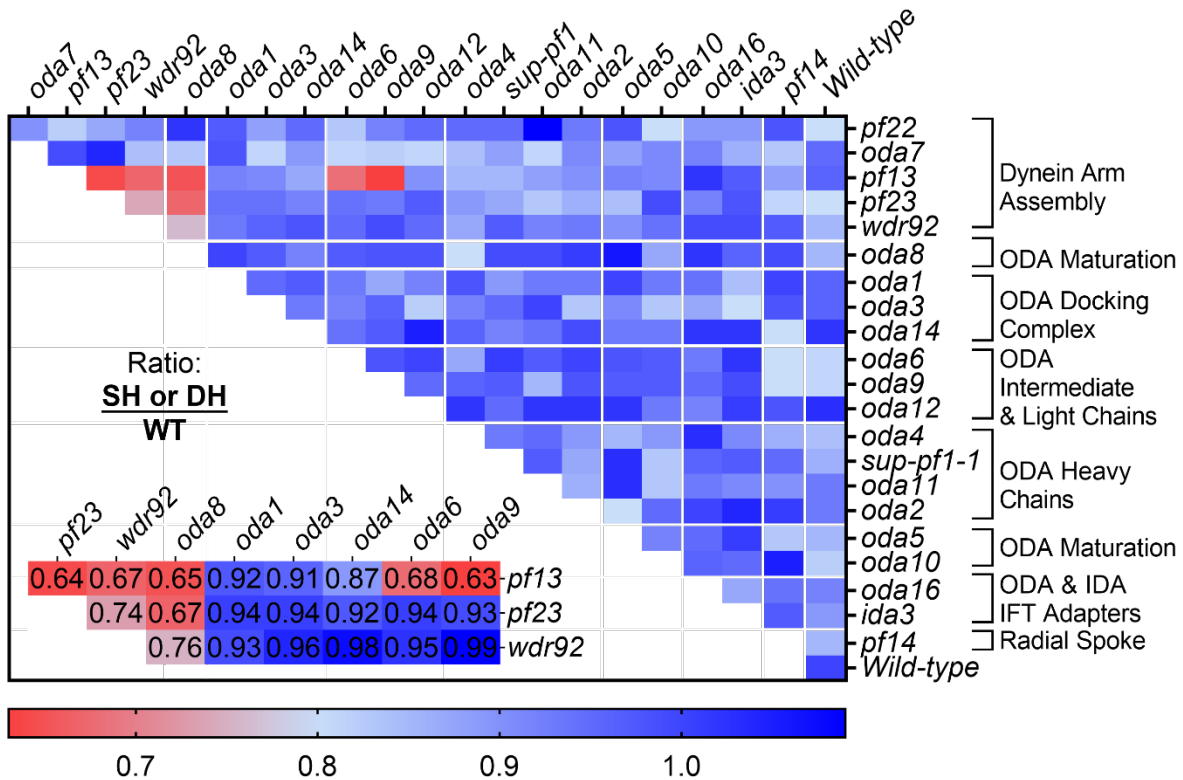


Figure 8: A Matrix of diploid cilia lengths following regeneration in cycloheximide. Each strain and a wild-type control was deciliated and allowed to regenerate for 40 min in 10 μ g/ml cycloheximide. Three biological replicates were measured for each heterozygous diploid. One biological replicate was measured for the wild-type diploid. For each replicate, 100 individual cilia were measured, and the average length was calculated. Each box shown in the heat map represents the ratio of the average length of the pooled biological replicates for each single (SH) (rightmost column) or double heterozygote (DH) / average length of the wild-type diploid (WT). Cooler colors (blue) indicate that the cilia length of the tested heterozygotes is closer to wild-type. Warmer colors (red) indicate that cilia length is shorter than wild-type. An inset of the candidate hits in red is shown in the bottom left corner with the cilia length ratio values. Created with GraphPad Prism.

oda16 and *ida3*, as well as the maturation factors *oda5* and *oda10* also complement. Non-complementation was observed when one of the mutations was in an assembly factor gene. SSNC was observed in the *pf13-1/PF13*; *oda6/ODA6* and *pf13-1/PF13*; *oda9/ODA9* double heterozygous diploid strains, which contain one DNAAF and one dynein structural protein, the intermediate chain. The remaining candidate strains that show SSNC are all double heterozygotes for mutations in dynein assembly factors and the dynein maturation factor ODA8 (Figure 8, inset

lower left). Previously, an interaction between PF23/DYX1C1 and WDR92 was observed by yeast two-hybrid and immunoprecipitation.^{137,138}

2.3.5 Generation and Screening of Null *pf23* Alleles

As mentioned previously, SSNC can occur via three mechanisms: poison, sequestration, and combined haploinsufficiency. The latter is the most straightforward model to test, and the mutant alleles of *wdr92* and *oda8* tested in our screen are null by immunoblots and predicted null, respectively. However, the *pf23-1* allele contains an in-frame deletion of exon 5 and surrounding introns and produces a smaller loss-of-function PF23 protein. Therefore, we decided to create a null allele of *PF23* to test the combined haploinsufficiency SSNC model.

We previously utilized a CRISPR/Cas9 site-directed insertional mutagenesis approach to insert the *aphvii* hygromycin resistance cassette into exon 1 of the *PF23* gene.¹¹⁸ The wild-type strain CC-5908 was transformed with an *aphvii* hygromycin resistance construct. We obtained three independent strains from two separate transformations. These three strains were renamed *pf23-2*, *pf23-3*, and *pf23-4*, respectively¹¹⁸ (Figure 9). Meiotic analysis of all three strains showed that *pf23-2* and *pf23-3* produced meiotic inviability, while crosses with *pf23-4* produced primarily tetrads with four viable progeny. Long-range sequencing of *pf23-2* and *pf23-3* showed that these strains contain translocation breaks between the *pf23* gene and chromosome 5 and 3, respectively.¹¹⁸ Because *pf23-4* did not show any meiotic abnormalities, it is unlikely that it possesses a translocation. Therefore, we used strain *pf23-4* for further analysis.

Immunofluorescence analysis of gametic wild-type and *pf23* mutant strains show that the *pf23-1* strain has short, stubby cilia approximately 2 microns long, while the *pf23* null strains assemble very short cilia that average one micron in length (Figure 10A). Immunoblot analysis using an anti-PF23 antibody¹³⁷ shows that all three strains lack the PF23 protein, compared to the

pf23-1 strain that produces a slightly smaller PF23 protein (Figure 10B). ODA intermediate chain IC69 appears unaffected.

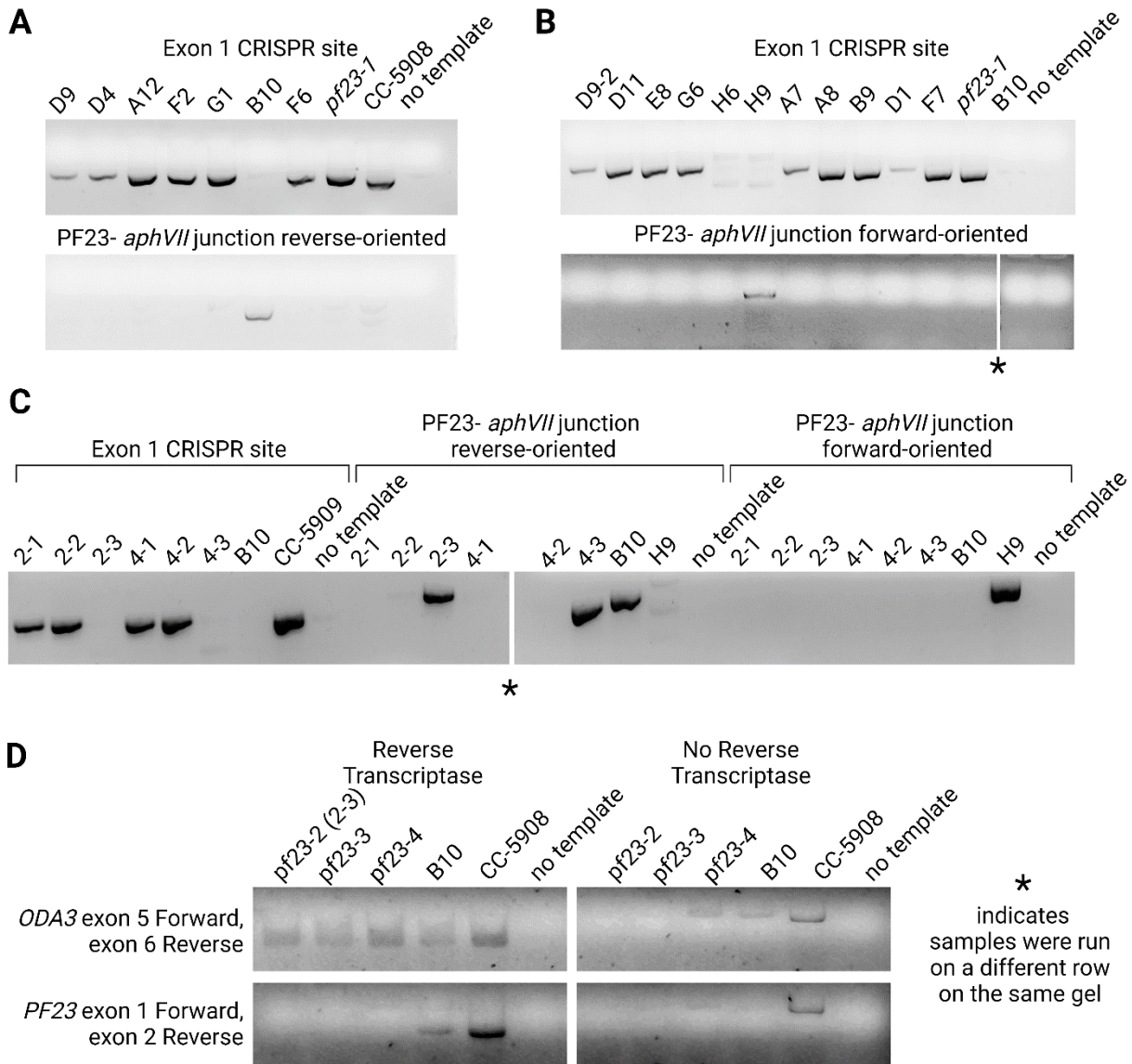


Figure 9: Isolation and analysis of wild-type strains transformed with *aphvii* targeted to exon 1 of the *PF23* gene. (A) PCR screening of 7 transformants from *PF23* CRISPR insertional mutagenesis. One colony, B10 fails to amplify the exon 1 region targeted by the primers and amplifies the *aphvii*-*PF23* junction in exon 1. (B) Strain H9 was retrieved by screening an additional 11 strains from the same transformation. The insertion is oriented in the forward direction. (C) A second transformation produced strains 2-3 (*pf23-2*) and 4-3 (*pf23-3*), the insertion in both strains is oriented in the reverse direction. (D) cDNA analysis of *PF23* CRISPR transformants to detect whether mRNA is disrupted. A band was amplified in strain B10, and it was excluded from further analysis. Strains 2-3, 4-3 and H9 (*pf23-2*, *pf23-3*, and *pf23-4* respectively) failed to generate a cDNA amplicon for exons 1 and 2. Created with BioRender.com.

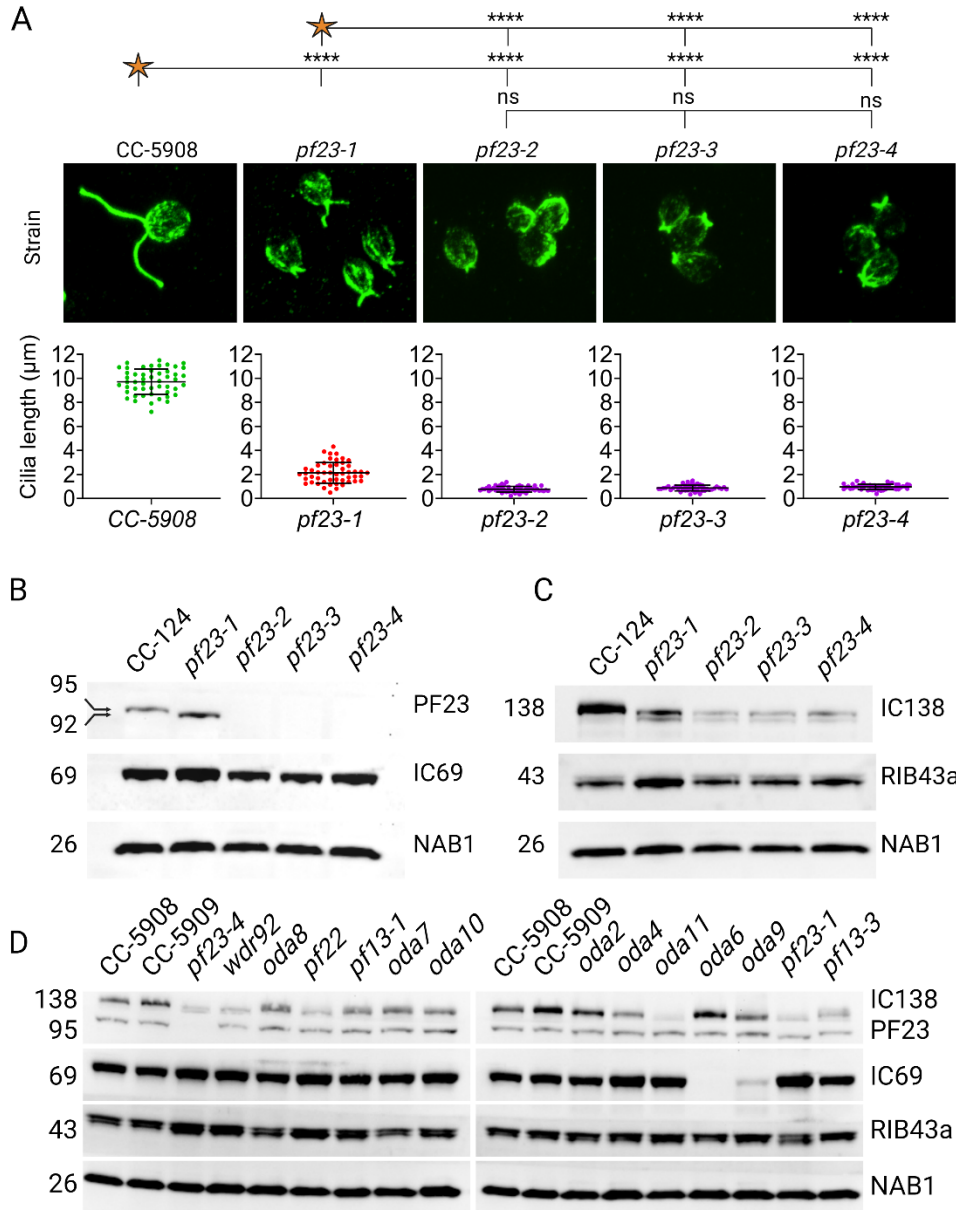


Figure 10: Characterization of null *pf23* alleles generated by CRISPR/Cas9 site-directed insertional mutagenesis. (A) Immunofluorescence staining of gametic cells using acetylated α -tubulin to visualize cilia length of wild-type, *pf23-1*, and the three *pf23* null strains. The quantification of length for each strain is positioned directly below its corresponding image. (B) Immunoblot probing whole cell extracts for PF23 and IC69 intermediate chain. (C) Each of the strains in B are probed with IC138 antibody and RIB43a antibody. NAB1 is used as a loading control. (D) Each mutant sample is probed with antibodies against IC138, PF23, IC69, and RIB43a. NAB1 is used as a loading control. Created with BioRender.com

Unexpectedly, the *pf23-1* strain, and *pf23-2*, *pf23-3*, and *pf23-4* all show reduced levels of the I1/f intermediate chain IC138 (Figure 10C). In addition, there are two bands in these strains compared to only one in wild-type, and they migrate slightly faster than the wild-type band. This altered abundance and pattern for IC138 is also observed in the *wdr92* mutant, but not other assembly factors *oda8*, *pf22*, *pf13-1*, *oda7*, and *pf13-3*. Abundance of a microtubule inner protein (MIP) RIB43a also appears unaffected in these strains (Figure 10D). This suggests that loss of *pf23* or *wdr92* function may specifically affect IC138 stability and influence post-translational modification.^{183–185}

2.3.6 A Null *pf23* Mutant Completely Lacks All ODAs and IDAs in the Cilia

We characterized the effects of the *pf23* null allele on dynein arm assembly using mass spectrometry of isolated axonemes (Table 3). However, the *pf23-4* cilia are extremely stubby and difficult to isolate. Mutations in *CNK11*, a NIMA-related kinase, partially suppresses the cilia length defects in *pf7* (*CCDC40*) and *pf8* (*CCDC39*) strains without rescue of the motility defects.¹⁸⁶ Another strain, *tpg1*, contains a mutation in the tubulin polyglutamylase gene *TLL9*. The *tpg1* mutation fails to rescue the cilia length defect in *pf7*, but partially rescues cilia length in the mutant *wdr92; tpg1-2* without restoring the dynein arm.¹⁸⁷ We made a *pf23-4; cnk11-3* double mutant strain. The proteomics data of *pf23-1* axonemes show almost complete loss of the IDA proteins, while ODA species are moderately reduced by approximately 50 to 60 percent.¹³⁶ Our analysis reveals that the *pf23-4* strain results in the complete absence of both ODAs and IDAs from the isolated axonemes (Table 2, red shading). Light chain DLC7b is also missing (red shading), and the other light chains are severely reduced (brown shading) (1% - 6%). Furthermore, ODA docking complex proteins are moderately reduced by approximately 60 percent (tan shading). Components

of other axonemal proteins including tubulin, MIA, radial spokes, N-DRC, and the central apparatus remain largely unaffected, or mildly reduced (green shading). Interestingly, there is a drastic loss of the I1/f tether component FAP44 (tan shading), but the tether-head protein FAP43 is retained.

Table 2: Mass spectrometry analysis of axonemes of wild-type strain WT 4-2P and *pf23-4; cnk11-3*.

Protein	Normalized <i>pf23-4; cnk11-3</i>	Protein	Normalized <i>pf23-4; cnk11-3</i>
Outer arms		ODA docking proteins	
ODA2	-	ODA1	0.435
ODA4	-	ODA3	0.435
ODA11	-	ODA14	0.233
ODA6	-		
ODA9	-	Tubulins	
Inner arms		Tubulin beta	1.1
PF9	-	Tubulin alpha	0.96
DHC10	-	Dynein arm associated	
BOP5	-	FAP44 (I1/f tether)	0.10
IC97	-	FAP244 (I1/f tether)	0.0027
LC7	-	FAP43 (I1/f tether)	1.37
FAP120	-	FAP73 (MIA2)	0.84
DHC2	0.002	FAP100 (MIA1)	0.61
DHC3	-	FAP57 (BOP2)	0.87
DHC4	-	FAP61 (RS2)	1.86
DHC5	0.0027	FAP91 (RS2)	1.25
DHC6	0.0027	FAP184 (RSS)	0.93
DHC7	-	FAP263 (RSS)	1.087
DHC8	0.0018	DRC4 (PF2)	0.71
DHC9	-	DRC1 (PF3)	0.61
DHC11	-	CCDC146 (MBO2)	1.13
IDA7	-	Other structures	
IDA4	-	Hydin	1.29
MOT24	-	CPC1	1.5
Light chains		PF16	0.91
DLC7b	-	PARCG	0.83
TCTEX1	0.018	FAP166	0.47
TCTEX2	0.032	RIB72	1.14
ODA12	0.064	RIB43a	0.76
ODA13	0.011		

Table 2: Mass spectrometry analysis of axonemes of wild-type strain WT 4-2P and *pf23-4; cnk11-3*. Table 3 shows the relative abundance of peptides from axonemes of *pf23-4; cnk11-3* strains, normalized to wild-type. Numbers were derived from conversion of Log2 values. A hyphen (-) or red shading indicates that the peptide was undetectable or extremely low. Proteins with brown shading were decreased to 6% or less, while proteins with tan shading were decreased detected at levels between 20-44%. - Indicates less than 1/1000. Not detectable.

2.3.7 Cilia Length Phenotypes Due to SSNC is Restricted to a Subset of Assembly Factors

To validate the phenotypes observed in the SSNC screen, we repeated the cilia regeneration assay. In this assay, the regeneration time was extended to 180 mins with cycloheximide to determine whether the phenotype is rescued with increasing time (Figure 11).

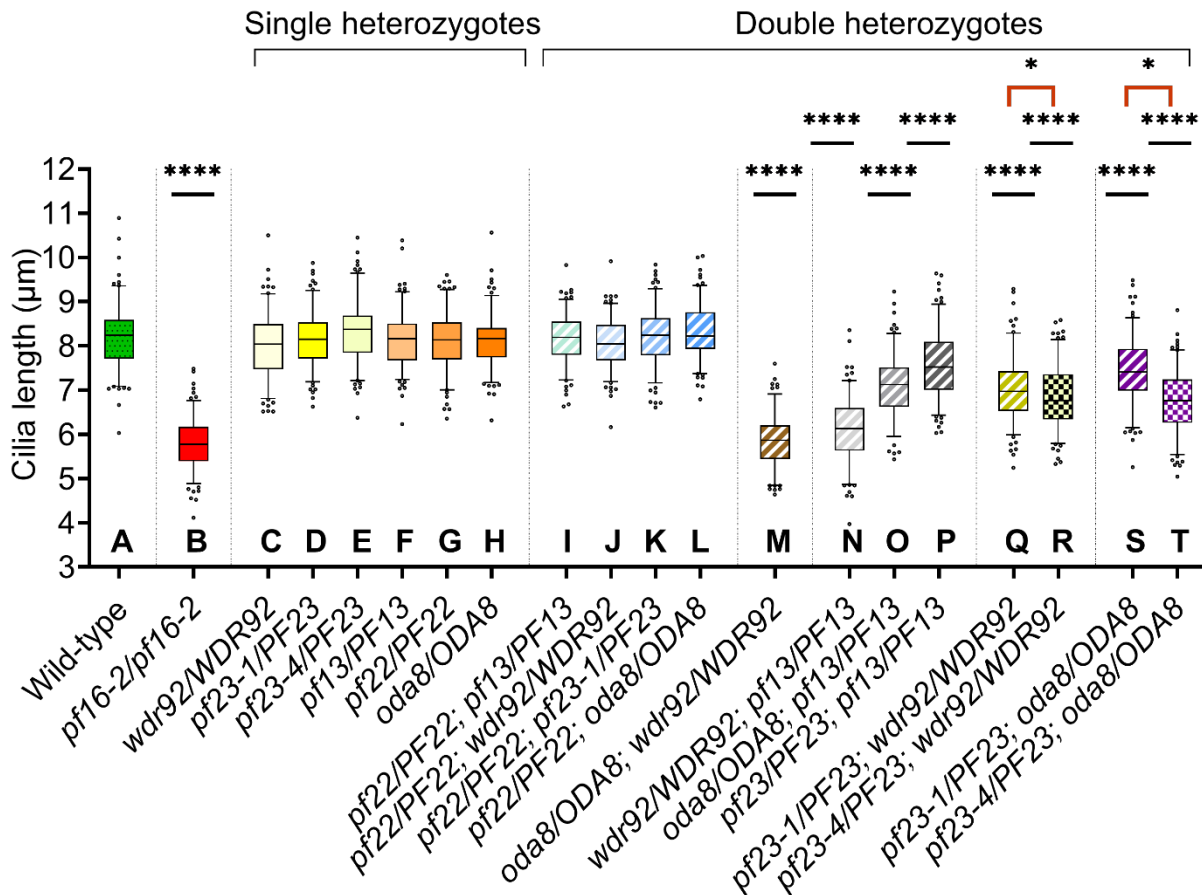


Figure 11: Cilia length of gametic diploids after 180 minute regeneration. Gametic diploids of the indicated genotypes were deciliated and allowed to regenerate for 180 minutes in 10 µg/ml cycloheximide. Three biological replicates of 50 cilia each were collected for each strain. Statistical analysis is a One-Way ANOVA. The cilia length of each strain is compared to the wild-type diploid. Solid green fill indicates wild-type and single heterozygotes are represented by various other solid fill colors. Striped fill indicates double heterozygotes while checkered fill indicates a double heterozygote generated using a null allele of *pf23* (*pf23-4*). Comparison done using a one-way ANOVA with corrections for multiple testing. Created using GraphPad Prism.

As expected, the wild-type strain regrew cilia to approximately 8 microns (Figure 11, column A), while the *pf16-2/pf16-2* diploid grew cilia 5.9 microns long (Figure 11, column B). The assembly factor single heterozygous diploids regrew wild-type length cilia, confirming that these mutations are recessive (Figure 11, columns C - H) . Additionally, diploids heterozygous for *pf22* mutations in combination with *oda8*, *pf13*, *pf23-1* or *wdr92* do not show a cilia phenotype (Figure 11, columns I - L). We tested 6 double heterozygotes with SSNC candidate assembly factor genes. Strain *oda8/ODA8; wdr92/WDR92* (Figure 11, column M) presented with the most severe phenotype; its regenerated length resembled that of the *pf16-2/pf16-2* homozygous diploid. Strains doubly heterozygous for *pf13* and *wdr92* (Figure 8, column N), *pf13* and *oda8* (Figure 11, column O), or *pf13* and *pf23* (Figure 11, column P) also showed varying degrees of regeneration defects, with the *pf13/PF13; wdr92/WDR92* strain being the shortest of these three. We also tested double heterozygotes *pf23-1/PF23; wdr92/WDR92* (Figure 8, column Q) and *pf23-1/PF23; oda8/ODA8* (Figure 8, column S) and observed length regeneration phenotypes. To test whether allele-specific effects would occur in double heterozygous strains with *pf23-1* hypomorphic or *pf23-4* null alleles, we generated diploids *pf23-4/PF23; wdr92/WDR92* and *pf23-4/PF23; oda8/ODA8* strains. As shown in Figure 11, columns R and T, respectively, the double heterozygotes with the *pf23-4* allele have a more severe regeneration defect than with the *pf23-1* allele (columns Q and S). These data suggest that the *pf23* alleles show allele-specific effects; the more severe phenotype of the null *pf23-4* allele likely reflects loss of assembly of ODAs and IDAs in this strain compared to *pf23-1*.

2.3.8 PF23 Protein Exhibits a Dosage-Dependent Reduction in Heterozygous Diploids

The most frequently occurring mechanism associated with SSNC is combined haploinsufficiency; both genes involved are heterozygous for null alleles. Previous examples suggest that double heterozygosity will cause further decreases in the proteins involved. To test

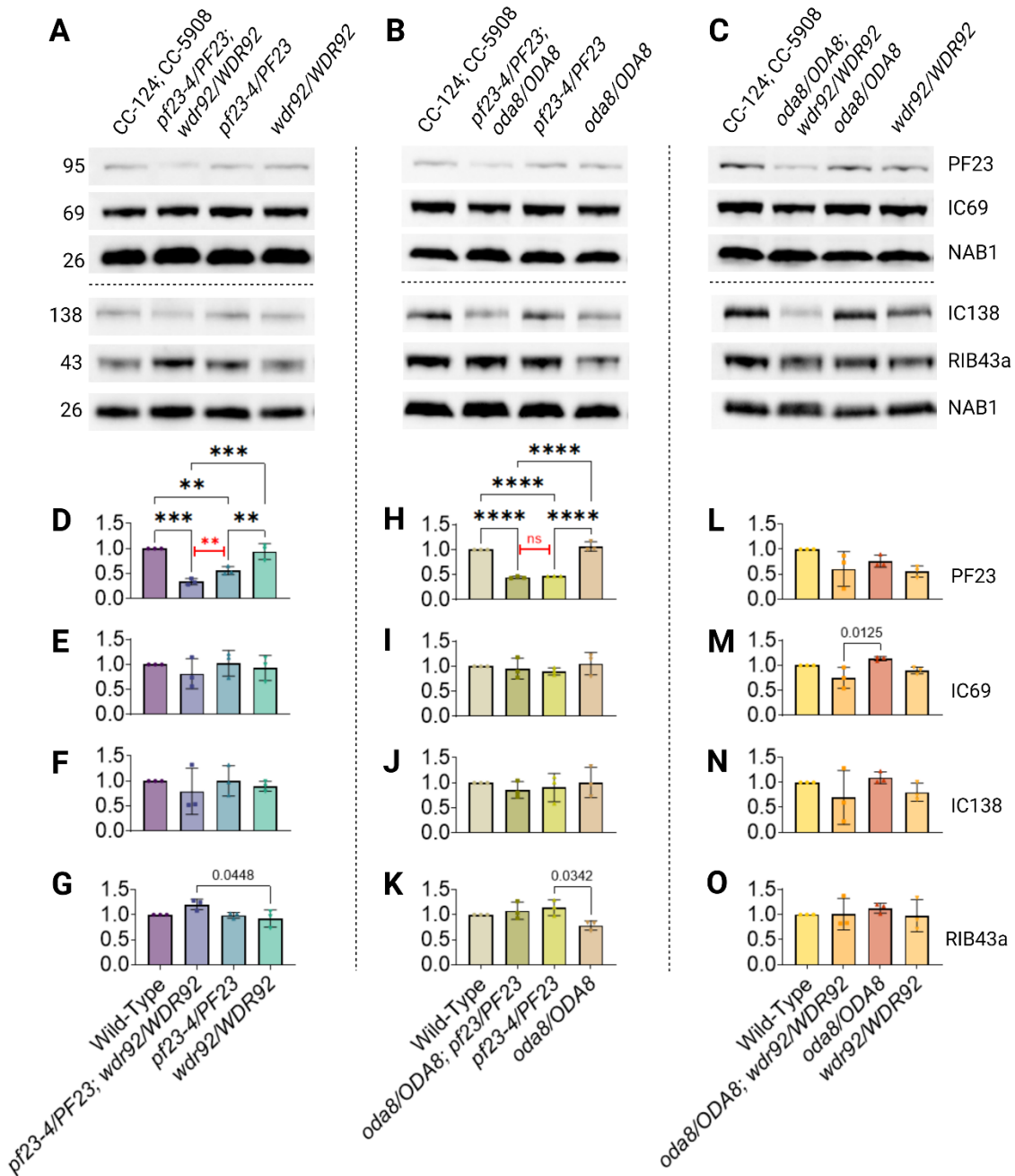


Figure 12: PF23 dynein arm assembly factor shows a dosage-dependent phenotype in heterozygous strains. (A) The *pf23/PF23; wdr92/WDR92* heterozygote extract is probed for PF23, IC69, IC138, and RIB43a and quantified (D-G). (B) and (C) Single and double heterozygotes are probed with the same antibodies as in A, and quantified in H-K, and L-O respectively. Created with BioRender.com and GraphPad Prism.

this mechanistic model, we examined the *pf23-4/PF23; wdr92/WDR92*, *pf23-4/PF23; oda8/ODA8*, and *oda8/ODA8; wdr92/WDR92* diploids. We performed immunoblot analysis on whole cell extracts of gametic steady-state diploids to ask whether PF23 protein abundance is altered in single or double heterozygous strains with mutant alleles *pf23-4*, *wdr92*, and *oda8*. As shown in Figure 12A, PF23 protein abundance is at wild-type levels in the *wdr92/WDR92* strain. Interestingly, in the *pf23-4/PF23* single heterozygote, PF23 abundance is reduced by half (55%), and is further reduced in the *pf23-4/PF23; wdr92/WDR92* double heterozygote (33%, Figure 12D). This difference in PF23 reduction is statistically significant between the two strains using a t-test analysis ($p = 0.0192$, Figure 12A, red significance bar). Analysis of the *pf23-4/PF23; oda8/ODA8* diploid shows a reduction in PF23 protein (47%), but this reduction is identical to the reduction in the *pf23/PF23* strain (47%, not significant by t-test, Figure 12B,H, red significance bars). There was no statistical difference in PF23 abundance between wild type and the *oda8/ODA8; wdr92/WDR92* diploid, and the *oda8;ODA8* and *wdr92/WDR92* single heterozygous diploids (Figure 12C). In addition, we probed these diploid samples with antibodies against ODA intermediate chain IC69, IDA 11/f intermediate chain IC138 and the MIP protein, RIB43a. These results show that PF23 protein shows a 50% reduction in the *pf23-4/PF23* strain that is solely due to the *pf23-4* allele. As mentioned earlier, the IC138 protein is reduced and altered in the *pf23* and *wdr92* mutant haploid strains. The data in Figure 12 suggests that half the normal complement of PF23 is sufficient for proper modification of IC138 (Figure 12F, 9J and 9N, see Figure 12B for comparison).

2.4 Discussion

2.4.1 *Chlamydomonas* Diploid Strains Have a Larger Ciliary Protein Pool

The investigation of SSNC requires a diploid genome. Because *Chlamydomonas reinhardtii* is haploid, we selected vegetative diploid cells using auxotrophic and drug resistance markers. Our analysis of haploid and diploid cells shows differences in their swimming behavior and morphology. The diploid cells are larger (Figure 5B,3F) and we propose that this is likely to contribute to a slower swimming velocity (Figure 5C) since the cilia must move a larger cell body with the same length cilia.

Having twice the genetic material of haploid cells is likely to lead to an increase in biosynthetic capacity.¹⁵³ In *Saccharomyces cerevisiae*, diploid cells are larger, and have twice the number of ribosomes compared to haploid cells.¹⁸⁸ Although this has not been measured in *Chlamydomonas*, it is likely that the same principle applies. In the absence of cycloheximide, diploid cells regenerate cilia at a slightly faster rate than haploid cells, even though they eventually reach the same terminal lengths (Figure 7B). In cycloheximide, diploid cells also regenerate cilia faster than haploids and these cilia are longer (Figure 7C). We suggest that the pool of ciliary proteins in diploid cells is larger than the pool in haploid cells; this would be consistent with more ribosomes and machinery available for protein biosynthesis. Genes needed for ciliogenesis are upregulated after deciliation^{189–191}. Inhibition of new protein synthesis shows that the size of the pool of proteins needed to regenerate cilia is important, and that both existing proteins and novel protein synthesis are required to regenerate full-length cilia. Our findings in diploid cells suggest the pool in diploid cells is larger yet the cells still regulate ciliary length. It is this limiting pool of proteins in the presence of cycloheximide that provides the sensitized background for our screen.

Cilia length is tightly regulated in *Chlamydomonas*.¹⁹² Differences in cell size of mutants in *Chlamydomonas* long flagellar mutants (*lf1-lf5*¹⁹³⁻¹⁹⁵) or short flagella (*shf1-shf3*^{196,197}) mutants, dynein assembly factors) have not been reported, with one exception. Loss of the NimA kinase, CNK2, results in a 40% increase in ciliary length and an increase in cell size.¹⁹⁸ Diploid cells remain able to regulate the ciliary length even when assembly is faster, and the pool is bigger.

2.4.2 Challenges With Modeling SSNC in *Chlamydomonas*

The aim of this work is to identify potential SSNC candidates in *Chlamydomonas* diploids using pre-existing mutant strains. We aim to use this knowledge to consider SSNC as a potential genetic mechanism in PCD patients without associated genes. As mentioned earlier, SSNC can occur via three different mechanisms (poison model, sequestration model, and combined haploinsufficiency). SSNC in its truest form is very rare, and the small number of candidate hits we obtained from our screen supports this finding from other organisms.⁸⁷ The poison model requires allele-specificity at both loci, the sequestration model requires allele-specificity at one locus, and in combined haploinsufficiency, both alleles are usually nulls⁸⁷. The genetic mechanism of the strains we selected are well-characterized. Apart from the *pf23-1*, *oda10*, *sup-pf1-1*, *pf14*, and *oda2* CLiP strains, all the mutations are null alleles. While some strains are characterized as null alleles through protein and cDNA analysis, others are predicted null based on whether the mutation occurs early in the protein (Table 1). Thus, our potential to detect different mechanisms of SSNC in motile cilia genes is restricted by the number of alleles we were able to test. The predominant model of SSNC is likely to be combined haploinsufficiency due to the large proportion of null alleles tested. Cells seem to be able to compensate for the potential loss of one-

half of the proteins tested and assemble cilia. It is possible that the cells can regulate the level of mRNAs needed to assemble full-length cilia for most of the genes tested.

2.4.3 The *pf23* Null Mutants Provide New Insights Into ODA and IDA Assembly in *Chlamydomonas*

Axonemal dynein arm assembly has been studied in many organisms. However, there are unanswered questions about the process of assembly and the interaction of DNAAFs with each other and dynein arms. Yeast two-hybrid and co-immunoprecipitation analyses of two DNAAFs, PF23 and WDR92, show that they interact indirectly in a protein complex with other assembly factors and chaperone proteins.¹³⁸ A complex identified on sucrose gradients with the PF23 protein requires wild-type WDR92 for stability. A small fraction of PF23 forms an oligomeric complex with the dynein heavy chains in wild-type cells but is absent in the *wdr92* mutant. A different complex of PF23 is formed only in the *wdr92* mutant.¹³⁷

The *Chlamydomonas* PF23 protein has three different domains: an N-terminus CS domain, a DYX domain in exon 5, and three TPR-repeat domains in the C-terminal region of the protein. The *Chlamydomonas pf23-1* strain possesses an in-frame deletion that removes all of exon 5 that includes the DYX domain, and portions of the flanking introns 4 and 5.¹⁹⁹ Prior mass spectrometry analysis of *pf23-1* reveals that the cilia of this strain lack all IDAs, with a moderate reduction in ODAs. Studies of *DYX1C1* (the ortholog of PF23) mutants in zebrafish using morpholino knockdown showed that ODAs and IDAs were completely lost in most cases, in some instances, there was only partial loss of ODAs^{199,200}. It is difficult to ascertain whether the loss of PF23 was complete in these treated zebrafish since the phenotype readout was based on the severity of embryo deformities and not on protein expression. *DYX1C1* variants/mutations in human patients

and mice, respectively showed loss of IDAs and ODAs. The variants observed in the human patients result in premature truncation of *DYX1C1*, but the effect of these variants on the protein was not assessed. It is likely that these mRNA products undergo NMD. Electron microscopy and immunofluorescence were used to assess the extent of dynein arm loss, but there is no quantification of ODAs and IDAs in the cilia. These findings differ from the mass spectrometry data from the *pf23-1* strain. Based on the differences in ODA and IDA loss between *pf23-1* and the *pf23-4* strain, we propose that the DYX domain (deleted in *pf23-1*) may be primarily responsible for IDA assembly, while the CS and TPR domains may be more involved with assembly of ODAs. Since ODAs are reduced around 50% in the *pf23-1* strain, our data also indicates that the DYX domain, CS domain, and TPR repeats may work cooperatively to properly assemble ODAs.

An intriguing finding is that the ODA docking complexes are also reduced. It is known that the ODA-DC assembles onto axonemes in the absence of dynein arms²⁰¹ but potentially, the dynein arm interaction may stabilize this binding. Our data also show that structural components that interact with dynein arms (MIA, radial spokes, NDRC, MBO2) do not require the dynein arms for docking. *Chlamydomonas* proteins FAP44 and FAP244 that interact with the I1/f IDA appear to be an exception; they are reduced by 90% in the *pf23-4* preparations. FAP43 is a paralog of FAP244 and is increased by 30%. This has been observed for the FAP57 and FBB7 paralogs. When FAP57 is missing, there is increased FBB7 protein in the axoneme.^{202,203} Importantly, our work overturns the longstanding notion that *DYX1C1/PF23* has a different function than in other organisms. It is not associated with just the assembly of IDAs but affects assembly of all ODAs and IDAs.

Many mutants that affect the assembly of both ODA and IDAs result in short cilia. This include both double mutants between an *oda* and *ida*^{136,179,204} mutants as well as the dynein assembly mutants. We do not know why the length of cilia when both ODAs and IDAs are missing is short, but these mutants again point out this finding. Despite the high conservation of motile cilia genes between humans and *Chlamydomonas*, there can be differences between the motile cilia phenotypes observed in humans and *Chlamydomonas*. One example is the striking short cilia phenotype in *Chlamydomonas* DNAAF mutants that is not as prominent in human mutant cilia.

2.4.4 Assembly Factors PF23 and WDR92 Have a Unique Role in IC138

Assembly or Modification

Immunoblots of *pf23-1* and *pf23-4* with an antibody against IDA I1/f intermediate chain shows that IC138 migrates faster in the *pf23* mutants than in wild-type. Previous studies showed that phosphorylation is important for IC138 regulation and function.^{184,196} IC138 is hyperphosphorylated in *mia* mutants that show altered swimming waveform, and the protein shows altered mobility.²⁰⁵ The presence of two lower bands suggests that PF23 may affect post-translational modification (PTM) of IC138. Previous studies examined ciliary IC138, and it is the only phosphorylated component of the I1/f IDA heavy chain complex.¹⁸³ This phosphorylation is performed by casein kinase 1 (CK1) that is anchored to the axoneme; it is required for activation of IC138.¹⁸⁵ The altered mobility and band pattern of IC138 in *pf23* mutants may be due to a change in phosphorylation of the protein.²⁰⁶ We observed that the altered bands are identical in the *pf23-1* and *pf23-4* strains (Figure 10C). This suggests that loss of the PF23 DYX domain is sufficient to disrupt IC138 assembly/modification. IC138 gel migration is also altered in the *wdr92* mutant in a similar pattern (Figure 10D). Previous studies show that the complex that contains

PF23 and WDR92 interacts with HSP90 co-chaperone proteins RUVBL1/2, which functions in the assembly of multi-protein complexes.¹³⁸ Perhaps loss of either PF23 or WDR92 could cause this complex to destabilize. This finding could provide a new role for PF23 and WDR92 in IC138 assembly, where IC138 is initially phosphorylated in the cytoplasm through the cooperative activities of PF23, WDR92 and an unknown kinase to prepare it for ciliary transport, followed by axonemal IC138 phosphorylation and activation by CK1.

2.4.5 SSNC Among Assembly Factors in *Chlamydomonas*

Based on our results, most of the genes encoding axonemal structural proteins do not seem to show SSNC. The high abundance of axonemal proteins may be sufficient to compensate for any perturbations that may arise from a loss of one of the two copies of two different structural genes. The exceptions are the strains *pf13-1/PF13; oda6/ODA6*, and *pf13-1/PF13; oda9/ODA9* heterozygous diploids that show SSNC. The ODA6 and ODA9 proteins (IC69 and IC78) depend on each other for stability.¹²⁸ ODA6 is completely missing in the *oda6* mutant, and severely reduced in the *oda9* strain (Figure 10D). Since stability of ODA6 and ODA9 are dependent on each other and influenced by loss of PF13, we suggest that SSNC may be the result of a combinatorial loss of protein.

Our screen identified assembly-factor specific SSNC candidates. Notably, we did not detect SSNC in any diploids heterozygous for the *pf22* mutation. PF22 interacts with PF13 and ODA7 and may act downstream of PF13 and ODA7.²⁰⁷ Other candidates in our SSNC screen, the *pf13-1/PF13; wdr92/WDR92* and *pf13-1/PF13; pf23-1/PF23* diploids, also warrant further analysis. The PF13 and PF23 proteins interact by co-immunoprecipitation, but no interaction was

identified between PF13 and WDR92.¹⁹⁹ PF13 is excluded from the R2TP-like complex that contains PF23 and WDR92.¹³⁸

2.4.6 PF23 Protein Demonstrates a Combined Haploinsufficiency SSNC Model

Immunoblots of diploids with single and double heterozygosity of *pf23*, *oda8* and *wdr92* provide potential insights into the mechanism behind SSNC in our screen. The level of PF23 protein is dosage sensitive. In *pf23-4/PF23* heterozygotes, PF23 is reduced by one-half. PF23 expression is not upregulated in response to the loss of one gene copy and does not operate in a self-regulating positive-feedback loop in steady-state diploid cells. These data also suggest that half the normal complement of protein product is sufficient for proper function; it is recessive. It also demonstrates that the *PF23* gene does not show a haplo-insufficiency (dominant) inheritance model. The *pf23/PF23; oda8/ODA8* diploid shows a reduction in the level of PF23 to approximately 50% (Figure 12B) but it is likely to be simply a consequence of heterozygosity of *PF23*. Thus, we do not know the mechanism responsible for SSNC with *PF23* and *ODA8*.

Unlike the example above, in the double heterozygote *pf23-4/PF23; wdr92/WDR92*, PF23 expression is further reduced to approximately 30% of wild-type levels (Figure 12A). First, PF23 is unaffected in the *wdr92/WDR92* single heterozygote. We were unable to obtain an antibody against WDR92 to assess whether WDR92 expression was reduced in the *wdr92/WDR92* heterozygote. In the future, we would like to examine the dosage of other assembly factors in heterozygotes, but we did not have antibodies to the other proteins. This was a common problem, and it reduced our ability to examine dosage of other assembly factors.

One hypothesis to explain our SSNC results is that reduction of both proteins below a critical threshold compromises the stability of PF23. One reason we may have failed to observe a

phenotype in steady state double heterozygous diploids is 50% of the PF23 protein is sufficient to provide assembled dyneins that are needed for ciliary maintenance. The transcription of PF23 is upregulated 6.4 fold after deciliation.¹⁹¹ When deciliation happens in the presence of cycloheximide, there may be insufficient protein to assemble dyneins. We suggest that the pool of PF23, like many other proteins, is insufficient for cilia regeneration without the upregulation of mRNA and new protein synthesis. The instability of PF23 and the lack of new synthesis forces the cell to attempt to rebuild the cilia with insufficient resources.

2.4.7 Second-site Non-Complementation as an Inheritance Model in PCD

Thus far, there have been no reports of SSNC (or DI) in human PCD patients. The body of work presented here reinforces the idea that PCD genes follow a predominantly recessive pattern. Because PCD is a rare disease, the likelihood of finding a patient with two heterozygous mutations is also rare. However, it should not be discounted since a handful of examples exist for other rare diseases discussed in the introduction. Of the patients who are missing a disease-associated gene for their PCD diagnosis, a small subset is heterozygous for mutations in one or more genes single gene.^{15,39,208,209} This implies that either the correct causative gene was missed during the analysis due to the presence of a complex variant, the patient bears mutations in a novel PCD gene, or the second hit is in a different gene than the one already identified. Although our steady-state double heterozygous diploids do not show obvious motility or cilia defects, the possibility of SSNC should be considered when looking at human PCD patients. One group of individuals worth considering are those with very mild PCD phenotypes. Their PCD phenotype may be due to the nature of the single gene mutations they carry; it may also be that there are heterozygous interactions between two different genes. However, in the case of PF23 and WDR92, our immunoblot data clearly show

that meaningful changes in protein levels are occurring in steady state, unperturbed diploids. These changes may be exacerbated under stress conditions and produce PCD phenotypes. The implications of this work are that individuals who are double heterozygotes for two motile cilia genes (particularly assembly factors) may encounter difficulties with recovering from assaults that damage their cilia. Taken together, we propose that a model of SSNC should be considered when examining new or existing PCD patients as part of their genetic diagnosis when a clear-cut answer is challenging.

2.5 Materials and Methods

2.5.1 Strains and Diploid Generation

A list of all the strains used in this study is found in Table 1. To generate diploid strains, single mutant haploid strains with *ac17* or *AC17*; *TG-aphviii* selectable genotypes were mated and then placed onto acetate-free plates supplemented with 10 μ g/ml paromomycin. Plates were incubated in constant light at 25°C for 3-5 days until diploids appeared. Each diploid colony was screened by PCR for heterozygosity at the mating-type locus before further analysis. Available PCR markers were used to genotype strains where appropriate. Primers are listed in Table S1. Strain CC-5485 with *aphviii* insertions was used to obtain strains CC-5908 and CC-5909.

2.5.2 Deciliation and Regeneration

For deciliation and regeneration assays, cells were streaked onto R (rich) medium plates for two days at 25°C.^{210,211} They were then placed into 1ml of R medium in a 1.5 ml Eppendorf tube and rocked under light for 3 hrs to allow cilia to assemble. The cells were placed on ice, spun at 10,000 x g for 30 sec and resuspended in 1 ml cold deciliation solution (10mM Tris pH 7.5, 150

mM D-mannitol and 1mM CaCl₂). pH shock was performed with 30μl 0.5N acetic acid followed by 30μl 0.5M sodium hydroxide and then checked for deciliation by phase microscopy with a 40x objective. Cells were then spun and resuspended in 500 μl R medium with or without 10μg/ml cycloheximide (Sigma Aldrich) and allowed to regenerate cilia for the times specified. A 40 min timepoint was selected because it allowed screening to be completed in a reasonable amount of time. Cells were fixed with a 1:10 dilution of 2% glutaraldehyde (Sigma Aldrich) in 0.2M phosphate buffer pH 7.5 (0.31g NaH₂PO₄ and 1.09g Na₂HPO₄ in 50 ml water). Cells were then allowed to adhere to glass slides coated with poly-L-Lysine solution (Sigma Aldrich). Excess cell volume was aspirated, and the slides were air dried before imaging.

2.5.3 Imaging and Cilia Length Measurement

For initial diploid screening of cycloheximide treated cells, fixed slides were imaged using phase contrast microscopy on a Zeiss AxioPhot with a 20x Neofluar objective lens and a NA of 2.0(Carl Zeiss AG, Oberkochen, Germany). Images were captured using a Phantom Miro eX2 camera and Phantom Camera Control Application 2.6 (Vision Research, Wayne, NJ) using 640 x 480 resolution. Cilia length was quantified using ImageJ. For immunofluorescence staining, protocol was followed according to Payne et.al.¹¹⁸. The primary antibody used was anti-acetylated α -tubulin mouse monoclonal clone 6-11B-1 (1:500 dilution, Sigma, T7451-200, lot #077M4751V). The secondary antibody was Alexa Fluor 488 donkey anti-mouse IgG (1:1,000 dilution, Invitrogen, A21202, lot #2266877). Images were false color stained using ImageJ.

2.5.4 Genome Editing

CRISPR genome editing protocol and associated reagents are described in detail in Payne et. al.¹¹⁸

2.5.5 Axoneme Isolation and Mass Spectrometry

Axonemes of wild-type strain WT 4-2P (generated from a cross between CC-124 and CC-125), strains *pf23-4; cnk11-3* (2-3, 3-1 and 5-1), and *cnk11-3* (1-7, 1-4, and 5-1) were prepared as sets of three biological replicates using the dibucaine method. Briefly, 10 plates of cells for each strain were grown for two days on TAP plates at 25°C, then resuspended in 100 ml of M-N/5 medium¹⁴⁹ with stirring for 3 hrs at 25°C. Cells were washed using 10mM HEPES pH 7.4, spun, resuspended in 25 mM dibucaine, then deciliated by pipetting up and down for 2 minutes. The dibucaine was inactivated by adding 0.5 mM EGTA. Cells were spun, the supernatant was collected, and then underlaid with 25% sucrose. Cilia were treated with 0.1% NP-40 to release the membrane and matrix fraction, and axonemes were collected by centrifugation at 30k x g for 30 min. 100 micrograms of protein was used per sample. Just prior to mass spectroscopy analysis, the cilia pellet was suspended in 150 µL of 100 mM HEPES, pH 8.0, mixed briefly, and probe sonicated for 5 pulses. The sample was then reduced with 10 mM Tris (2-carboxyethyl) phosphine hydrochloride (TCEP) and alkylated with 25 mM iodoacetamide prior to digestion with trypsin (1:20) at 37 °C overnight. The digested sample was acidified with 1% trifluoroacetic acid, then purified with Sep-Pak C18 SPE column (Waters, Milford, MA). The extracted peptides were dried down and were then submitted for Tandem Mass Tag (TMT) labeling.

Tandem Mass Tag (TMT) Labeling

Each sample was added with 50 μ L of 100 mM HEPES/20% anhydrous acetonitrile, pH 8.5 buffer. Samples were labeled according to the TMT 10-plex reagent kit (ThermoFisher, Waltham, MA) per the manufacturer's instructions (only 7 channels were used in this study). Labeled digests were combined into a 2 mL microfuge tube, acidified with formic acid, subjected to Sep-Pak C18 solid phase extraction, and dried down.

High pH Reverse Phase Fractionation

The dried peptide mixture was dissolved in 110 μ L of mobile phase A (10 mM ammonium formate, pH 9.0) and 100 μ L injected onto a 2.1 x 150 mm XSelect CSH C18 column (Waters) equilibrated with 3% mobile phase B (10 mM ammonium formate, 90% ACN). Peptides were separated using a gradient as previously described with the following parameters at a flow rate of 0.2 mL/min (8). Peptide fractions (total 96) were collected corresponding to 0.8 min each. Pooled samples were generated by concatenation in which every 12th fraction (i.e., 1, 13, 25, 37, 49, 61...; twelve fractions total) was combined. The pooled fractions were acidified, dried down and resuspended before injection.

LC-MS Analysis

Each fraction was reconstituted with 25 μ L of 0.1% trifluoroacetic acid. Samples (5 μ l volumes) were transferred to autosampler vials for LC-MS analysis on an Orbitrap Fusion Lumos (Thermo Fisher Scientific, San Jose, CA) mass spectrometer coupled with a U3000 RSLCnano HPLC (ThermoFisher Scientific). The peptide separation was carried out on a 75 μ m x 50 cm PepMap C18 column (ThermoFisher Scientific) at a flow rate of 0.3 μ l/min and the following gradient: Time = 0–4 min, 2% B isocratic; 4–8 min, 2–10% B; 8–83 min, 10–25% B; 83–97 min, 25–50% B; 97–105 min, 50–98%. Mobile phase consisted of A, 0.1% formic acid; mobile phase B, 0.1% formic acid in acetonitrile. The instrument was operated in the data-dependent acquisition

mode in which each MS1 scan was followed by Higher-energy collisional dissociation (HCD) of as many precursor ions in 3 second cycle (Top Speed method). The mass range for the MS1 done using Fourier Transform Mass Spectrometry (FTMS) was 375 to 1500 m/z with resolving power set to 120,000 at 400 m/z and the automatic gain control (AGC) target set to standard with a maximum fill time of 50 ms. The selected precursors were also fragmented in the FTMS using an isolation window of 0.7 m/z, a normalized AGC target of 200%, a maximum fill time of 105 ms, fixed HCD collision energy of 38%. Dynamic exclusion was performed with a repeat count of 1, exclusion duration of 30 s, and a minimum MS ion count for triggering MS/MS set to 25000 counts.

Proteomic Data Analysis.

MS/MS samples were analyzed using Proteome Discoverer 2.4 (ThermoFisher Scientific). The SEQUEST search engine in the Proteome Discover was set to search Mouse proteome database (Uniprot.org). The digestion enzyme was set as trypsin. The higher energy collisional dissociation (HCD) MS/MS spectra were searched with a fragment ion mass tolerance of 0.02 Da and a parent ion tolerance of 10 ppm. Oxidation of methionine and acetylation of N-terminal of protein were specified as a variable modification, while carbamidomethyl of cysteine and TMT labeling on lysine residues or peptide N-termini were specified as static modification. MS/MS based peptide and protein identifications and quantification results exported as excel sheets from Proteome Discover. Samples were further normalized and analyzed as previously described (9, 10).

2.5.6 Immunoblotting

Immunoblotting was performed using gametic whole cell extracts. One plate of cells per strain was grown on TAP medium for 2 days at 25°C, then placed at room temperature for 3 days to allow cells to become gametic. Each plate was then resuspended in 10 ml of M-N/5 and rocked in light at room temperature for 3 hours. Cells were then spun at 2,000 xg for 5 min, resuspended in 10 ml of autolysin²¹² for 1 hour. Next cells were spun at 2,000 xg for 5 min and resuspended in 600-750 µl of cell lysis buffer (20 mM Tris-HCl pH 7.5, 5 mM MgCl₂, 300 mM NaCl, 5 mM Dithiothreitol [DTT], 0.1% Triton-X100, ²¹³ with 20 µM PMSF and Protease Inhibitor Cocktail for plants (Sigma, p9599, lot #086K4075). The cell suspension was then pulled 10 times through a 22 ½ gauge needle and syringe to promote cell lysis. The lysate was spun at 21,000 xg for 30 min to remove cell bodies and debris. The supernatant was transferred to a fresh 1.5 ml Eppendorf tube and protein concentration was measured using Bradford (Bio-Rad Protein assay Dye reagent Concentrate (#5000006, lot 64227541). Samples were frozen at -80°. For protein electrophoresis, 5x sample buffer (3.78g Tris, 5g SDS, 25g sucrose, volume to 90 ml, pH to 6.8, volume to 100 ml, and add 0.04g bromophenol blue) with freshly added β-mercaptoethanol to a final concentration of 5% was added to the sample at 1X concentration and heated in a dry bath for 10 min at 70°C. 50 µg of each sample was loaded onto a 4-20% Novex Tris-Glycine gel (XP04205BOX, XP04202BOX) and run at 225 volts for 45 min. Following transfer onto Immobilon-P 0.45µm PVDF membranes (Millipore Sigma), each membrane was incubated with Invitrogen™ No-Stain™ Protein Labeling Reagent (A44717) according to manufacturer's instructions. Subsequent blotting steps followed standard procedures. For antibody probing, the membranes were cut horizontally at the appropriate size marker for the protein being examined. Each section of membrane was incubated with its respective primary and secondary antibody sequentially. Primary

antibodies used were rabbit anti-PF23 CT299¹³⁷(1:1000, a gift from Dr. Stephen King), rabbit anti IC138 (1:2000, a gift from Dr. Winfield Sale and Dr. Lea Alford), rabbit anti-RIB 43a (1:2000, a gift from Dr. Mary Porter), rabbit anti-NAB1 (1:10,000, Agrisera, catalog #AS08 333, lot #1311), and monoclonal mouse anti IC69 clone 1869A (1:10,000, Sigma, D-6168, lot #92H4862). Secondary antibodies used were goat anti-rabbit HRP (Sigma-Aldrich, A6154-1ML, SLCL2476) at 1:5000, 1:5000, 1:10,000, and 1:10,000 dilutions respectively. Goat anti-mouse HRP (catalog 82-8520, lot #WD321502) was used at 1:10,000 dilution. Membranes were visualized using the Invitrogen iBright 1500 Imager with the universal channel to detect total protein stain and chemiluminescence.

2.5.7 RNA and cDNA Isolation and Analysis

Cells for RNA isolation were collected from R plates grown in bright light for two days at 25°C. RNA was prepared using Trisol Reagent (Ambion, catalog 15596018, lot#265712) and quality was assessed using a 0.8% agarose gel. cDNA was generated using SuperScript IV VILO MasterMix (ThermoFisher)²⁰³.

2.5.8 Statistical Analysis

Statistical analyses were performed using GraphpadPrism 9 software. Comparisons were performed using a One-Way ANOVA with corrections for multiple testing unless otherwise indicated.

2.5.9 Whole Genome Sequencing and Analysis

Whole genome sequencing was performed according to a previous protocol.¹⁶⁴ In instances where SnpEff^{214,215} was unable to identify the causative mutation, the whole genome sequencing

data was manually analyzed using IGV and alignment to reference sequences CC-124 and CC-125.

2.6 Supplemental Tables

Table S1: PCR primers designed to genotype strains used in this work

Strain	Locus	Forward Primer	Reverse Primer	Bands (digest)
<i>oda1</i>	Cre16.g666150	TGCTTTAAACATCTG GCTTG	CTTGTGCAAACGGG TCAC	Mutant + wild-type (<i>SacI</i>)
<i>oda2 CLiP</i>	Cre11.g476050	CTGTACTGCATGACC TGGTC	TCTCCTCGTTCTTGG GGTAG	No band in mutant
<i>oda3-1</i>	Cre17.g703850	CAGAAGAAGCTGCG TGAG	AGTCCTGCTCCATCT TGA	Mutant + wild-type (<i>NruI</i>)
<i>oda4-1</i>	Cre09.g403800	AAGACTCTGGAGGA CAAGCT	AACCAGCATGGCAT TGCCAC	Detects wild-type
<i>sup-pf1-1</i>	Cre09.g403800	AGTGCCAGTTTGCT CTTG	GACTTGAGCTCCGA CAACTC	Mutant + wild-type (<i>DrdI</i>)
<i>oda5</i>	Cre01.g029750	CAGTGTGGGCGTTT GAAAA	ATCTACAACCCATCC CCACC	Mutant + wild-type (<i>BslI</i>)
<i>oda6-95</i>	Cre12.g506000	CAGTTTGGCCGCTTT CCA	GTAGTCAACATCCTT GGGCC	Mutant + wild-type (<i>HaeIII</i>)
<i>oda7-1</i>	Cre01.g029150	ACAAAATGGACTCT ACCGCA	ACTTCAGGTCCGCCA GT	No band in mutant
<i>oda8</i>	Cre01.g043650	CTGCAACTGGTCGTG AACT	CTGAGCGTCTGCAG ATGC	Detects wild-type
		TTATAATTTAAATATA ATAAACTACCTCGCC GCGTGCCACC	GTCACAGGCTCATC GTCAAG	Detects mutant
<i>oda9</i>	Cre12.g536550	GGCGATGAAGTCCA AAGC	CGTCGTCCCAGTACT TGAAG	Detects wild-type*
		AGTGGGAGATCTAC GACGAG	CCGCCTTCTTGCCGC A	Detects mutant*
<i>oda11-1</i>	Cre03.g145127	CGGACCTGCGCCCA ATAA	GCACGTCACCCTTCA GAAT	Detects mutant*
<i>oda12-2</i>	Cre12.g527750	GTCTCGATTTGTAC CATGG	CATACACCGTTACA GCCTTG	No band in mutant
<i>oda14-f28</i>	Cre14.g617550	GGTGGAGGACATGA TTTGGG	CTCCTCCAGTGTGAT GAAGC	No band in mutant
<i>pf14</i>	Cre06.g291700	TACAACACTAGTGCTCG CCTGA	GCGTATGTGTTGCCT CGTAC	Mutant + wild-type (<i>MseI</i>)
<i>pf22-1</i>	Cre01.g001657	CCCCATGCTCCCCTT GACTACA	GCCCTCGGGGCTGTC ATCC	Detects wild-type*
		GCCTGCCGGCTGTAC GTATGA	CACCCCGCCGTCCA GCAG	Detects mutant*
<i>pf23-1</i>	Cre11.g467560	CATTGGGTACTGGG ATGATGGAAC	TGCAGCCGATGACT CCTTATAAGTTT	Detects mutant
		ACACACACACATGC GCAAT	TCCGTAAGTAACTCC GTCGC	Detects wild-type

Strain	Locus	Forward Primer	Reverse Primer	Bands (digest)
<i>wdr92-2</i>	Cre16.g672600	ATGCTGCAAGGTGG TGTTG	CACACACCAGCAGT CCCT	Detects wild-type
		ATGCTGCAAGGTGG TGTTG	GCACCAATCATGTC AAGCCT	Detects mutant
<i>ida3</i>	Cre03.g205000	ACTTGCTTTCTCAG GCACT	CATGAGACTCCTTCC GTGT	Mutant + wild-type (<i>SfcI</i>)
<i>CC-124</i>	Mating-type minus	GCATGGCCTCTTAAT CAGAC	TTTGGAGTCCTCTCG TCAAG	**
<i>CC-125</i>	Mating-type plus	TCTCCATGGGGTGTA TCATC	TTTGGAGTCCTCTCG TCAAG	***
<i>pf23-2</i>	Cre11.g467560	TGTAAATGGAGGCG CTCGTTG	GATCGCCAAGCCCT GTTGC	Detects reverse insertion
<i>pf23-3</i>	Cre11.g467560	TGTAAATGGAGGCG CTCGTTG	GATCGCCAAGCCCT GTTGC	Detects reverse insertion
<i>pf23-4</i>	Cre11.g467560	TGTAAATGGAGGCG CTCGTTG	GTCCAGCGCGAACA GATAGG	Detects forward insertion
<i>PF23 exon 1</i>	Cre11.g467560	GATCGCCAAGCCCT GTTGC	GTCCAGCGCGAACA GATAGG	Detects wild-type
<i>ATG17</i>	Cre16.g651350	AAGAAGGAACACGC CAAAAC	GTAGGATCGGTTGCT GACG	Band in wild-type
<i>PHD2/AC17</i>	Cre03.g194200	AGGCCCAGAAGA AGGAGATT	AGCCGGTCCAAGA TAACTA	Mutant + wild-type (<i>HaeIII</i>)
<i>CC-5908/ CC-5909</i>		AAGAAGGAACACGC CAAAAC	GTATCGGAGGAAAA GCTGGC	<i>atg17; aphviii junction</i>

Where indicated, the PCR product is digested with a restriction enzyme to distinguish between wild-type and mutant genotypes. Primers separated by a dashed line are used to genotype wild-type and mutant alleles of the same gene separately. 'No band in mutant' indicates the presence of an insertion that is too large to amplify during the extension time needed to amplify the PCR products of the same primer in wild-type. *Designed using the method for allele-specific primers (ASP)²¹⁶ ** The mating-type primers can be run simultaneously to generate two bands that distinguish between both mating-types.

Chapter 3: A Gap-Free Genome Assembly of *Chlamydomonas reinhardtii* and Detection of Translocations Induced by CRISPR-Mediated Mutagenesis

Zachary L. Payne, Gervette M. Penny, Tychele N. Turner, and Susan K. Dutcher*

From:

A gap-free genome assembly of *Chlamydomonas reinhardtii* and detection of translocations induced by CRISPR-mediated mutagenesis

Payne, Z. L., Penny, G. M., Turner, T. N., & Dutcher, S. K. (2023). A gap-free genome assembly of *Chlamydomonas reinhardtii* and detection of translocations induced by CRISPR-mediated mutagenesis. *Plant Communications*, 4(2), 100493. <https://doi.org/10.1016/J.XPLC.2022.100493>

This article was published as a Gold Open Access article in which copyright is retained by The Authors and the article is available for reuse under a Creative Commons Attribution CC BY 4.0 license.

My contribution to this work was the generation, screening, and characterization of CRISPR transformants in the *PF23* gene. This is represented in Figure 6. A more comprehensive characterization of these strains is discussed in Chapter 2.

3.1 Abstract

Genomic assemblies of the unicellular green alga, *Chlamydomonas reinhardtii* provided important resources for researchers. However, assembly errors, large gaps, and unplaced scaffolds as well as strain-specific variants currently impede many types of analyses. By combining PacBio HiFi and Oxford Nanopore long-read technologies, we generated a *de novo* genome assembly for strain CC-5816, derived from crosses of strains CC-125 and CC-124. Multiple methods of

evaluating genome completeness and base-pair error rate suggest the final telomere-to-telomere assembly is highly accurate. The CC-5816 assembly enabled previously difficult analyses that include characterization of the 17 centromeres, rDNA arrays on 3 chromosomes, and 56 insertions of organellar DNA into the nuclear genome. Using Nanopore sequencing, we identified sites of cytosine (CpG) methylation, which are enriched at centromeres. We analyzed CRISPR/Cas9 insertional mutants in the *PF23* gene. Two of the three alleles produced progeny that displayed patterns of meiotic inviability that suggested the presence of a chromosomal aberration. Mapping Nanopore reads from *pf23-2* and *pf23-3* onto the CC-5816 genome showed that these two strains each carry a translocation that was initiated at the *PF23* gene locus on Chromosome 11 and joined with Chromosomes 5 or 3, respectively. The translocations were verified by demonstrating linkage between loci on the two translocated chromosomes in meiotic progeny. The three *pf23* alleles display the expected short cilia phenotype and *pf23-2* lacks the PF23 protein by immunoblotting. Our CC-5816 genome assembly will undoubtedly provide an important tool for the *Chlamydomonas* research community.

3.2 Introduction

The haploid nuclear genome of the unicellular green alga, *Chlamydomonas reinhardtii*, resides in 17 chromosomes with a total base pair length of approximately 120 megabases (Mb).²¹⁷ *Chlamydomonas* has been a valuable model organism for the study of conserved functions of cilia,²¹⁸ photosynthesis,²¹⁹ the production of biofuels,²²⁰ and sexual reproduction.²²¹ The *Chlamydomonas* research community is currently equipped with a wide range of tools and techniques at their disposal to facilitate the study and manipulation of this organism,²²² including a mutant library derived from insertional mutagenesis,¹²¹ molecular toolkits for cloning and

synthetic biology,^{213,223} targeted gene editing strategies,^{224,225} and an annotated reference genome.^{114,217}

The U.S. Department of Energy (DOE) Joint Genome Institute (JGI) genomic assembly of *Chlamydomonas reinhardtii* has provided an important resource for *Chlamydomonas* researchers.^{114,217} Despite over a decade of improvements to the assembly, including the use of BACs and fosmids to anchor unplaced sequences, the current version (https://phytozome-next.jgi.doe.gov/info/Creinhardtii_v5_6 (v5.6)) is contained in 53 scaffolds assembled from >1,500 contigs. Nearly 2 Mb of sequence remains unplaced. Multiple regions in the assembly are not representative of wild-type strains CC-124 and CC-125 due to either mis-assemblies or chromosomal rearrangements specific to strain CC-503 that was used for sequencing. These shortcomings contributed to our decision to use sequencing platforms that produce reads >10 kilobases (kb) in length. Concurrently, a PacBio version of the genome of CC-4532 is available on BioRxiv,¹¹⁵ and at Phytozome (https://phytozome-next.jgi.doe.gov/info/CreinhardtiiCC_4532_v6_1). It is contained in 60 scaffolds.

Genomes assembled from short read technologies, though highly accurate (>99.9%), are often unable to resolve tandemly or segmentally duplicated sequences, low complexity regions, and other repetitive sequences within genomes when these sequences are longer than the reads themselves.^{226,227} Thus, assemblies obtained from only short reads tend to contain gaps, and short or unplaced contigs. Long-read, single-molecule sequencing technologies from Pacific Bioscience (PacBio) and Oxford Nanopore Technologies (ONT) have revolutionized many aspects of genomics that include improvements to reference genome assembly projects,^{228–230} structural variant analyses,^{231–234} and comparative genomics.^{235,236} The balance of accuracy and read length that has been achieved by HiFi Circular Consensus Sequencing (CCS) from PacBio and Nanopore

sequencing from ONT improves the ability of assembly programs to reconstruct sequence data obtained from these technologies. Read lengths with HiFi range from 10-20 kb and reach hundreds of Kbs or even Mbs with ONT and depend on the quality of isolated DNA and the library preparation method.^{237,238} These reads can span many difficult-to-assemble regions and provide insights into previously unassembled portions of genomes from many organisms. Each of these sequencing technologies has its strengths and limitations. For example, Nanopore reads can reach unprecedented read lengths. However, the base-level quality is only ~95% accurate. On the other hand, while HiFi reads are ~99% accurate, they are shorter in length than Nanopore reads.²³⁸ Recently, highly contiguous or even telomere-to-telomere genome assemblies have been generated for human as well as a variety of crops and model organisms by combining long-read technologies, including the telomere-to-telomere assembly of the human genome,^{229,239,240} watermelon,²⁴¹ rye,²⁴² rice,²⁴³ *Arabidopsis thaliana*,²⁴⁴ and multiple drosophilid species.²³⁶ These assemblies utilized complementary features of more than one technology to assemble highly contiguous and even telomere-to-telomere chromosomes in some cases. Multiple variations of hybrid strategies have been successful. One attractive strategy employed for the assembly of human chromosome 8 combines the use of HiFi and Nanopore long-read technologies.²²⁹ A large fraction of the assembly is composed of contigs derived from HiFi reads. The remaining gaps are composed of sequences derived from Nanopore reads. These were merged to produce a highly accurate and contiguous assembly.²³⁸ The success of hybrid approaches has spurred the development of a plethora of publicly available bioinformatic tools aiming to maximize the strengths of each sequencing technology. Various strategies have been streamlined for labs to include in the assembly workflow.²⁴⁵⁻²⁴⁷ As a result, there is an influx of new assemblies for unsequenced organisms as well as improvements to existing assemblies.

We used a combination of high-coverage HiFi and Nanopore data coupled with multiple assembly strategies to develop a reference-quality *Chlamydomonas reinhardtii* genome assembly *de novo* using strain CC-5816, derived from a meiotic cross between wild-type strains CC-124 and CC-125 that was subsequently backcrossed to CC-124 three times. The final assembly consists of 17 scaffolds that correspond to each of the chromosomes and contains no gaps. We have assessed several regions; these include repetitive regions on chromosomes 11 and 15 that are not present in current *Chlamydomonas* assemblies, highly methylated centromeric regions, and insertions of organellar DNA from both the mitochondria (NUMTs) and chloroplast (NUPTs) present throughout the genome.

Analysis of structural rearrangements, especially when proximal to repetitive or duplicated sequence, remains difficult with fragmented assemblies. We have taken advantage of this genome assembly as a reference to examine CRISPR/Cas9 generated strains. Meiotic analysis suggests that the genome editing generated large chromosomal aberrations in two of three CRISPR/Cas9 mediated strains from our group and three of six obtained from other groups. We used Nanopore sequencing in the strains generated in our lab to identify the lesions as a translocation between chromosomes 5 and 11 in one strain and between chromosomes 3 and 11 in the other.

3.3 Results

3.3.1 Assembly of the CC-5816 Genome Using PacBio HiFi and Nanopore Reads

We sought to establish a new *Chlamydomonas* reference genome given the shortcomings of the current CC-503 v5 assembly (Supplemental Figure S1). The unusually high GC nucleotide

content of *Chlamydomonas* (64%) presents a considerable challenge for many sequencing platforms, particularly amplification-based methods.²⁴⁸ The presence of a cell wall creates another challenge with respect to isolating DNA of sufficient quality, quantity, and length required for long-read sequencing. The strain used for the initial genome project, CC-503, was isolated following mutagenesis with the goal of producing mutants that reduce cell wall integrity,²⁴⁹ which helped to increase DNA isolation yield.¹¹⁴ However, it is now clear that this method has produced undesired structural changes in the genome.¹¹⁵ We reasoned that single-molecule-based methods for sequencing would circumvent issues of nucleotide bias in the final dataset. In addition, we optimized an existing HMW DNA isolation protocol utilizing the QIAGEN MagAttract HMW DNA Isolation Kit to improve the size and yield of DNA fragments necessary for long-read sequencing technologies without the use of a cell-wall mutant (Supplemental Figure S2).

We sequenced *Chlamydomonas reinhardtii* wild-type strain CC-5816 on one PacBio HiFi SMRT cell and obtained ~18 Gb of CCS reads at approximately 150x coverage of the estimated 120 Mb nuclear genome (Supplemental Figure S3). We used both Hifiasm²⁵⁰ and Canu^{246,251} assemblers for *de novo* assembly at various coverages (Supplemental Figure S4A). We utilized a Nanopore assembly of strain CC-1690 (also referred to as 21gr) for validation of our assemblies²⁵² (Supplemental Figure S4B). CC-1690 shares a close lineage with CC-5816. It was derived from the meiotic products of a single zygote isolated in 1945 by G. M. Smith in Massachusetts.^{32,253} Whole-genome alignment revealed CC-5816 is highly syntenic with CC-1690. A Hifiasm assembly using the entire dataset produced the most contiguous assembly and contained no obvious mis-assemblies when compared to CC-1690 (Supplemental Figure S4; Supplemental Table S1). We obtained a raw genome assembly of 395 contigs that covered 99.34% of the CC-

1690 nuclear sequence by whole-genome alignment (Figure 1A). Nine of the largest contigs make up 50% of the assembly. They range in length from 5,298,489 to 9,193,794 base pairs (bp). By

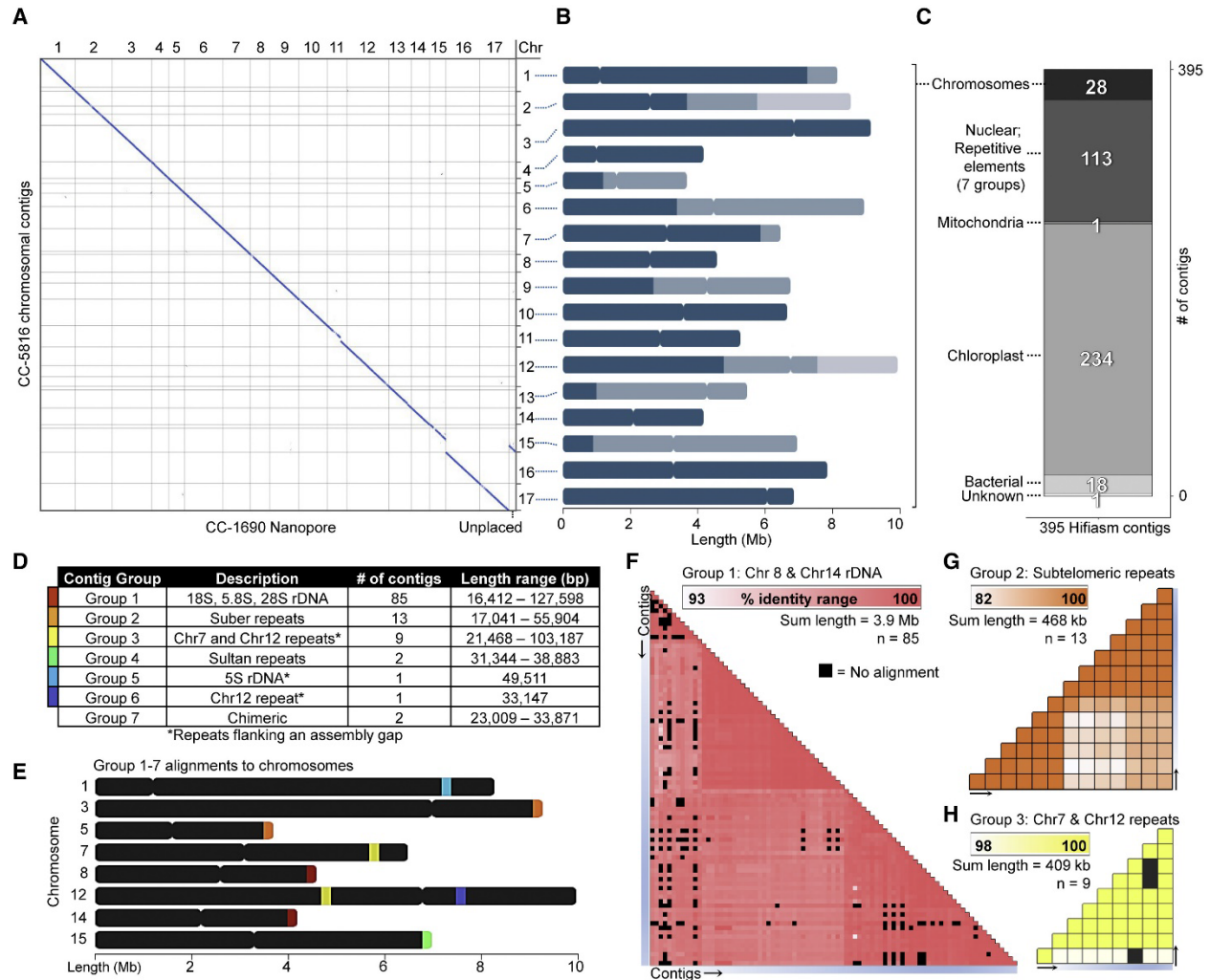


Figure 1. Hifiasm assembly generates highly contiguous assembly using PacBio HiFi data. (A) Dot plot of the 28 largest contigs from CC-5816 that align completely and uniquely to the CC-1690 genome assembly. An unplaced scaffold in the CC-1690 genome assembly was assembled onto chromosome 15 in CC-5816. All alignments were reoriented to the same direction to aid in visualization. (B) Ideogram plots of the 28 largest contigs scaffolded into 17 chromosomes. Contigs were scaffolded based on synteny to CC-1690. Contigs are represented as solid colors on each chromosome ranging from dark to light blue. The borders between colors correspond to an assembly gap between contigs. (C) Bar chart categorizing the possible origin of all contigs based on alignments to CC-1690, chloroplast and mitochondrial sequences, and potential contaminants. (D) Each of the 113 nuclear, repetitive contigs were grouped based on the type of repetitive sequence found on each. The two contigs from Group 7 had poor read coverage and may derive from low abundant chimeric reads or transposition events. (E) Ideogram plots illustrating approximate locations within the nuclear genome where repetitive contigs from groups 1-6 align. (F - H) Percent identity heatmaps among the 3 most abundant repetitive contigs filtered from the final assembly are shown. (F) rDNA arrays map to one end of both chromosomes 8 and 14, (G) Suber repeats appear proximal to telomeric sequence, and (H) a repetitive element flanking assembly gaps on chromosomes 7 and 12.

comparison, the CC-503 v5.6 genome assembly at the contig level contains 1,547 contigs, with the 141 longest contigs ranging in length between 215,409 to 1,410,767 bp making up 50% of the assembly. The 28 longest Hifiasm contigs contained 99.28% of the alignments covering CC-1690 nuclear base sequences (Figure 1B) and align to the 17 chromosomes.

We identified 235 contigs containing predominantly organellar sequence and compared them to consensus genomes previously assembled from mitochondria and chloroplast derived from *Chlamydomonas*.¹¹⁶ A single mitochondrial (MT) contig in the Hifiasm draft assembly was 30,743 bp, twice the length of the consensus ~15.8 kb linear mitochondrial genome.¹¹⁶ We determined that to be a mis-assembly from HiFiasm, as we did not observe this mis-assembly in the MT contig generated with Canu. We confirmed this mis-assembly by inspecting read coverage across the junction connecting the duplicate MT genomes and observed a lack of reads connecting the two terminal inverted repeats. Alignment of this contig to the consensus MT genome did not reveal any sequence variation. The chloroplast (CP) was represented by 234 contigs ranging in size from ~21.7 to 93.4 kb. No single contig represents the entire ~205 kb chloroplast genome, likely due to the abundance of repetitive sequence.¹¹⁶ 100% of bases from the CP consensus genome aligned to this set of CP contigs and 99.93% of bases from the contigs produced an alignment. These results confirm the accuracy of the *Chlamydomonas* MT and CP genomes from Gallaher et al.,¹¹⁶ and suggest few differences among strains. Eighteen contigs ranging in length from 26,083 to 71,538 bp originate from *Chryseobacterium*; these may be contaminants. There is one short 1533 bp contig of unknown origin (Figure 1C).

The remaining 113 contigs collectively contain 4,985,725 bp. Each of these contigs show >99% alignment coverage from the 28 chromosomal contigs using BLAST and 89.53% alignment

using NUCmer. These 113 contigs are extremely short; the largest is 127,598 bp (Figure 1D). Multiple sequence alignment of these contigs reveal that 109 of the contigs fall into four groups based on high sequence identity to each other, while the 4 remaining contigs were dissimilar to each other and to the other 109 contigs (Figure 1D). Inspection of repeat content using Tandem Repeats Finder²⁵⁴ and RepeatMasker²⁵⁵ revealed that this set of 113 contigs contain ~66% repetitive sequence (compared to ~22% genome-wide). We used BLAST and NUCmer alignments to determine the genomic origins of these contigs and found that, consistent with the multiple sequence alignment, they fall into seven groups (Figure 1E). They are identified as (1) 18S, 5.8S, 28S rDNA arrays (Figure 1F), (2) subtelomeric Suber repeats (Figure 1G), (3) repeats flanking two assembly gaps on chromosomes 7 and 12 (Figure 1H), (4) subtelomeric Sultan repeats,²⁵⁶ (5) 5S arrays spanning the assembly gap on chromosome 1, (6) repeats flanking a second assembly gap on chromosome 12, and (7) chimeric mis-assemblies or transposition events. We refer to these as Groups 1-7, respectively. Group 7 contigs contained transposable elements (TEs) embedded between short nonadjacent nuclear sequences. Only three and five reads mapped to these contigs and were not considered further. The initial draft assembly, consisting of the 28 chromosomal contigs, was evaluated for completeness using BUSCO²⁵⁷ and Augustus²⁵⁸ to identify highly conserved universal single-copy Chlorophyta orthologs (referred to as BUSCOs). We identified 1516 of the 1519 (99.7%) BUSCOs. Addition of the filtered contigs in this evaluation did not recover any additional BUSCOs. Per-base quality score (QV) was evaluated by comparison of k-mers between the 28 contigs and read set using Merquy.²⁵⁹ This produced a genome-wide QV score of 60.07, or one incorrect base every 1,015,521 bp. These results confirm that a full genomic representation of all unique CC-5816 sequence was indeed present within the 28 largest contigs in

the assembly. After scaffolding, only 11 gaps remained between adjacent contigs, which correspond to the 17 chromosomes of *Chlamydomonas reinhardtii* (Figure 1B).

To fill in the remaining 11 gaps in the assembly, we sequenced CC-5816 using Nanopore technology. Six flongle flow cells were used to optimize our protocol prior to sequencing on an R9 flow cell. In total, we obtained roughly 6.5 Gb of sequence, or approximately 50x coverage, with a read N50 of 39,357 bp and a max read size of 338,467 bp (Supplemental Figure S3). We assessed the results of various gap filling strategies utilizing the Nanopore reads. We assembled the basecalled reads using three different assemblers: Canu,²⁴⁶ Flye,²⁶⁰ and Necat.²⁶¹ Eighteen combinations of hybrid Nanopore assemblies were generated using QuickMerge.^{245,262} QuickMerge uses sequence from a donor assembly to fill gaps in an acceptor assembly. Using QuickMerge, the HiFi assembly was gapfilled with either one of the hybrids ONT assemblies, or iteratively using the Canu, Flye, and Necat assemblies in various combinations to create a total of 20 HiFi-Nanopore hybrid assemblies. We also tested a more conservative gapfilling strategy using TGS-GapCloser.²⁴⁷ This method uses sequence from individual reads that align to the ends of two adjacent contigs to fill gaps. Two assemblies were generated using TGS-GapCloser; the first contained HiFi and Nanopore reads while the second used only Nanopore reads. Finally, to ensure accurate sequence consensus and removal of potential artifacts generated from these gapfilling pipelines, RaCon was used for polishing by using aligned HiFi and Nanopore reads in different combinations. All assemblies were carefully assessed at each step for completeness and accuracy by noting the number of gaps filled, checking for recovery or loss of BUSCOs, concordance of k-mers between reads and assembly for QV scores, and improvements in coverage of HiFi and Nanopore reads. Assemblies generated with significantly reduced metrics in any of the previously listed categories were not considered further. Only assemblies with zero gaps were considered as

candidate assemblies for final curation. In total, 43 gapless assemblies were considered for final curation (Supplemental Table S2). An assembly using TGS-GapCloser to fill gaps using first HiFi, then Nanopore reads, and no RaCon polishing (assembly titled v0.2 in Supplementary Table S2) had the highest BUSCO (99.74%; 1515/1519) and QV (57.73) scores among the gapless assemblies (Supplemental Table S3). Low coverage regions (less than 5x coverage) 5 bp and longer were manually inspected and corrected by comparing read coverage across the corresponding region in other high-ranking assemblies, inspecting the raw reads for discrepancies in alignment to the assembly, and aligning available reads to each other to help determine the local consensus (Supplemental Table S4). Reads were then realigned, and the edited regions evaluated to determine whether improvements were made to the region. Many of the changes were obvious and fixed by simply deletion or insertion of nucleotides based on the consensus of the raw reads. Alternate assemblies that had better read coverage across specific regions were used to replace sequence. We were unable to improve read coverage in four regions located on chromosomes 1, 2, 4, and 5 and were unchanged, but are noted in Supplemental Table S4. Small errors such as single base substitutions and local expansions or collapse errors were fixed by running Inspector²⁶³ (Supplemental Table S2), which detects sudden changes in read coverage to identify and correct small-scale errors. Metrics previously mentioned to determine completeness and accuracy were again checked before accepting any changes. The final telomere-to-telomere assembly size is 113,900,589 bp. One-half of the whole assembly is contained in 8 contigs that are each longer than 6,857,676 bp. BUSCO produced an initial score of 1515/1519 using Augustus.²⁵⁸ Three of the missing BUSCOs were located running BUSCO with metaeuk.²⁶⁴ and the last was recovered by comparing the expected amino acid sequence with aligned gene models. Merquy produced a QV score of 59.38 or a per-base error rate of 1.15×10^{-6} . All bases in the assembly are supported by

either HiFi or Nanopore reads except for 4 bp at the left telomere of Chr10 and 1 bp at the right telomere of Chr12. At least 99.997% of bases are covered by more than five reads from either HiFi or Nanopore (Supplemental Table S5).

3.3.2 CC-5816 Haplotypes, Repeat Content, Cytosine Methylation, and Gene Content

We characterized general genomic features of CC-5816. Using Illumina whole genome sequencing (WGS) paired-end reads from CC-5816 parental strains CC-124 and CC-125, we created a haplotype map for each chromosome by comparing haplotype specific k-mers (hapmers) between the read sets and genome assembly. We used the distribution of these hapmers to assign phase blocks and show that 74% of the haplotype derives from CC-124, while only 17% originates from CC-125 (Figure 2A). The nucleotide content of the assembly remains unchanged from previous estimates; it contains 64% G and C bases. The genome-wide repeat content determined by either RepeatMasker or Tandem Repeats Finder varied greatly, likely due to their methods of detection (Supplemental Table S6). RepeatMasker uses an established database that includes annotated TEs and repeat sequences to compare against the query sequence. It estimated a repeat content of 18.88%. Tandem Repeats Finder, which uses a non-biased approach to detect stretches of tandemly repeating sequence, estimated a repeat content of 7.72%. The union of these two programs together masked 22.37% of bases as repetitive sequence across the genome. Using the union of these results, we found that chromosomes 11 and 15 possessed strikingly high repeat contents. They are 34.34% and 55.71%, respectively. Chromosomes 4 (27.48%) and 5 (25.59%) have higher averages as well. Examining the spatial organization of the repetitive elements on chromosomes 11 and 15 revealed that they are not distributed equally across each chromosome.

Instead, they fall within concentrated regions roughly 860 kb and 1.6 Mb in length, respectively, next to their respective centromeres (Figure 2B and C). 83.68% of the 1.6 Mb region on chromosome 15 were flagged as repeats, while the 860 kb region on chromosome 11 contains 100% repetitive bases. It is likely the most repetitive region in the genome. Both regions are partially missing in alignments to both CC-1690 and CC-503 v5 assemblies. Inspection of read coverage across these regions in CC-5816 did not reveal any evidence of mis-assemblies, expansions, or other errors; read coverage was consistent throughout those regions. Using Nanopore reads, we assessed the frequency of CpG sites methylated to 5-methylcytosine (5mC) using Nanopolish, which performs well based on benchmarking studies.²⁶⁵⁻²⁶⁷ We found that average per-site 5mC frequencies for individual chromosomes range between 1.36 to 3.97% and genome-wide at an average frequency of 2.13%. This is between the two previous estimates of 0.75%²⁶⁸ and 5.38%²⁶⁹ which used whole genome bisulfate sequencing. Potential reasons for the range of genome-wide averages may be attributable to the life stage in which the cells are analyzed or the bioinformatic tools used to analyze sequencing data.^{265,266,270} Despite the difference in average genome-wide 5mC frequency, locations of individual hypermethylated regions identified by Lopez et al. are validated by our Nanopore dataset. These hypermethylated sites predominantly overlap centromeres (Figure 2A) and other repetitive regions largely missing or incomplete in previous assemblies. These include the previously mentioned repetitive region on chromosome 11 (Figure 2A and B). Centromeres were identified on all seventeen chromosomes by the presence of *ZeppL-1_cRei* LINE TE clusters^{271,272} (Supplemental Table S7). Based on the length of *ZeppL-1_cRei* clusters, centromeres in CC-5816 range in length from approximately 252-480 kb. We saw a 15-fold enrichment in average per-site 5mC frequencies at CpGs across all centromeres (23.55%)

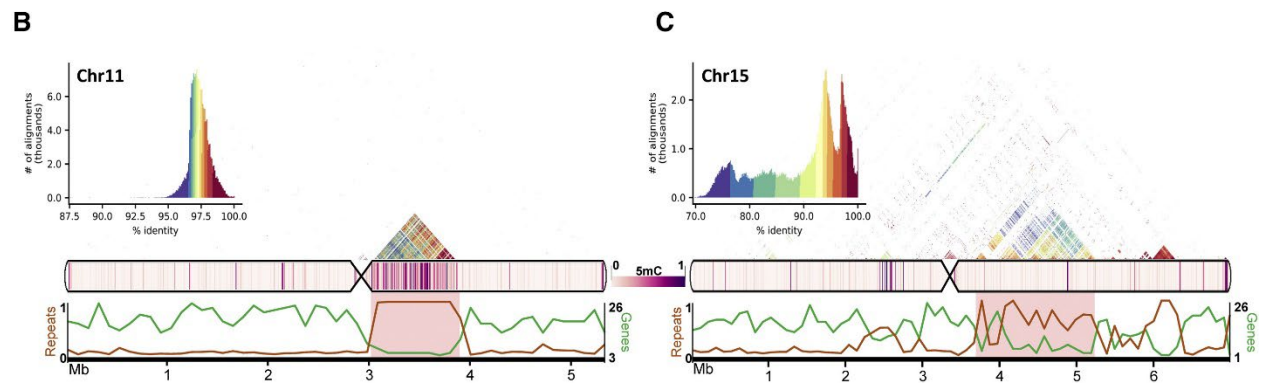
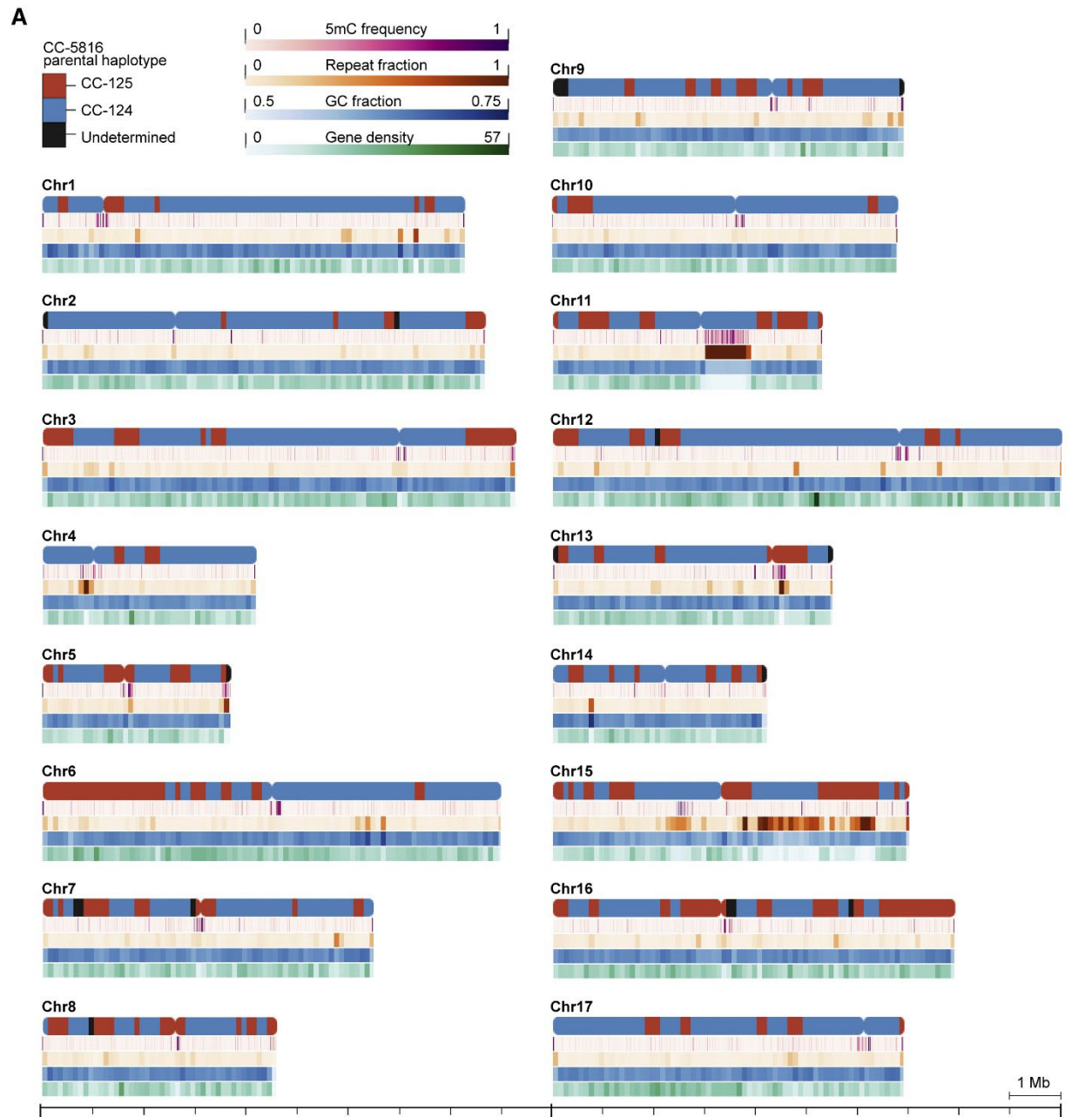


Figure 2. Telomere-to-telomere assembly of CC-5816. (A) Gap-free, telomere-to-telomere genome assembly of *Chlamydomonas reinhardtii* mating-type plus strain CC-5816. CC-5816 was obtained from a single meiotic product from multiple crosses between wild-type strains CC-125 and CC-124 and then backcrossing three times to CC-124. Genome features are shown for each of the 17 chromosomes. Approximate centromere locations are based on the location of *ZeppL-1_cRei* clusters and tetrad analysis and are denoted by inward curvature. For each chromosome, five plots from top to bottom show: the parental haplotype blocks (red, blue, and black), 5-methylcytosine (5mC) frequency (magenta), repeat fraction determined by Tandem Repeats Finder (orange), GC fraction (blue), and gene density (green) plotted along the lengths, with a scale bar at the bottom for reference. The parental haplotype was determined by creating libraries of 16-mers from the CC-5816 assembly as well as short read Illumina data from CC-125 and CC-124. 16-mers unique to one of the two parental strains were used to determine phase blocks. Repeat and GC fractions were calculated by the fraction of bases masked with Tandem Repeats Finder and the fraction of G and C nucleotides within 100 kb nonoverlapping windows across each chromosome. Gene density was calculated by counting the number of unique gene loci per 100 kb window. (B and C) Ideogram and plots for chromosomes 11 and 15 displaying several features (top to bottom): distribution and heatmap of intrachromosomal sequence identity from all-by-all alignment of 2 kb windows across each chromosome (color scales are independent for each chromosome), 5mC frequency heatmap (magenta), and line plots of repeat fraction (orange) and number of genes (green) per 100 kb window. Highly repetitive regions on each chromosome mentioned in the main text are highlighted in red within the line plots. Note that the appearance of some regions containing larger or inconsistent window sizes compared to others is due to consecutive windows with equivalent values. For example, the repetitive region between 3 Mb and 4 Mb on chromosome 11 appears as having a larger window size in many of the data tracks, but this is due to multiple windows with equivalent values next to each other.

compared with other nuclear CpGs (1.55%). For individual chromosomes, the average 5mC frequency across centromeres ranges between 4.26 to 34.53%. Regions annotated as repetitive sequence by RepeatMasker or Tandem Repeats Finder are also hypermethylated compared to non-repetitive regions (4.67% vs 1.42%). We mapped CC-503 gene models²⁷³ to CC-5816 and saw that coding sequence (CDS) is hypomethylated with respect to non-coding sequence (0.98% CDS; 3.11% non-coding). We then examined 5mC frequencies in the chloroplast and mitochondria. Previous studies have shown high methylation frequencies in chloroplast DNA derived from cells undergoing gametogenesis, especially in mating-type plus gametes.²⁷⁴ We found that the frequency of methylation across the chloroplast derived from CC-5816 gametes is 24.52%, more than double that of the previous estimate made from mating-type plus gametes previously. The mitochondrial genome was methylated at a much lower frequency than chloroplast in gametes (3.96%). Previous attempts to detect methylation from the mitochondrial genome of *Chlamydomonas* were unsuccessful.²⁷⁵ To our knowledge, this is the first report of mitochondrial 5mC methylation in *Chlamydomonas*.

We utilized a combined dataset composed of IsoSeq derived from CC-124 mRNA and a publicly available multi-isolate IsoSeq dataset²⁷³ to identify potentially novel splicing events and gene loci. We compared gene models generated from IsoSeq to v5.7 models (Supplemental Table S8). Six of the 19,548 v5.7 transcripts could not be mapped initially to CC-5816 and were checked for potential mis-assemblies surrounding adjacent genes. Cre12.g532400.t1.2 and Cre16.g650850.t1.2, are annotated as Tam3-transposase and are likely a strain-specific insertion. Cre12.g539700.t1.2 is redundant with two other genes that are located next to each other, they are Cre04.g229450 (e-175) and the combination of Cre04.g229398 and Cre04.g229422, which IsoSeq reads suggest as one transcript. Cre11.g467557.t1.1 is found near a large gap in v5 and is split when aligned to CC-5816. IsoSeq reads suggests in CC-5816 that the two split parts of this model are from the 5' and 3' ends of Cre11.g467551 and Cre11.g467552, respectively. Both models flank an assembly gap in v5. Cre17.g703300 is annotated as a ribonuclease III and has a high hmmsearch score to PlantFAM Chlorophyte protein family regulator of Ty1 transposition protein 103 ($e = 2.8e-65$) that includes nearby gene Cre17.g703450 ($e = 4e-27$). Cre16.g655430 is an unannotated, green algal specific gene with no domain predictions. It is in a region on Chr17 that is highly variable between CC-125 and CC-124. This transcript is likely to be missing in CC-5816 due to the difference in haplotype between CC-5816 and CC-503 genomes. Read coverage from both HiFi and Nanopore was normal across each of these loci. We conclude that these six transcripts are strain specific, redundant, nonessential, or TEs and do not suggest mis-assemblies in CC-5816. A total of 78,827 IsoSeq transcript models were generated that correspond to 12,711 unique genes. SQANTI3²⁷⁶ was used for comparing IsoSeq models to RNA-seq data and v5.7 transcript models by comparing overlaps of internal splice sites, which matched 10,935 v5.7 genes to 11,561 IsoSeq genes. 29,968 IsoSeq transcripts precisely matched a v5.7 model, 16,827 IsoSeq transcripts

excluded exons and/or retained introns but utilized known splice sites, and 27,344 contained novel splicing events. 1,150 IsoSeq gene models were classified as novel. It is likely some portion of these novel genes that overlap a v5.7 gene correspond to models which were unable to be matched by automated means. 110 of these novel genes contain transcripts that overlap a v5.7 model, each reciprocally covering at least 60% of the other's length, and 174 contain no overlap to a v5.7 model. 6,835 of the v5.7 genes did not match an IsoSeq model. 5,956 of these do not contain transcripts with overlap to the IsoSeq datasets, indicating detectable transcription is presumably not present for all genes in the combined IsoSeq dataset. We examined transcripts that were present in the centromeric regions (Supplemental Table S9). Assuming an even distribution of genes with approximately one gene every 10 kb based on the number of IsoSeq gene loci and genome size, 350 genes are expected. We find only 51 gene models from IsoSeq mapping to a centromeric region, eight of which have only very small overlap with the centromere boundaries (Supplemental Table S10). Chromosomes 6, 15, and 16 each contain six IsoSeq gene models, 4 and 11 contain none, and the average number of genes is three. We performed a multiple sequence alignment of the 557 centromere transcript models that revealed 80 separate clusters of transcripts with greater than 60% identity to each other (Supplemental Table S9). To determine the composition of each cluster, we took a random transcript from each cluster and performed a BLAST search as well as examine RepeatMasker annotations within the gene models (Supplemental Table S10). Thirty-nine gene models were identified as likely TEs, the majority being LINEs. Four were unidentifiable, but each are similar to four unannotated genes (Cre02.g093300, Cre07.g333850, Cre09.g399812, and Cre14.g622550).

3.3.3 Organellar Sequences Are Present Throughout The Nuclear Genome of CC-5816

Gene transfer between host and endosymbiont has played a large role in eukaryotic genome evolution.²⁷⁷ Organellar sequences continue to be identified in sequenced eukaryotic nuclear genomes and there is growing evidence that mitochondrial and plastid DNA continues to insert into nuclear sequence and may play a role in human diseases including cancer.²⁷⁸ Two independent groups observed *de novo* integration of plastid DNA (NUPTs) in the tobacco nuclear genome.^{279,280} Nuclear integrants of mitochondrial DNA (NUMTs) have been observed and the frequency increased by mutations in *S. cerevisiae*.^{281,282} Similar experiments to those performed in tobacco have been attempted in *Chlamydomonas reinhardtii* using a drug resistant gene inserted into the chloroplast that would only confer resistance if the gene translocated to the nucleus.²⁸³ However, no evidence of active DNA transfer was detected, and no apparent plastid sequences were identified in the genome assembly. Several studies since then have found varying levels of organellar sequences spread throughout the genome, depending on the BLAST parameters applied to the search and the available version of the genome assembly at the time.^{284,285} Using BLASTn

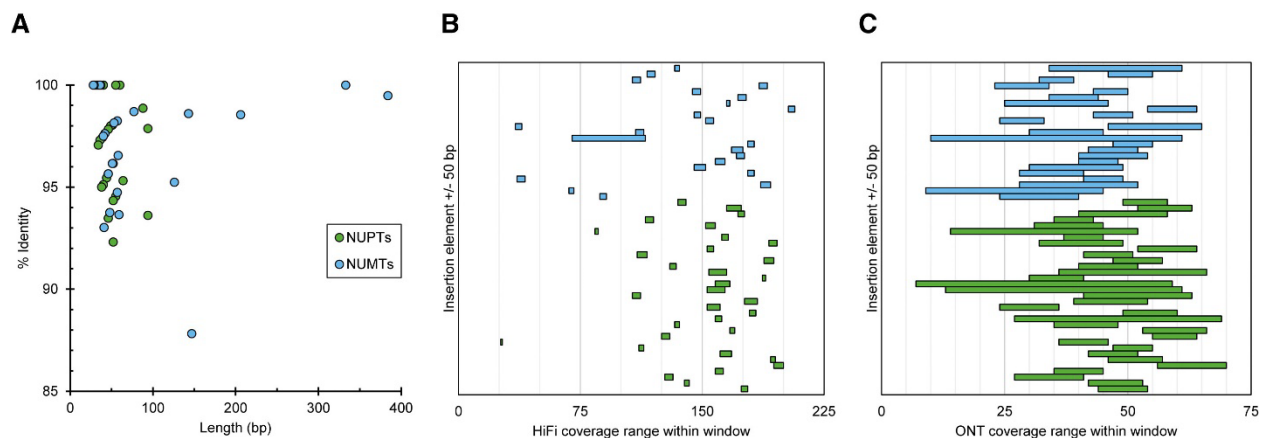


Figure 3. Characterization of organellar sequences in the nuclear genome. (A) Organellar insertions plotted by their length (x-axis) and percent identity by BLASTn to their respective *Chlamydomonas* organelle (y-axis). (B) The range of per-base coverage (x-axis) across each organellar insertion +/- 50 bp (y-axis) from PacBio HiFi reads. (C)

The range of per-base coverage (x-axis) across each organellar insertion +/- 50 bp (y-axis) from ONT reads. In each panel, NUPTs are colored green and NUMTs are colored blue.

with conservative parameters (See Materials and Methods), we found 33 NUPTs and 23 NUMTs ranging between 87.8 to 100% in identity to the aligned organellar sequences (Figure 3A and Supplemental Table S11). All insertions are individually short in length, ranging from 28 to 384 bp. HiFi and ONT coverage across these elements and the surrounding context did not reveal any evidence of mis-assemblies (Figure 3B and 3C). To assess the likelihood of obtaining false positives, we used two independent methods. First, we randomized seventeen sequences with 64% GC nucleotides of equivalent length to the *Chlamydomonas* chromosomes each containing 64% GC nucleotides. BLASTn did not find any positive results from these random sequences. Second, each insertion was used as a query for BLASTn against the NCBI database (Supplemental Table S12). The most common result for each sequence was alignment to the respective *Chlamydomonas* organelle; there were a few hits to other organisms. These two tests provide strong evidence for the presence of organellar DNA in the nuclear genome.

We characterized the NUPTs and NUMTs. Each chromosome has at least one NUPT or NUMT (Figure 4A). To determine if the locations of NUPTs or NUMTs has any correlation with other features in the nuclear genome, we looked at the distribution of these elements with respect to annotated repetitive elements, genes, nucleotide content, and methylation frequency (Figure 4B). We generated 100 sets of shuffled NUPTs and NUMTs of similar size for each analysis to compare against a random distribution. We considered all annotated features within 50 bp of NUPTs and NUMTs in our analyses. We saw differences in the frequency of various genomic

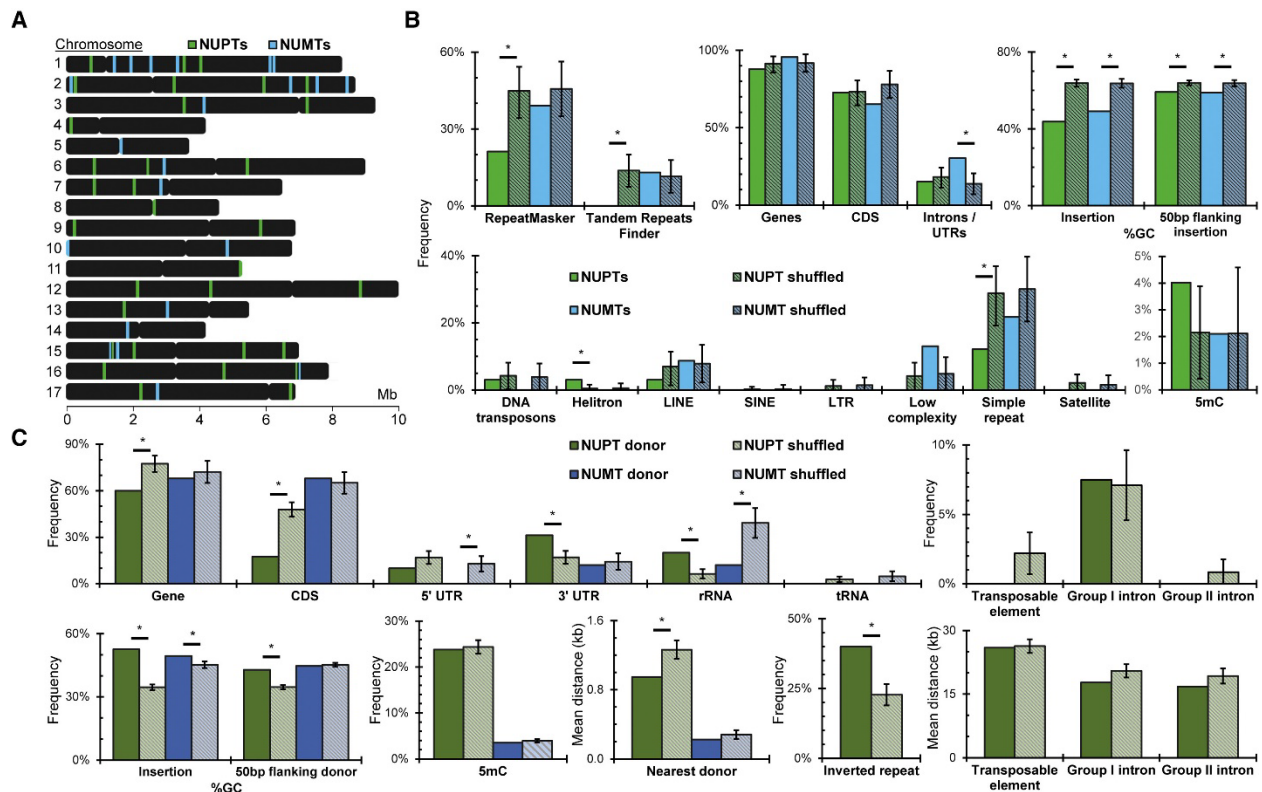


Figure 4. NUPTs and NUMTs originate from specific sequences and are located near specific elements within the nuclear genome. (A) Ideogram showing approximate nuclear locations of nuclear integrants of plastid DNA (NUPTs, green) and nuclear integrants of mitochondrial DNA (NUMTs, blue). The width of colored lines is resized for easy identification and are not correlated with insertion lengths. (B) Frequency of genomic elements proximal to NUPTs (green) and NUMTs (blue) within nuclear sequence compared to 100 sets of randomly shuffled coordinates of equal sizes (NUPT simulations, green with black stripes; NUMT simulations, blue with black stripes). (C) (Top row, left to right) Frequency of plastid NUPT donors (dark green) and mitochondrial NUMT donors (dark blue) within 50 bp of annotated genes, CDS, 5' UTRs, 3' UTRs, rRNAs, and tRNAs. Frequency of NUPT donors within 50 bp of mobile elements, including transposable elements, group I, and group II introns. (Bottom row, left to right) Frequency of G and C bases within NUPT and NUMT donor sequences and the 50 bp flanking. Per-base frequency of 5mC detected at CpGs within NUPT and NUMT donors. Mean distance between each NUPT and NUMT donor and the nearest donor. Frequency of NUPT donors within 50 bp of either of the two inverted repeats. Mean distance between each NUPT donor and the nearest transposable element, group I, and group II intron. Each are compared to 100 sets of randomly shuffled coordinates of equal sizes (NUPT donor simulations, pale green with black stripes; NUMT simulations, pale blue with black stripes). Plastid annotations were duplicated upstream and downstream for these analyses to account for circular genome conformation. Error bars in (B and C) depict standard error of the mean (SEM) for 100 simulated NUPTs and NUMTs. Asterisks (*) indicate $p < 0.05$ from a two-tailed one-sample t-test assuming a normal distribution.

elements appearing in proximity to tested sites depending on whether the tested site was a NUPT, NUMT, or a random site. Repetitive elements in general were underrepresented adjacent to NUPTs (RepeatMasker, $p=0.01$; Tandem Repeats Finder, $p=0.03$). Specifically, we found simple repeats

to be statistically underrepresented adjacent to NUPTs ($p=0.04$). Despite the underrepresentation of repetitive elements, helitron transposons were near NUPTs more frequently than expected by chance ($p=0.03$). NUMTs on the other hand did not appear to have any significant correlation with any repetitive elements, aside from possibly low complexity regions, the element nearest to our p -value threshold of 0.05 ($p=0.1$). We then looked at the proximity of NUPTs and NUMTs with respect to v5.7 genes and saw that NUMTs were preferentially located near intronic and UTR regions ($p=0.02$), while NUPTs did not appear to have any correlation with genes. The average GC contents of both chloroplast and mitochondrial sequences are very different from the *Chlamydomonas* nuclear genome (34.57% for chloroplast and 45.24% for mitochondria). Therefore, it is not surprising to find that sequences putatively originating from these organelles are on average lower in GC content than the nuclear genomic average of 64% (NUPTs, 43.8% GC, $p=6.64\times 10^{-18}$; NUMTs, 49.1% GC, $p=7.76\times 10^{-9}$). We looked at the 50 bp flanking each insertion and found that, to a lesser degree, GC content was lower than expected (NUPTs, 59.2% GC, $p=6.64\times 10^{-18}$; NUMTs, 58.8% GC, $p=7.76\times 10^{-9}$). Several studies have shown that organellar insertions in nuclear DNA are often hypermethylated, especially before accumulating mutations.^{286,287} We observed a small, but not statistically significant ($p=0.28$), enrichment of 5mC frequencies at NUPT CpGs (4%) compared to non-NUPT CpGs (2.1%). We next asked whether NUPTs or NUMTs derive from specific regions within the chloroplast or mitochondria (Figure 4C). For each NUPT and NUMT, we used the BLAST alignments with highest identity to determine the likely origin of the donor. Insertions with more than one equally likely donor were included in the analyses. We again randomly sampled 100 sets of coordinates of equal size to the actual donor sequences from the chloroplast and mitochondria for comparison against. For NUPT donors within the chloroplast, we saw an underrepresentation of annotated

genes within 50 bp of donor sequences ($p=1.2\times 10^{-3}$), and even more specifically with coding sequence ($p=4.1\times 10^{-9}$). We found NUPT donor regions enriched for 3' UTRs ($p=8.9\times 10^{-4}$), rRNA sequence ($p=9.9\times 10^{-6}$), and GC nucleotides (donor, $p=9.9\times 10^{-6}$; 50 bp flanking, $p=9.9\times 10^{-6}$). We then calculated the distance of each donor to its nearest neighboring donor to determine if there was any clustering. The mean distance between each donor and the nearest neighboring donor is shorter than in any of our random samples by an average of ~ 317 bp ($p=3.9\times 10^{-3}$). We identified clustering of NUPT donors within two inverted repeat regions ($p=1.6\times 10^{-5}$) and observed a weak signal for NUPTs clustered near elements associated with mobile DNA, namely Group I and Group II introns,²⁸⁸ which were closer to NUPTs on average, though not statistically significant from our tests (Group I introns, $p=0.09$; Group II introns, $p=0.11$).

3.3.4 Ribosomal DNA Arrays

We next looked at the location of ribosomal DNA (rDNA) in CC-5816. There are 4 main arrays in CC-5816, two 5S arrays on chromosomes 1 and 8, and two 18S, 5.8S, and 28S arrays on chromosomes 8 and 14 (Figure 5A and 5B), and ~ 12 singular or partial rDNA units scattered throughout the rest of the genome. The 5S array on chromosome 8 was completely assembled using only HiFi reads (Figure 5A). The 5S array on chromosome 1 is $\sim 3x$ longer with highly identical rDNA units (Figure 5A). This array was only correctly assembled after incorporating Nanopore reads. Consistent with observations from strain CC-1690,²⁵⁶ 18S, 5.8S, and 28S rDNA are located on the right arms of chromosomes 8 and 14 and are organized tandemly in an array (Figure 5B). Based on alignment of PacBio Isoseq data, one 18S, 5.8S, and 28S unit is ~ 6.46 kb

in length followed by a ~1.98 kb spacer sequence to create a periodicity of ~8.42 kb. The 18S, 5.8S, and 28S arrays are likely incomplete in length based on

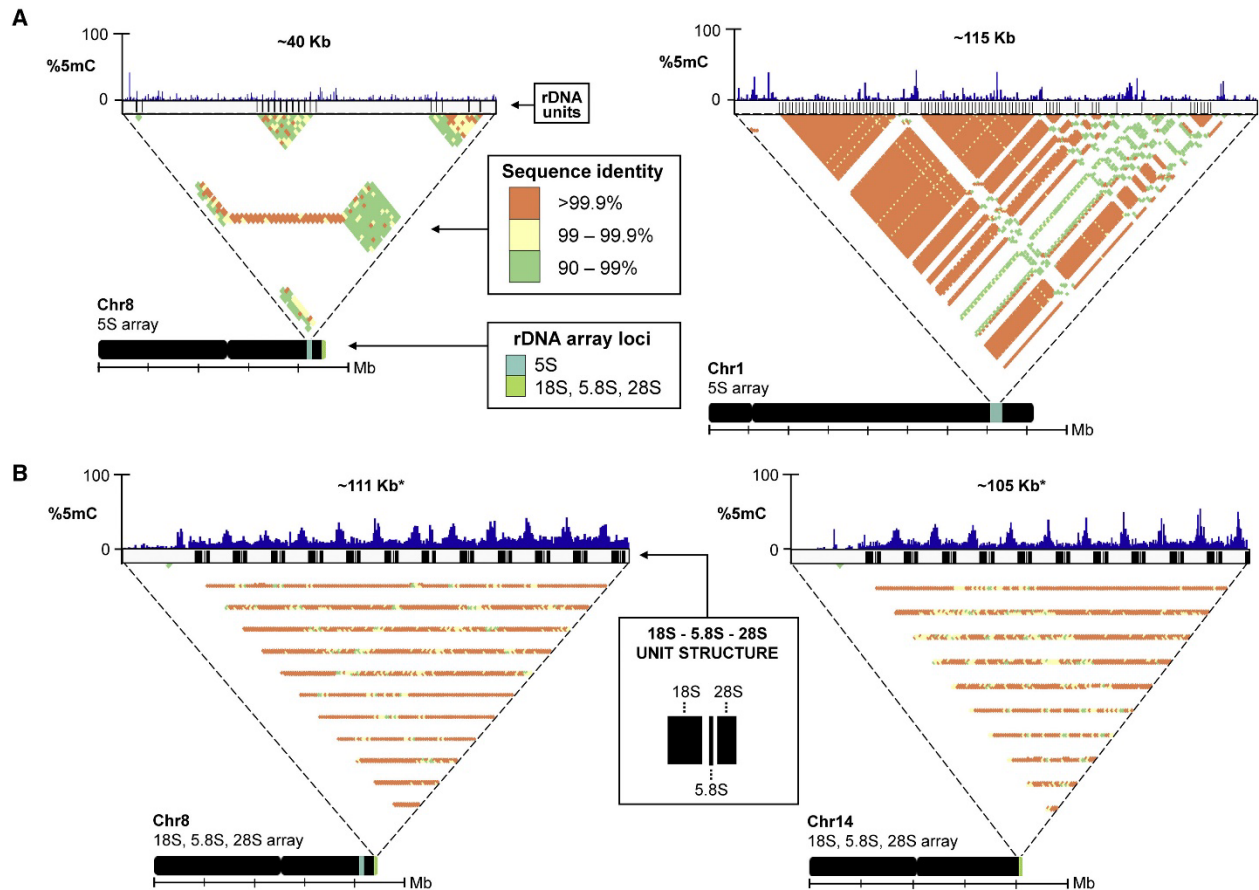


Figure 5. Ribosomal DNA arrays.

(A) Characterization of 5S arrays on chromosomes 8 (left) & 1 (right) with approximate length of the region in the assembly, 5mC frequency, unit structure, percent identity heat map, and ideogram illustrating location of arrays (5S, light blue; 18S, 5.8S, and 28S, lime green). (B) Characterization of 18S, 5.8S, and 28S arrays on the ends of chromosomes 8 (left) and 14 (right). The sequence identity and array loci legends in (A) apply to panel (B) as well. Asterisks (*) indicate length in the final genome assembly.

higher coverage than the genomic average and the presence of 85 additional contigs containing only these arrays.

3.3.5 Gene Editing of The *PF23* Gene by CRISPR/Cas9.

The *PF23* gene contains 11 exons (Figure 6B, I) that encode a dynein assembly factor (DNAAF) protein, which is needed for assembling axonemal dynein arms in the cilia. It is known as DXY1C1/DNAAF4 in mammals.¹⁹⁹ The only allele of the *PF23* gene in *Chlamydomonas* (*pf23-1*) contains an in-frame 494 bp deletion that removes all of exon 5 and parts of the two flanking introns (Figure 6B, II). This generates a protein lacking 27 amino acids.¹³⁶ Although this allele has been extensively characterized, the study of null alleles often provides further insights into function and could reconcile differences in phenotypes between *Chlamydomonas* and human variants in *DYX1C1*. We utilized a site-directed insertional mutagenesis approach using CRISPR/Cas9 to generate null alleles of *PF23*. A Cas9 gRNA PAM site at the beginning of exon 1 of the *PF23* gene was chosen, as this site would likely result in disruption of the gene. Cas9 protein, the gRNA construct and an *aphVII* gene that confers resistance to hygromycin with reverse-oriented homology arms,²⁸⁹ were transformed into either CC-5908 or CC-5909 strain (Supplemental Table S16) to insert the *aphVII* gene into exon 1 (Figure 6A). Following transformation and selection on hygromycin medium, we isolated three independent strains (4-3, 2-3, and H9) that fail to swim in liquid cultures, which is the phenotype of the *pf23-1* allele. PCR analysis using primer pairs that are upstream of exon 1 and within the *aphVII* construct (*PF23-aphVII* junction) shows that the *aphVII* construct is inserted into exon 1 of *PF23* in all three strains (Figure 6C, Supplemental Table S13, S14). The *aphVII* construct is inserted in the reverse orientation in strains 4-3 and 2-3

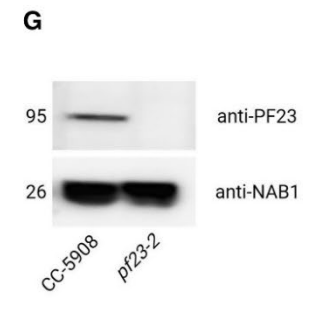
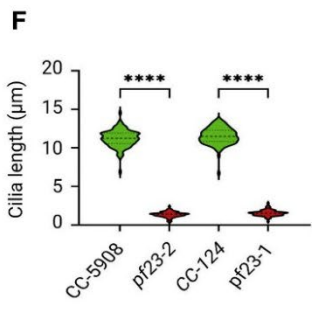
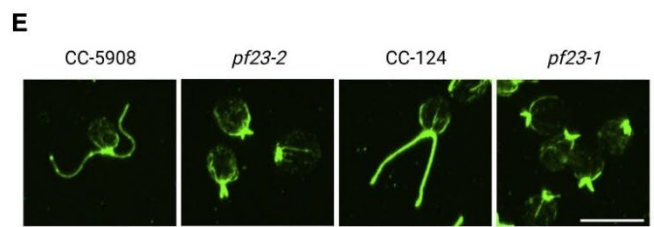
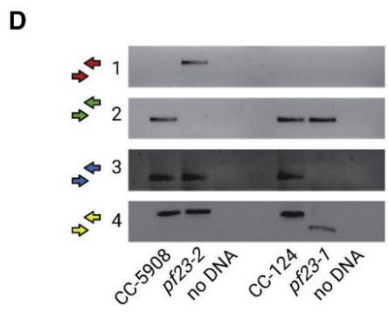
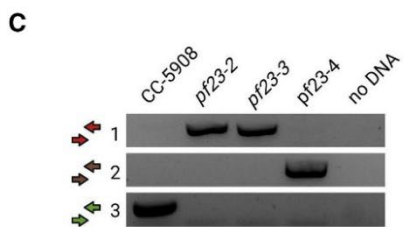
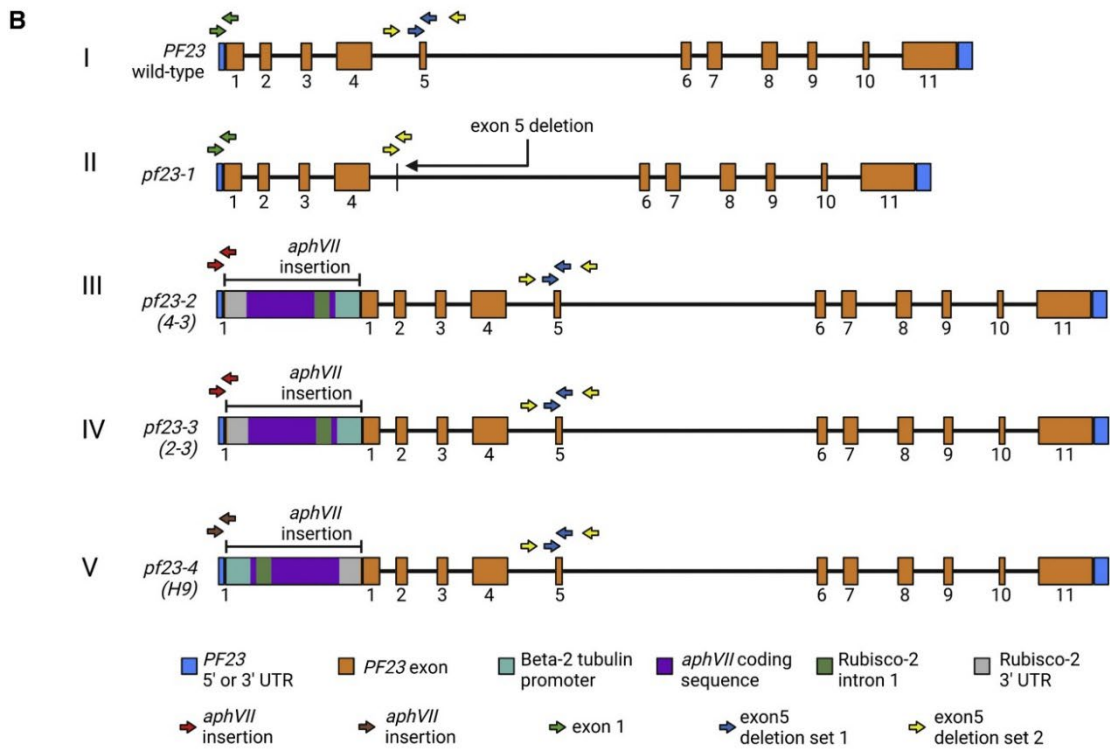
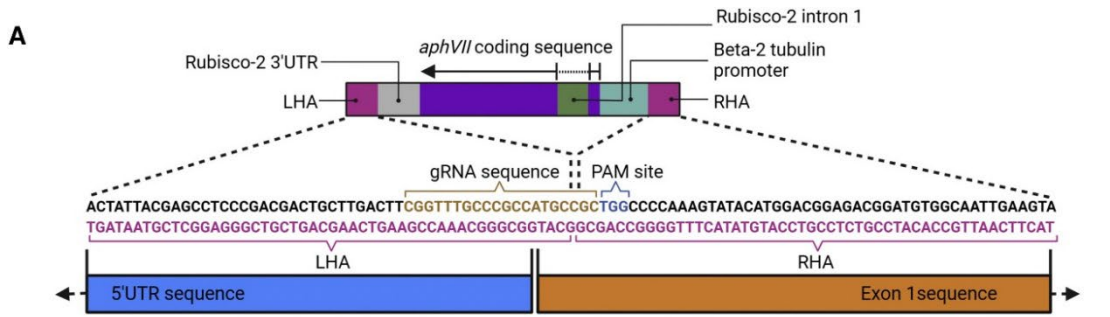


Figure 6: Characterization of null *pf23* CRISPR-generated alleles

(A) The *aphVII* construct includes the Beta-2 tubulin promoter, Rubisco-2 3'UTR, and *aphVII* coding sequence with Rubisco-2 intron 1 sequence. The construct is flanked at the left and right ends with a left homology arm (LHA) and right homology arm (RHA) respectively that correspond to regions in the 5'UTR and exon 1 segments of the *PF23* gene. The dashed lines indicate that the homology arms in the *aphVII* construct recombine with the homologous sequences in the 5'UTR and beginning exon1 sequences of the *PF23* gene. Only a portion of the gene is shown for reference. The 5'UTR and Exon 1 sequences extend to the left and right respectively, indicated by black arrows. The LHA and RHA sequences are in pink, the guide RNA (gRNA) in tan, and the PAM site in blue. Cas9 cleavage at the PAM site allows a break in the *PF23* gene followed by recombination of the RHA and LHA to allow insertion of the *aphVII* construct into exon 1 of *PF23*. Maps generated to scale using BioRender. (B) Colored arrows indicate regions of PCR amplification by primers listed in Supplemental Table S13. I - The wild-type *PF23* gene. II - The *pf23-1* allele lacks exon 5 and portions of the flanking introns that is indicated by the black arrow. III - The *pf23-2* strain is expected to contain an insertion of the *aphVII* construct in reverse orientation within exon 1 (black arrow and bars indicate region and directionality). GreenGenie2 was used to annotate the correct *PF23* gene using Nanopore sequencing assembly (this study) and a cDNA sequence of *PF23* (Yamamoto et al., 2017). IV - The *pf23-3* strain also contains an insertion of the *aphVII* construct in reverse orientation. V - The *aphVII* insertion in the *pf23-4* strain is in the forward orientation. Maps generated to scale using BioRender. (C) PCR to detect *aphVII* hygromycin insertion in *pf23* CRISPR-generated strains. Primers in exon 1 and *aphVII* (*PF23-aphVII* junction) show that *aphVII* has inserted in the reverse orientation in *pf23-2* and *pf23-3* (row 1, red arrows), whereas *aphVII* is present in the forward orientation in *pf23-4* (row 2, brown arrows). Primers spanning the exon1 CRISPR insertion site only amplify in wild-type strain CC-5908 that lacks the insertion (row 3, green arrows). (D) Comparison of the mutations present in *pf23-2* and *pf23-1* strains. Primers spanning the *PF23-aphVII* junction amplify only in the *pf23-2* strain containing the insertional construct (row 1, red arrows). Primers flanking the CRISPR site in exon 1 fail to amplify in *pf23-2* due to the large insertion and use of a short extension time during PCR (row 2, green arrows). Primers within exon 5 fail to amplify in *pf23-1* that contains a deletion of exon 5 and parts of the surrounding introns (row 3, blue arrows). This deletion is absent in the *pf23-2* CRISPR generated strain and wild type; those strains both amplify PCR fragments that are 955 bp long (row 4, yellow arrows), while *pf23-1* generates a 494 bp fragment. Colored arrows indicate primer binding sites in (A). (E) Immunofluorescence of strains with wild-type length cilia (CC-5908) and CC-124 compared to CRISPR-generated strain *pf23-2* and a strain containing the *pf23-1* allele that have short cilia. The scale bar is 10 microns. (F) Quantification of cilia length of strains. One hundred individual cilia (one per cell) were measured for each strain. Asterisks indicate a p-value <0.0001 using an independent two-sample two-tailed t-test. (G) Immunoblot of the *pf23-2* strain shows that *PF23* protein is completely absent from this strain. The NAB protein (Nucleic acid binding)1 is used as a loading control. Created with BioRender.com

as expected (Figure 6B, III-IV and Figure 6C, rows 1-2). However, in strain H9, *aphVII* integrated in the forward orientation (Figure 6B, V and Figure 6C, row 3). Figure 6D (row 1) shows that the *aphVII* insertion is present in *pf23-2* but not wild-type strains CC-5908 and CC-124 (see also Figure 6B, III). Primers flanking the exon 1 gRNA site fail to amplify in *pf23-2*. This suggests the insertion of a large fragment of DNA (Figure 6D, row 2). Our analysis also shows that the mutation in *pf23-2* is distinct from the original *pf23-1* allele that contains an exon 5 deletion (Figure 6D, rows 3 and 4, Supplemental Table S13, S14). To confirm that the short cilia phenotype is linked to *aphVII* insertion into the *PF23* gene, we performed two backcrosses on each strain followed by meiotic analysis. Analysis of 7 tetrads from 4-3, 12 tetrads from 2-3 and 12 tetrads from H9 shows

complete segregation of the short cilia phenotype with hygromycin resistance and PCR amplification of the *PF23-aphVII* junction. These results confirm that the short cilia phenotype results from disruption of the *PF23* gene. Consequently, strains 4-3, 2-3 and H9 were renamed *pf23-2*, *pf23-3*, and *pf23-4*, respectively. The *pf23-4* strain shows wild-type levels of viability in tetrads (n=30). However, the 7 tetrads from strain *pf23-2* and the 12 tetrads from strain *pf23-3* produced ~50% inviable meiotic progeny. This suggests the presence of large chromosomal aberrations that cause aneuploidy and death following meiosis. This observation is investigated further in the section below on meiotic analysis. Immunofluorescence analysis shows that strain *pf23-2* is unable to grow full length cilia. The cilia are short, stubby, and resemble the original *pf23-1* strain (Figure 6E and F). To confirm that the *pf23-2* strain is a protein null, immunoblot analysis with a polyclonal antibody against PF23 protein was performed (Yamamoto et al., 2017). Figure 6G shows that the *pf23-2* strain completely lacks the PF23 protein.

3.3.6 Meiotic Analysis of *pf23* null CRISPR-Generated Strains

Tetrad analysis has been used extensively to analyze the meiotic outcomes in *Neurospora* and *Saccharomyces* strains that are heterozygous for a translocation, which reduces the viability of meiotic progeny. Examination of translocations in *S. cerevisiae* and *N. crassa* by tetrad analysis shows that tetrads with 4 viable progeny, 2 viable progeny and no viable progeny are the most common classes.^{290,291} Tetrads with four viable progeny are ascribed to alternate segregation that generates progeny with two wild-type chromosomes and two balanced translocation chromosomes. Tetrads with only 2 viable progeny are ascribed to alternate segregation with recombination between the breakpoint and the centromere, or nondisjunction. Tetrads with no

viable progeny are ascribed to adjacent segregation with all progeny having unbalanced chromosomal complements.

Meiotic inviability in strains *pf23-2* and *pf23-3* after mating to a wild-type strain suggests the possibility of large chromosomal aberrations/rearrangements present in the genome of these CRISPR strains. Meiotic crosses of *pf23-2* by *pf23-2* produced fully viable tetrads (N= 25) as did meiotic crosses of *pf23-3* x *pf23-3* (N=23) (Supplemental Table S15). Moreover, meiotic crosses of *pf23-2* x *pf23-3* suggest that the rearrangements in in these two strains are not identical, as the viability of the meiotic progeny from this cross is reduced further than either single strain; only 4 tetrads produced four viable progeny and 12 tetrads produced no viable progeny (N=20). Using our optimized HMW DNA extraction protocol (see Materials and Methods; Supplemental Figure 2), we performed whole genome Nanopore sequencing of *pf23-2* and *pf23-3*. We obtained 1.24 Gb of sequence or 10x coverage for *pf23-2* and we obtained 0.69 Gb of sequence or 6x coverage for *pf23-3*. We used a combination of *de novo* genome assembly and mapping of reads from *pf23-2* and *pf23-3* to the CC-503 v5 and CC-5816 genome assemblies to identify structural variation between the two CRISPR-generated strains (Supplemental Figure S5). We determined that the *pf23-2* strain carries a translocation between chromosomes 5 and 11, referred to as t(5;11) and t(11;5) (Figure 7A-C). Breakpoints at exon 1 of *pf23* on Chr11 were identified using both CC-5816 and CC-503 v5. However, we were only able to identify the precise location of the breakpoint on Chr5 using CC-5816, as CC-503 lacks 14 kb of sequence in this region (Supplemental Figure S5). The breakpoint on translocation partner t(5;11) from strain *pf23-2* was not covered entirely by a single read, which indicates a large insertion. To resolve the length of the insertion, we assembled *pf23-2* Nanopore reads *de novo* using Flye (Figure 7D). The resulting assembly

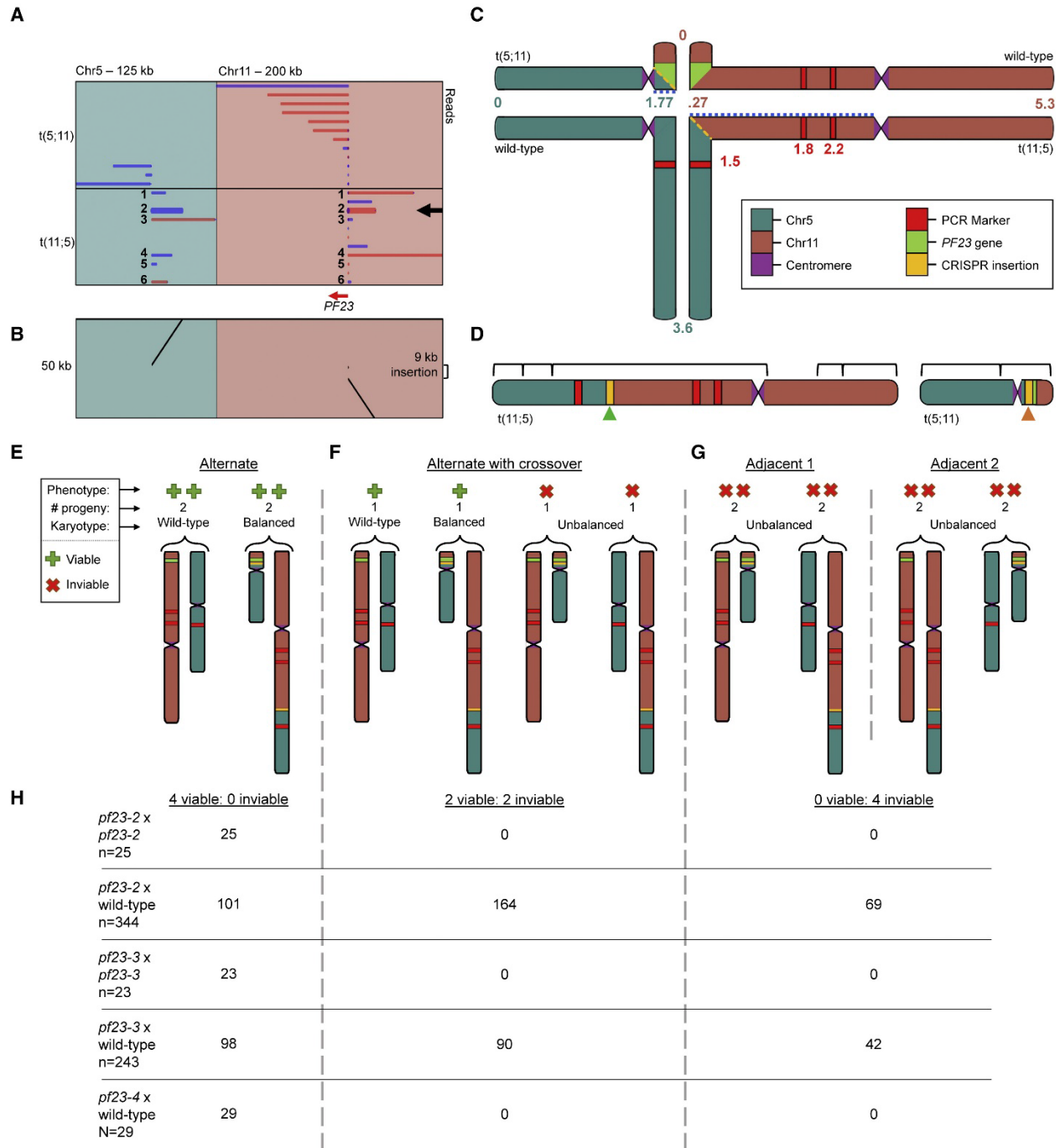


Figure 7. Translocations in *pf23-2* and *pf23-3* were induced by site-directed CRISPR/Cas9 mutagenesis.

(A) Alignments to CC-5816 from *pf23-2* Nanopore reads selected within the *PF23* gene locus. Each row corresponds to a single aligned *pf23-2* Nanopore read. Blue and red lines along the x-axis indicate forward and reverse alignments, respectively. The read in bold indicated by the black arrow highlights one example of a chimeric read mapped with respect to CC-5816 which overlaps the translocation break point in *pf23-2*. Alignments to Chromosomes 2 and 12 are due to the RBCS2 intron and Beta2-tubulin promoter, respectively, which are used in the insertional cassette. (B) Dotplot of the bolded read in (A). (C) Quadrivalent structure of Chr5, Chr11, t(5;11), and t(11;5) predicted to form during meiosis I in a *pf23-2* × wild-type cross. Similar information for *pf23-3* can be found in Supplemental Figure S6. Coordinates are in Mb and based on CC-5816 to illustrate approximate location of breakpoints in translocation. Alternate segregation of chromosomes containing a single crossover between the breakpoints and centromeres results in one-half of progeny being inviable due to deletions in either chromosome. (D) *pf23-2* Nanopore reads were assembled *de novo* using Flye as validation to determine k-mer overlapping of putative translocation junctions. Brackets indicate regions supported by an assembled contig. A contig spanning the entirety of a highly repetitive region downstream of the Chr11 centromere could not be found. The region denoted by the green arrow is supported by linkage of PCR-based markers shown in red, *de novo* genome assembly with Flye, and six individual reads spanning the entire breakpoint, including Chr5, the connecting *aphVII* insertion cassette, and Chr11. The breakpoint denoted by the orange arrow has reads from either Chr5 or Chr11 connected to an *aphVII* insertion cassette. *De novo* genome assembly with Flye was used to determine if the breakpoint could be assembled *de novo* into a contig, indicating the presence of unique overlapping k-mers from these reads. (E-G) Diagram depicting possible meiotic products from meiosis (C) for (E) alternate segregation without a crossover (4 viable progeny), (F) alternate segregation with a single crossover event between a break point and centromere (2 viable and 2 inviable progeny), (G) adjacent-1, and adjacent-2 segregation (all inviable). (H) Table of the number of tetrads containing either 4 viable, 2 viable, or 0 viable progeny from the meiotic crosses in this study. The parent strains in each cross are shown in the left-most column with the number of tetrads scored (n). Note that panels C and E-G contain pictures corresponding to chromosomes from *pf23-2* × wild-type crosses.

revealed the insertion size to be ~22 kb (Supplemental Figure S5). We then determined that *pf23-3* carries a translocation between chromosomes 3 and 11, referred to as t(3;11) and t(11;3) (Supplemental Figure S6). Breakpoints in *pf23-3* were identified using both CC-5816 and CC-503.

Since the number of reads across the translocation breakpoints was not large, we verified the translocations with meiotic crosses by determining if linkage was observed between the translocation chromosomes predicted from the Nanopore sequencing. We examined meiotic progeny from 344 tetrads from crosses of *pf23-2* by two different CC-125 × CC-124 derived meiotic strains named 1-1 and 3-3. We examined 243 tetrads from crosses of *pf23-3* by 1-1 or CC-124 (see Materials and Methods). As observed in fungal tetrads heterozygous for a translocation, we found tetrads with 4, 2, and 0 progeny^{290,291} From *pf23-2* crosses, we retrieved 101 tetrads with 4 viable progeny (Figure 7E), 164 tetrads with 2 viable progeny (Figure 7F) and 69 tetrads with no viable progeny (Figure 7G). Tetrads with 4 viable progeny should show pseudolinkage of genes

on the two translocated chromosomes. This means that SNVs on chromosomes 5 and 11 will be linked to each other and will not show independent assortment. We monitored PCR based markers (Figure 7H and Supplemental Table S15) on chromosomes 5 and 11 in control crosses of CC-125 x CC-124. The genes on chromosomes 5 and 11 show independent assortment and therefore are unlinked in 28 tetrads (Figure 7H and Supplemental Table S15). In the *pf23-2* x 1-1 (or 3-3), we found no recombination in 90 tetrads that showed 2:2 segregation of hygromycin resistance; and three tetrads with recombination. Nine tetrads that did not show 2:2 segregation of the *pf23* phenotype were found and may arise by nondisjunction. For the tetrads that produced 2 viable and 2 inviable progeny, 89% had one product with the *pf23-2* allele and one with the wild-type allele. We monitored recombination between the breakpoint and the centromere on chromosome 5 but were unable to find markers between the centromere and the breakpoint on chromosome 11 (Supplemental Table S15). We observed 21% of the tetrads showed recombination and 11% showed nondisjunction based on the lack of 1:1 segregation.

The *pf23-3* mutant is associated with a translocation between chromosome 3 and chromosome 11. Crossing either *pf23-4* or *pf23-1* by *ac17* showed that the two chromosomes assort independently (14:15:0 and 13:17:0, respectively) and that both genes are linked to their respective centromeres given the lack of tetratype tetrads. From *pf23-3* crosses by wild-type, we retrieved 98 tetrads with 4 viable progeny, 90 tetrads with 2 viable progeny, 18 progeny with only 1 viable progeny and 42 tetrads with no viable progeny. The class with only one viable progeny was more frequent in the *pf23-2* crosses. In tetrads with 4 viable progeny from the *pf23-3* x 1-1 or CC-124 crosses, we found no recombination in 98 tetrads with *ac17*, which was present in the parental strain (CC-5908). *AC17* encodes the pyruvate dehydrogenase E1 beta subunit and maps at 6.45 Mb on chromosome 3 (Dent et al., 2015). In the 32 tetrads that were tested and were

heterozygous for a PCR marker at 7.42 Mb, we observed no recombinants. For the tetrads that produced 2 viable and 2 inviable progeny, 95.6% had one product with the *pf23-3* allele and one with the wild-type allele. The other 4 had one with four non-swimmers, one with four swimmers, one with one non-swimmer and 4 swimmers, and one with 3 non-swimmers and one swimmer. In the 32 tetrads that were tested and heterozygous for the PCR marker at 7.42 Mb on Chromosome 3, we observed 3 recombinants. Of the 18 tetrads that had only one viable progeny, most were swimmers (N=14) and four of these showed resistance to hygromycin, which suggests that they are aneuploid and carry the translocation with the chromosome 11 where the cluster of *aphVII* genes are located near the centromere of chromosome 11 (Supplemental Figure S6).

3.3.7 Behavior of Other CRISPR-Generated Strains in Meiosis

Since we found two of the three CRISPR/Cas9 mutants in the *PF23* gene had translocations, we tested CRISPR generated mutants in three other genes. We obtained a CRISPR/Cas9 generated strain with mutant alleles in *CHR1* and *CHR2* that encode channelrhodopsins²⁹² as well as four mutant alleles in *FAP70* that are found in the central apparatus of cilia.²⁸⁹ Each was crossed by a wild-type strain and viability patterns were assayed. The generation of 2 viable and 2 inviable progeny as well as no viable progeny was considered indicative of a chromosome aberration. The *chr1; chr2* strain produced 94% viable progeny (N= 18) and was judged to be structurally intact. The four *fap70* strains showed reduced viability that ranged from 30 to 50% viability (N= 82 tetrads). In a second backcross, the viability remained lower than observed in the *pf23-2* and *pf23-3* crosses, which had 67 and 59% viability, respectively. However, three of the 4 *fap70* strains showed patterns of meiotic inviable suggestive of a chromosomal aberration (Supplemental Table S15). In the small subset of mutants tested,

insertions in *fap70* and *pf23* but not *chr1* and *chr2* show signs of a chromosomal aberration. Thus, five of nine of the CRISPR-generated insertions are associated with a translocation or a suspected translocation.

3.4 Discussion

A growing number of genetic and genomic tools are accessible to researchers; these include the telomere-to-telomere version of the human genome (T2T-CHM13)²⁴⁰ as well as CRISPR/Cas9-based methods for gene editing.^{293,294} The community studying the widely used model organism, *Chlamydomonas reinhardtii*, has quickly adapted, and produced similar tools tailored to this model organism. These include RNAseq experiments,^{191,273,295,296} epitope-tagging of proteins,²¹³ an insertional mutant library,¹²¹ and CRISPR/Cas9 site-directed mutagenesis techniques.^{225,289,297} These tools require a better reference genome assembly than the one assembled using short reads.^{114,217} Our telomere-to-telomere assembly of the seventeen chromosomes of CC-5816 provides a complete reference for noncoding sequences, repetitive and transposable elements, as well as DNA methylation. Another recent genome assembly¹¹⁵ has been generated but it has several gaps. Multiple genome sequences will be important for further genetic studies.

We evaluated various bioinformatic tools through stepwise assessment of multiple assemblies to determine which tools are most effective at generating high-quality genome assemblies from high coverage HiFi and Nanopore sequencing data. Using ~150x HiFi data, Hifiasm generated the most contiguous and accurate nuclear assembly, while Canu generated mis-assemblies in multiple regions. TGS-GapCloser and QuickMerge were tested, and both were successful in producing high quality assemblies. The order of assemblies used for gap filling with

QuickMerge greatly affected the quality of the output, so careful evaluation should be performed. We found the use of RaCon was detrimental to the quality of the assembly when used for polishing the entire assembly. However, using RaCon to correct short regions with low coverage improved the base quality score. For ~50x Nanopore data, we evaluated three different assemblers: Canu, Flye, and Necat, and found all three programs to be useful for comparing strategies for filling gaps and correcting regions with low coverage, as each varied in quality within different regions based on read coverage. Notably, Flye was the only assembler to generate a contiguous assembly (135 contigs and an N50 of ~2.2 Mb) from low coverage Nanopore data (<10x coverage)

Regions Resolved by Long Reads

Cumulatively, only 2,916 bp of our assembly has less than 5x coverage from both HiFi and Nanopore reads. Some DNA segments in CC-5816 are unaligned to CC-503 v5.6 or CC-1690. Considering only 1-to-1 alignments, there are 8,164,010 bp and 4,488,839 bp in CC-5816 with no alignments to CC-503 v5.6 or CC-1690, respectively. Most of this sequence is flagged as repetitive and resides on chromosomes 11 and 15. The alignment of IsoSeq reads suggests ~300 to 500 kb of this repetitive sequence may be transcriptionally active. Excluding repetitive DNA, there are a total of 1,999,696 bp and 932,474 bp of unaligned sequence when compared to CC-503 v5.6 and CC-1690, respectively. It will be interesting to see the extent of genomic variation among *Chlamydomonas* strains upon release of more high-quality assemblies.

The identification of a ciliary central apparatus-associated protein from single particle cryo-EM of *Chlamydomonas* axonemes was made possible with the new assembly.²⁹⁸ Currently in the v5.7 assembly, FAP221 (Cre11.g476376) and FAP360 (Cre49.g761347) are annotated as two different gene models. Nucleotide and amino acid sequence alignments to CC-5816 as well as IsoSeq models suggest that FAP221 and FAP360 are not paralogs, but actually one gene

(Supplemental Figure S7). Based on IsoSeq transcript models, 2,435 transcripts match splice junctions from more than one v5.7 gene model, indicating there may be many gene models in need of correction. This will be a key area for future work.

Based on previous studies, there are roughly 350 copies or 3 Mb of rDNA genes in the genome.^{256,299,300} However, our assembly only contains 12 full rDNA copies on chromosome 8, and 10 full and one partial copy on chromosome 14. Assembling repetitive arrays of this size remains challenging even with long reads. We have turned to assessing rDNA number using HiFi and Nanopore coverage across rDNA arrays compared with genome-wide coverage. We estimated that there are 2,758,766 to 2,809,246 bp of total rDNA sequence, which corresponds to 328 to 334 units. Using read coverage for each chromosome separately, we found that the chromosome 8 array has 1,393,494 bp of sequence, or 129 copies based on HiFi, and 658,050 bp or 78 copies based on Nanopore. The chromosome 14 array has 1,667,328 bp of sequence or 198 copies based on HiFi, and 2,140,753 bp or 245 copies based on Nanopore. Thus, our coverage data supports the previous studies.

Coverage from our long read data sets provides evidence for 56 sites of organellar DNA insertions into the nucleus (Supplemental Table S11). Previous work using short reads observed AT-rich sequence thought to be plastid in origin linked to telomere sequences.³⁰¹ We observed plastid sequences linked to telomere sequence on chromosomes 2, 3, 5, 9, and 17, and mitochondrial sequence on the chromosome 14 telomere supported by <5 reads. A contig with mostly plastid sequence contained ~2 kb of nuclear sequence was supported by one read. BLAST aligned the nuclear portion of this contig to 12 genes (Supplemental Table S17). Thus, the evidence for telomere-linked plastid sequence is marginal.

Many eukaryotes modify cytosines in CpG dinucleotides by the addition of a methyl group at the C-5 position. This modification plays a multitude of functions that include transcriptional repression or genomic stability.^{302,303} Methylation is not utilized to the same degree in all eukaryotes. For example, yeast display very low levels of 5mC (<0.4%) and this varies depending on the life stage.²⁷⁰ We found, using detection of base modifications in Nanopore reads, that the average genome-wide 5mC frequency in *Chlamydomonas reinhardtii* was 2.13% in gametic CC-5816 cells. This average falls between two previous estimates (0.75% and 5.38%), which were determined using whole-genome bisulfate sequencing.^{268,269} Technical explanations for this variation include differences in sequencing technologies, bioinformatics pipelines, or the genome assembly used for alignment of reads. We chose to use Nanopolish that uses a hidden Markov model to detect base modifications from Nanopore reads. Benchmarking studies have demonstrated Nanopolish's accuracy in detecting modifications across a broad range of methylation frequency contexts, though one caveat to consider is that it has been shown it may sometimes overestimate methylation in low 5mC frequency regions.^{266,267} Biological explanations include differences in strains or the life stage. Feng et al.²⁶⁹ saw a genome-wide methylation frequency of 5.38% in vegetative cells from the *MT+* strain CC-503 with the CC-503 v3 assembly for read alignment. Lopez et al.,²⁶⁸ used a different strain and the CC-503 v5 assembly. They detected 5mC frequencies <0.75% using both plus and minus mating-type strains and saw little difference between zygotic, gametic, and vegetative cells.

Centromeres in many organisms are hypermethylated.^{304,305} DNA methylation appears important for binding of the centromere specific histone H3 (CenP/CEH3). Our data show that the *Chlamydomonas* centromeres are highly methylated compared to the rest of the chromosomal arms. Centromeres are required for chromatid cohesion and segregation during both meiotic and

mitotic cells divisions. Future studies will be interesting to ask about the rates of chromosome loss and meiotic recombination on different chromosomes with varying amounts of DNA methylation.³⁰⁶

Translocations Induced by CRISPR-Mediated Mutagenesis

Both insertional and targeted base pair alterations have been attempted using a variety of techniques in conjunction with CRISPR/Cas9. Gene editing is associated with the generation of tandem arrays. The *aphVII* gene was inserted into *pf23-2* and *pf23-3* in tandem arrays that contains both complete and truncated copies. We found 14 and 9 full-length copies of *aphVII* in *pf23-2* and *pf23-3*, respectively. This phenomenon has been reported in insertional mutagenesis of *S. pombe*, where tandem repeats of *ura4⁺* transgenic DNA were inserted at a single site by non-homologous end-joining.³⁰⁷ Another group reported similar results after transformation of *Magnaporthe oryzae* using transformation cassettes containing the hygromycin gene (*aphVII*).³⁰⁸ In *Chlamydomonas reinhardtii*, this occurrence has also been observed following insertional mutagenesis of the nuclear genome.^{309,310}

A translocation occurs when a chromosome breaks and the fragmented pieces re-attach to a different broken chromosome. Creighton and McClintock³¹¹ took advantage of a maize line that was heterozygous for a translocation between chromosomes 8 and 9 and carried a cytologically visible knob. Screening recombinant progeny provided irrevocable evidence that recombination involved physical exchange of DNA. Comparable results were also observed in *Drosophila* by Stern in 1931.³¹² Many species of evening primrose carry multiple reciprocal translocations and form multi-chromosomal meiotic rings involving all 14 chromosomes.³¹³ Evening primrose plants produce gametes with normal chromosomes and balanced translocation chromosomes. Chromosome rearrangements generated by gene-editing have been reported in human cell

lines.^{314–318} This should not be unexpected as the broken ends of double strand breaks (DSBs) generated in a CRISPR/Cas9 experiment at target sites, and off-target sites within a cell may fuse to form chromosomal translocations or inversions. CRISPR/Cas9 gene editing techniques have been used to intentionally make chromosomal aberrations in *Arabidopsis*³¹⁹ and in mammalian cells. The engineering of chromosomal changes has produced large deletions and insertions³²⁰ as well as inversions and translocations.^{321–323}

Two of three strains we obtained by targeting the *PF23* locus show meiotic viability patterns that are consistent with translocations. As has been observed in *S. cerevisiae*,²⁹¹ the frequency of inviability changes with the location of the centromere relative to the breakpoint. The proximity of the chromosome 3 breakpoint to the centromere may be associated with the increased number tetrads with one viable progeny. The generation of translocations seems to be specific to CRISPR-mediated mutagenesis in *Chlamydomonas*. Previously, we analyzed 20 insertional strains by tetrad analysis and failed to find patterns of meiotic lethality that suggests chromosome aberrations.¹⁸⁰

We do not know the frequency of chromosome aberrations associated with gene editing events in *Chlamydomonas* as most researchers do not perform meiotic crosses with the edited strains. It will be important to determine how frequently chromosome aberrations are generated. Monitoring and minimizing these cells with chromosome aberrations will be crucial for future applications of genome editing in *Chlamydomonas*.

Chapter 4: A closer look at dynein assembly and maturation factors in *Chlamydomonas reinhardtii*

4.1 Introduction

4.1.1 ODA8 is an ODA Maturation Factor

Motile cilia are intricately structured organelles whose primary function is to provide locomotion to cells or to direct fluid flow. The motility of cilia is generated by the action of ATPase motors called dyneins, that are attached to the A-tubules of the axoneme. The heads of the dyneins connect to the adjacent B-tubules where they ‘walk’. This generates a sliding motion that leads to bending of the cilia.^{77,79} Dyneins are pre-assembled in the cytoplasm by dynein arm assembly factors (DNAAFs)^{82,169,324} and made axoneme binding-competent by ODA maturation factors ODA5, ODA10, and ODA8.^{140–142,325}

One of the intriguing hits from our SSNC screen is ODA8. We observed SSNC in double heterozygous diploids with ODA8 and PF23, WDR92, and PF13. ODA8 is known as a ‘maturation factor’. Work by Desai et. al.³²⁵ in *Chlamydomonas* shows that *oda8* is localized to the cytoplasm and the cilia, though it is much more concentrated in the cytoplasm. They also use an HA-tagged strain of ODA8 to show that ODA8 is markedly reduced in the cilia of *oda5* and *oda10*, the other two maturation factors. They demonstrate that ODA8 is not necessary for ODAs to bind to axonemes. Co-immunoprecipitation experiments reveal that the assembly of the α -, β , and γ chains with the IC69 intermediate chains is reduced in the *oda8* mutant, although the abundance of these

proteins in the cytoplasm is unaffected, or slightly higher than wild-type. These data show that ODA8 is important for proper assembly of the ODA complex before it enters the cilia. A later study identified human patients with variants in *LRRC56*, the human orthologue of ODA8. These patients presented with defective mucociliary clearance and situs abnormalities. They performed immunofluorescence imaging in *Trypanosoma*; these data suggest that ODA8 localizes with an IFT protein, IFT88. Loss of ODA8 in the Trypanosomes resulted in the failure of ODAs to assemble in the distal axoneme²⁴. Additional total internal reflection fluorescence (TIRF) microscopy studies demonstrate that in an *oda8; oda6; IC2::NG-TG* strain, trafficking of IC2 (IC69) is infrequent, axonemal binding is rare, and the quantities of ODA8 in the axoneme are extremely low. The authors suggest that ODAs mostly enter the axoneme by diffusion and are unable to dock properly to axonemes in the *oda8* mutant³²⁶. These data present an interesting consideration about ODA8; it does not fit the description of a canonical DNAAF in *Chlamydomonas*, since its loss only results in the failure of ODAs to assemble in the cilia and the phenotype resembles other *oda* mutants. Secondly, it is not a core IFT component,¹⁶² but it appears to have a function related to proper trafficking of ODAs into the axoneme. Therefore, I wanted to learn more about its localization in the cytoplasm, potential genetic interactions with other proteins, and whether ODA8 colocalized with DNAAFs.

4.1.2 An Overview of Dynein Arm Assembly Factor PF23 in *Chlamydomonas reinhardtii*

PF23/DYX1C1 was first discovered in association with dyslexia, but this association remains controversial.^{327,328} Homozygous mutations in DYX1C1 cause a PCD phenotype in mice, zebrafish, and humans. In human epithelial cells and *Chlamydomonas*, PF23 localizes to the

cytoplasm. ultrastructural analyses show that both IDAs and ODAs fail to assemble in mouse and human cilia. In *Chlamydomonas*, the *pf23* mutant displays severely reduced IDAs and moderately reduced ODAs caused by a deletion in the DYX domain, one of four domains in PF23.^{199,200} This deletion results in a dynein arm pre-assembly defect. A wild-type copy of *PF23* restores wild-type function but transformation with a truncated *pf23* protein results in partial rescue, which suggests an important function for the additional C-terminal TPR domains. Interactions that were reported between PF23 and DNAAF2/PF13¹⁹⁹ and with PIH1D3³²⁹ (other pre-assembly proteins) in human cell lines could not be verified in *Chlamydomonas*. PF23 function is still poorly understood, but it is believed to have a scaffolding role during dynein arm cytoplasmic pre-assembly.³³⁰

4.2 Results

4.2.1 ODA8 Localizes to the Cytoplasm, Basal Body Regions, and Cilia of *Chlamydomonas*

Based on the current knowledge of ODA8, I wanted to ask about ODA8 localization in *Chlamydomonas* cytoplasm using confocal microscopy imaging. I obtained an ODA8::HA-TG plasmid³²⁵ and transformed it into the *oda8* mutant using electroporation. I screened plates for colonies that looked flat and pale green, rather than heaped and dark green; the former often represents wild-type colonies that can hatch from the mother cell wall and move away from the original colony. I obtained 6 transformants that were positive for both the *oda8* mutation and the *ODA8* wild-type transgene by PCR (Figure 1A). Strains 1-3-14 and 1-3-16 were obtained from the same plate and could be meiotic products from the same zygote, so only one of these was selected

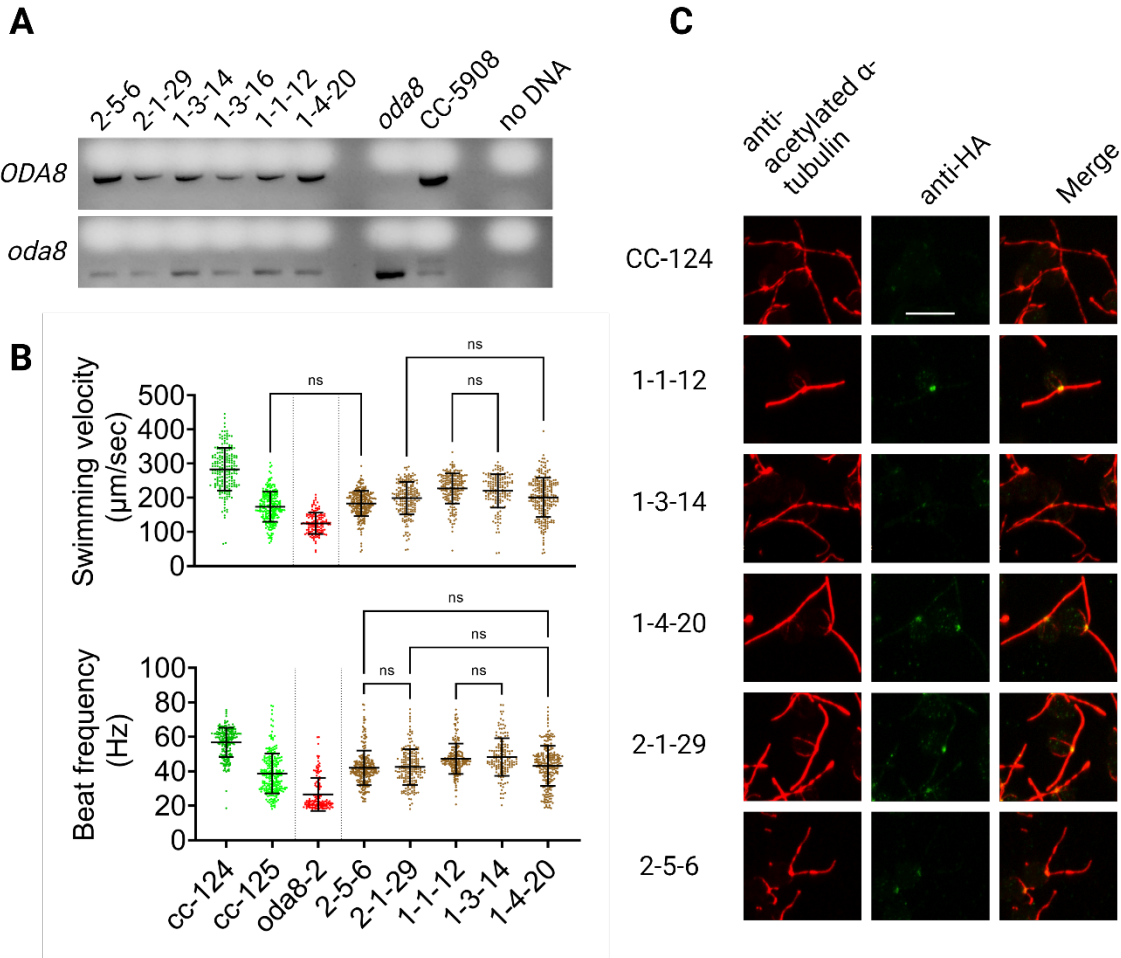


Figure 1: Screening and analysis of *oda8*; *ODA8::HA-TG* transgenic strains. (A) PCR analysis shows that transgenic strains (lanes 1-6) contain both the PCR product for the wild-type *ODA8* (top) and the mutant *oda8* (bottom). A mutant *oda8* strain and wild-type CC-5908 are shown for reference. (B) Quantification of swimming velocity (top) and beat frequency (bottom) of CC-124 and CC-125 wild-types and five transformants. (C) Immunofluorescence analysis of the five transformants assessed for swimming velocity in B. Scale bar measures 10 μm . Created with Biorender.com and GraphPad Prism.

for further analysis. All the other strains are independent transformants. To confirm rescue of the *oda8* mutation, I performed swimming velocity analysis of wild-types CC-124, CC-125, *oda8*, and five transformants. Figure 1B shows that swimming velocity of all 5 strains is rescued to the wild-type level of CC-125. Strain-specific differences have been shown between wild-type strains

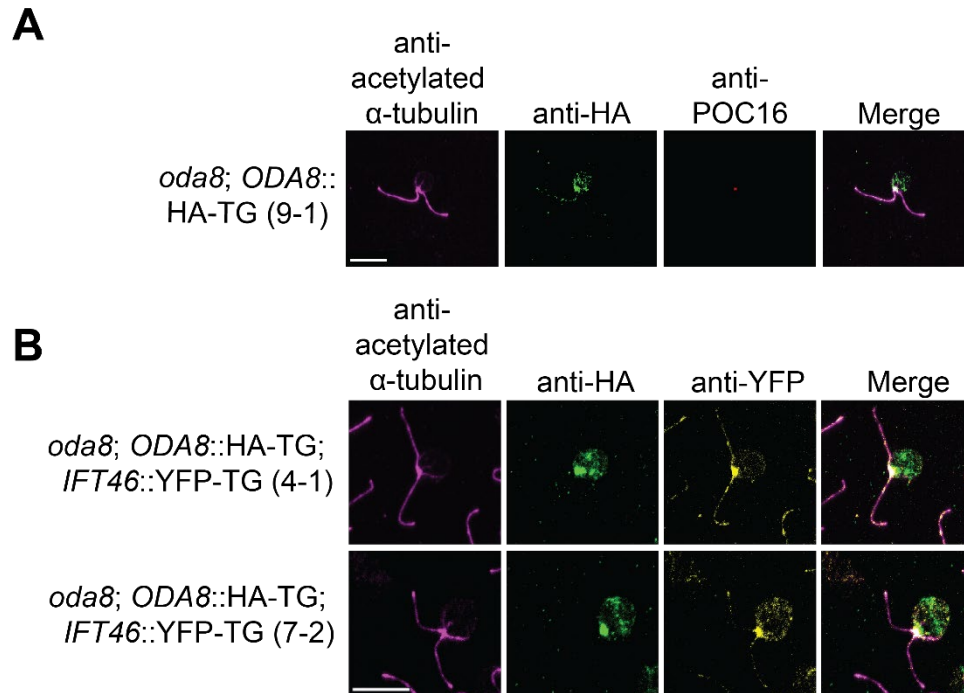


Figure 2: Assessment of ODA8 localization in *Chlamydomonas*. (A) Strain *oda8*; *ODA8*::HA-TG is stained for acetylated α -tubulin, HA-tagged ODA8, and basal body marker POC16. (B) . Two biological replicates of strain *oda8*; *ODA8*::HA-TG; *IFT46*::YFP-TG (4-1, top) and 7-2 (bottom) are stained with anti-acetylated α -tubulin, anti-HA and anti-YFP. (C) A *pf23-1*; *PF23*::HA-TG rescue strain is stained with anti-acetylated α -tubulin and anti-HA to assess PF23 localization in *Chlamydomonas* cytoplasm. The scale bar is 10 microns.

from the CLiP collection, strains CC-1690 and CC-5325.³³¹ Immunofluorescence analysis shows the HA tag attached to the ODA8 transgene is expressed. Strain 1-1-12 appeared to have the brightest signal by immunofluorescence, so this strain was selected for further studies (Figure 1C).

Additional immunofluorescence experiments show that ODA8 is present in the cytoplasm. There is also a weak ciliary signal. In many instances, ODA8 appears to form bright puncta, and many of them are concentrated around the base of the cilia at the region where IFT trains are loaded (Figure 2A).^{332,333} Co-staining with a basal body marker POC16³³⁴ shows that ODA8 puncta appear in the same region as POC16 (Figure 2A). This suggests that ODA8 is in the vicinity of the basal bodies.

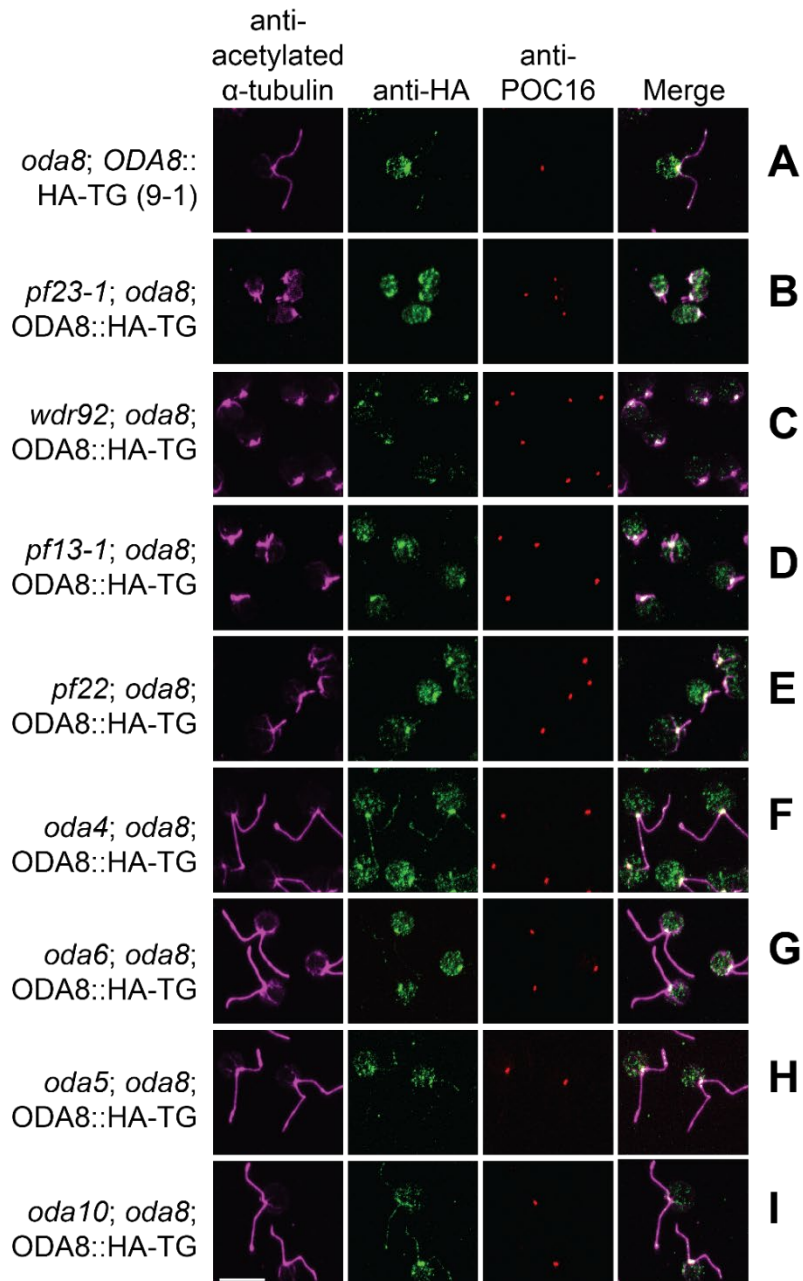


Figure 3: Analysis of ODA8-HA localization and abundance in dynein structural and DNAAF mutants. (A) An ODA8 transgenic strain from a cross between CC-125 and *oda8*; *ODA8*::HA-TG (1-1-12). (B-E) ODA8 transgenic strains crossed with DNAAF mutants. (F-G) ODA8 transgenic strains crossed with an ODA heavy chain and an ODA intermediate chain mutant, respectively. (H-I) ODA8 transgenic strains crossed with mutants in maturation factors ODA5 and ODA10, respectively. The scale bar is 10 microns.

ODA8 has been associated with IFT88 in *Trypanosomes*.²⁴ To ask whether ODA8 shows a similar localization pattern to IFT proteins in *Chlamydomonas*, we crossed the *oda8; ODA8::HA-TG* strain into the background of a strain with *IFT46::YFP-TG*.³³⁵ Interestingly, ODA8::HA appears to partially overlap the region where IFT46::YFP is localized in two independent strains from this cross (Figure 2B). This finding agrees with previous data and suggests that ODA8 could have some functional association with IFT. To gain some insight about ODA8 interaction partners, I wanted to ask whether ODA8 localization was dependent on the presence of dynein arm assembly factors (PF23, PF22, WDR92 and PF13), the dynein arm heavy chains and intermediate chains (ODA4 and ODA6, respectively) and accessory complex proteins ODA5 and ODA10.

Strains with mutations in each of these genes were crossed with *oda8; ODA8::HA-TG* (1-1-12). The double mutant strains with the ODA8 transgene were stained with an anti-HA antibody to see if ODA8 localization or abundance was affected. ODA8 localization to the basal body region appears slightly reduced in accessory complex proteins ODA5 and ODA10 (Figure 3H, 3I). Work by Desai and colleagues¹⁴¹ shows that ODA8 interacts genetically with ODA5 and ODA10 and it is unstable in these mutant backgrounds. However, no biochemical interaction of ODA8 with ODA5 and ODA10 was detected. ODA5 and ODA10 also have a localization pattern that is different from ODA8. These proteins localize to the proximal region of the cilia, with ODA10 only binding to one of the 9 axonemal doublets.^{141,142} Interestingly, WDR92 dynein arm assembly factor appears to affect ODA8 localization and abundance. In the *wdr92* mutant background, ODA8 puncta at the basal body region are smaller and less intense compared to the wild-type strain (Figure 3C). This needs to be confirmed with replicate experiments.

Recent work by the Avasthi lab³³⁶ demonstrates that the actin cytoskeleton is important for cilia assembly and localization of some proteins. The SAG protein, a mating-type agglutinin

present on the *Chlamydomonas* cell membrane is transported to the ciliary base and subsequently transported into the cilia for signaling during mating.³³⁷ Brae and colleagues show that disruption of the actin cytoskeleton either through a genetic mutant in the Arp2/3 complex or using Arp2/3 inhibitory drug CK-666 prevents SAG::HA from localizing to the basal body region. Thus, I wanted to ask whether an intact actin network was necessary for ODA8 localization to the basal body region. I treated *oda8*; *ODA8::HA-TG* cells with 250uM CK689 (inactive control) and 100μM or 250μM CK-666 (Arp 2/3 inhibitor) and performed immunofluorescence by co-staining

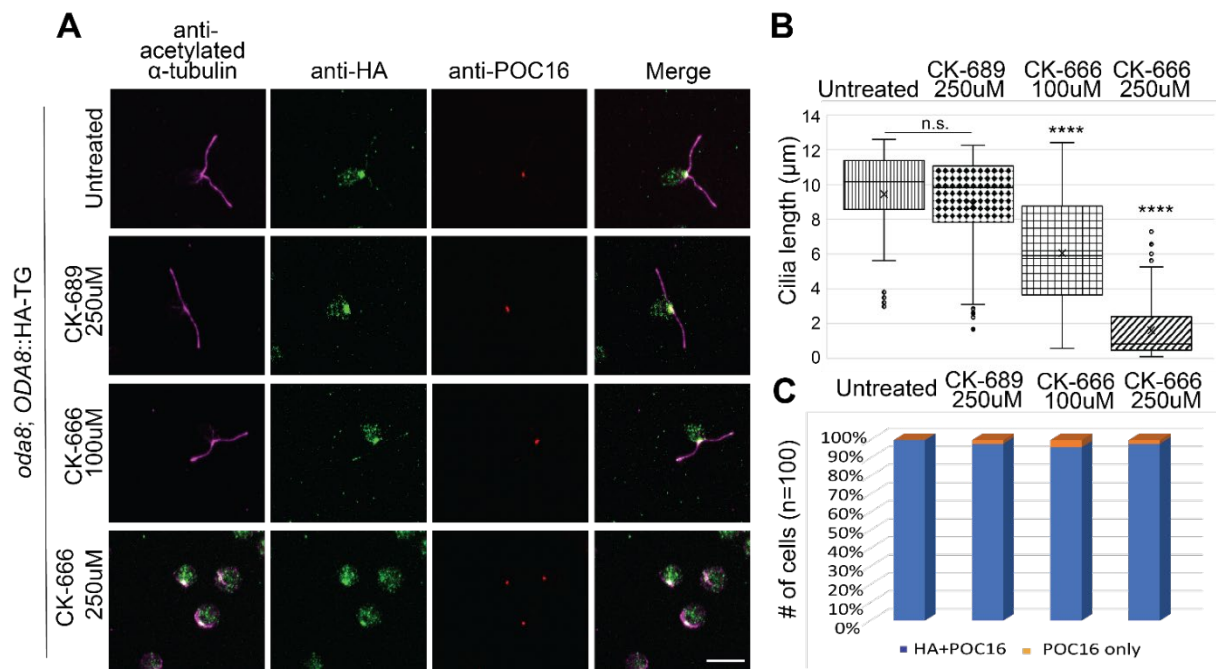


Figure 4: Actin cytoskeleton disruption affects cilia length but not ODA8 localization or abundance. (A) strain *oda8*; *ODA8::HA-TG* was treated for 1.5 hrs with CK-689 Arp 2/3 inactive control, or CK-666 Arp 2/3 complex inhibitor 1 at the concentrations indicated. Immunofluorescence staining was performed using anti-acetylated α -tubulin to observe changes in cilia length, and with anti-HA to measure perturbations to ODA8 localization or abundance. (B) Cilia length of the strains subjected to the experimental conditions in (A) are quantified. (C) Quantification of the number of cells in which ODA8 puncta co-localizes with POC16 for each condition in (A). The scale bar is 10 microns.

with anti-POC16, anti-HA, and anti-acetylated α -tubulin. As expected, treatment with CK-666 affects ciliary maintenance at steady state; cilia become shorter with increasing concentrations of the drug after a 1.5 hour incubation period (Figure 4A). However, it does not appear that Arp2/3

is necessary for ODA8 localization to the basal bodies since the staining indicates that puncta are still present at the basal body region identified by POC16 staining.

4.2.2 Dynein Assembly Factor PF23 Colocalizes With ODA Intermediate

Chain IC69

To learn more about PF23 localization in *Chlamydomonas*, I obtained strains with the *pf23-1* allele in the background in addition to the PF23::HA transgene.¹³⁶ First, I wanted to confirm PF23 cytoplasmic localization by immunofluorescence. I co-stained PF23::HA with anti-acetylated α -tubulin and anti-HA antibodies (Figure 5A). PF23 displays cytoplasmic localization, with a very strong signal that appears at the base of the cilia. This pattern resembles ODA8. Additionally, it appears that PF23 expression is upregulated following deciliation in a subset of cells.¹⁹¹ However, I was unable to test whether ODA8 and PF23 co-localized with each other since both strains contain an HA tag. I performed immunofluorescence on whole cells of *Chlamydomonas* using antibodies against the HA tag and IC69. Surprisingly, I observed that HA-tagged PF23 colocalizes with IC69 in some regions of the cell (indicated by white staining in merged images, Figure 5B).

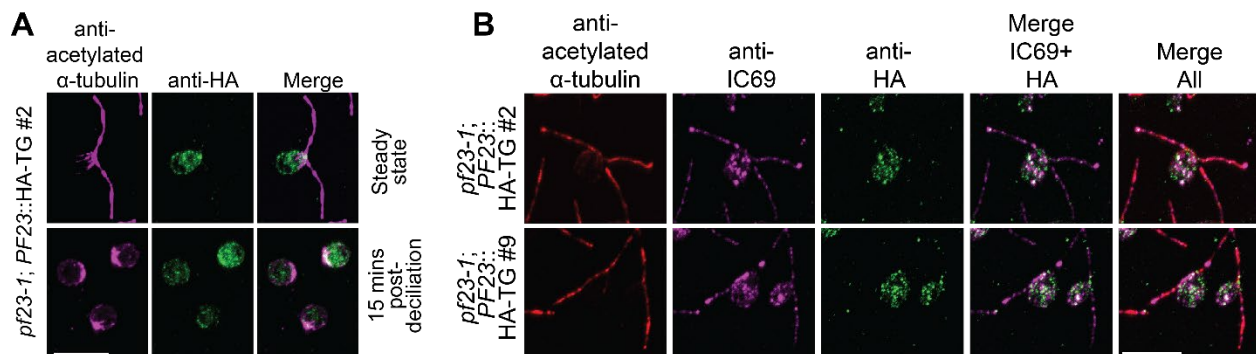


Figure 5: Localization dynamics of *pf23-1; PF23::HA-TG* (A) The PF23 HA-tagged transgenic strain is shown under steady-state conditions after growing in M-N/5 for 3 hours (top) and 15 mins post-deciliation (bottom). (B) The PF23 HA-tagged transgenic strain is co-stained for acetylated α -tubulin, IC69 and HA. Two independent strains are shown. A merged image that shows co-localization of IC69 and PF23::HA is shown in column 4.

4.3 Discussion

The biochemical role of ODA8 has been well studied regarding its role in dynein assembly. It is also known that there is a genetic interaction between ODA8, and ODA5 and ODA10, since loss of ODA5 or ODA10 results in a reduction in ODA8.³²⁵ However, no known physical interactors of ODA8 have been reported, although ODA8 appears to co-localize by immunofluorescence with IFT88.²⁴ The results I obtained with co-staining of IFT46::YFP-TG and ODA8::HA-TG appears to support an ODA8-IFT relationship, though additional experiments are needed to confirm this in *Chlamydomonas*.

I attempted to uncover genetic interactions of ODA8 with other assembly factors and dynein arm components, but these experiments returned negative results. It is imperative to obtain an antibody against ODA8, as this could yield more information about other proteins that ODA8 interacts with under native conditions. It is exciting that I was able to obtain results that indicate co-localization of PF23::HA-TG and IC69. This finding gives a preliminary indication that DyNAPs may exist in *Chlamydomonas reinhardtii*, and that dynein arm assembly factors and ODA structural proteins can accumulate in the same regions of the cell. Further immunofluorescence experiments that involve other DNAAFs are critical to continuing an investigation of this phenomenon in *Chlamydomonas reinhardtii*. Positive future results could support the DyNAP model and provide further insights into the dynein arm assembly process.

4.4 Materials and Methods

4.4.1 Strains and Reagents

The ODA8::HA-TG³²⁵ plasmid construct was obtained as a gift from Dr. David Mitchell (Suny Upstate Medical University). The *pf23-1*; *PF23*::HA-TG³³⁸ strain was a gift from Dr. Winfield Sale (Emory University). All other strains were obtained from the *Chlamydomonas* Resource Center (University of Minnesota). Crosses were performed according to standard procedures for the field.³³⁹

4.4.2 Transformation and Screening

To obtain the *oda8*; ODA8::HA-TG strain, I transformed the ODA8::HA-TG plasmid into the ODA8 strain using previously described methods with modifications.³⁴⁰ Briefly, cells were grown on TAP plates for 2 days at 25°C. They were then checked for the presence of cilia, spun down at 800 x g for 5 minutes. Cells were resuspended in MAX Efficiency™ Transformation Reagent for Algae (Invitrogen, A24229, lot #1886029) using the volume required to bring the cells to a final concentration of 8 x 10⁸ cells/ml. 125 µl of cells were placed into a 2mm electroporation cuvette (Bulldog Bio, 12358-346PT, lot #061020-2). 1 µg of ODA8::HA-TG plasmid was added to the cells along with 500ng of *aphviii* construct for a co-transformation to allow selection of transformed cells. The cells were electroporated using a NEPA21 (Nepa Gene, Japan) electroporator. The settings used were: Poring pulse at 250 V, 8 ms each, decay rate of 40%, 50 ms intervals, 2 pulses total, and Transfer pulse at 20V, 50 ms each, 40% decay rate, 50 ms intervals, 5 pulses total. The cells were immediately transferred to the 25°C incubator for 5 minutes for recovery. They were then resuspended in 10 ml of TAP + 150 mM mannitol in 15 ml conical

tubes, wrapped in aluminum foil to prevent exposure to light, and rocked continuously at 25°C overnight. The following day, the cells were spun down at 800 x g for 5 minutes, resuspended in 1 ml of TAP medium and spread onto 5 plates containing ¾ TAP + 100 µg/ml paromomycin. The plates were placed into the 25°C incubator for 3-5 days until transformants were grown. They were then picked into liquid TAP medium and screened visually for rescue by the presence of a wild-type swimming phenotype. The rescue was confirmed by PCR for both the wild-type ODA8 and the mutant *oda8* PCR products.

4.4.3 Swimming Velocity and Cilia Length Measurements

Swimming velocity was measured using previously described protocols.³⁴¹ To measure the cilia length, cells were allowed to grow cilia by resuspending them in M-N/5 medium for 3 hours. They were then fixed with 2% glutaraldehyde in phosphate buffer and allowed to settle onto Polylysine-coated slides. Cilia length measurements were performed using the protocol described in Materials and Methods, Chapter 2. For HA staining, the Anti-HA High Affinity Rat monoclonal antibody clone 3F10 (Roche, REF 11867423001, lot #42155800) was used at 1:500 concentration. The anti-rat HRP Alexa Flour 488 goat anti-rat-IgG antibody (Invitrogen API83P, lot number 2915317, 1:500 dilution) was used at a 1:1000 dilution.

4.4.4 Arp 2/3 Inhibitor Experimental Protocol

The cells used for this experiment were incubated at room temperature in light for 3 hours on a rocker in M-N/5. They were then spun down at 10,000 x g for 1 minute and resuspended in either CK-666 or CK-689 at the indicated concentrations for 1.5 hours at room temperature. The cells were then spun down again and resuspended in 1ml of autolysin with the appropriate

concentration of CK-666 or CK-689 for 40 minutes. The cells were then prepared for immunofluorescence using the protocol described in Materials and Methods, Chapter 2. The anti-POC16 antibody was a gift from Virginie Hamel and Paul Guichard.³⁴² It was used at a 1:750 concentration. The anti-rabbit HRP was used at 1:1000 concentration.

Chapter 5: Summary, Discussion, and Conclusion

5.1 Summary of findings

5.1.1 SSNC in *Chlamydomonas*

In this dissertation, I utilized the motile cilia model organism, *Chlamydomonas reinhardtii*, to investigate SSNC among motile cilia genes. In Chapter 2, I obtained motile cilia mutants across 20 loci from an existing repository, crossed them, and then subjected them to selection to generate 231 single and double heterozygous diploids and a wild-type diploid strain. None of the diploids show phenotypes under steady-state conditions. In a sensitized assay where cells the protein pool available to regenerate cilia is restricted by the addition of cycloheximide after deciliation, a select combination of DNAAFs show SSNC. I generated a null allele of the dynein arm assembly factor PF23 to assess the combined haploinsufficiency SSNC model in the *pf23-4/PF23; wdr92-1/WDR92* double heterozygous diploid. I show that the null *pf23* allele shows a more severe phenotype than the hypomorphic *pf23-1* allele; all ODAs and IDAs are missing from the cilia by mass spectrometry analysis. Additionally, PF23 and WDR92 appear to play a role in IC138 post-translational modification or assembly. I demonstrate by immunoblot analysis that PF23 exhibits a 50 percent dosage-dependent reduction in single heterozygotes. I also show that PF23 is further reduced in the *pf23-4/PF23; wdr92-1/WDR92* diploid in whole cell extracts of steady-state cells. Because both alleles are nulls, it is likely that the SSNC mechanism we observe in this strain is due to combined haploinsufficiency. This work indicates that SSNC can be a useful tool to learn

about the relationships between motile cilia genes in *Chlamydomonas* and reveal new insights about dynein arm assembly.

5.1.2 Null Alleles of the PF23 gene in *Chlamydomonas reinhardtii* contain translocations

To investigate the SSNC mechanism of combined haploinsufficiency in *Chlamydomonas* heterozygous diploids, I generated null *pf23* mutants *pf23-2*, *pf23-3*, and *pf23-4*. To achieve this, I used CRISPR/Cas9 targeted insertional mutagenesis of the *PF23* gene.³⁴³ In chapter 3, I show that the null *pf23* strains *pf23-2*, *pf23-3*, and *pf23-4* contain the insertional construct. Further analyses of these strains by my colleagues show that the *pf23-2* and *pf23-3* strains show meiotic inviability after crosses and that they contain translocations of the *PF23* gene with chromosomes 5 and 3, respectively. These findings imply that while CRISPR/Cas9 can be successfully applied to induce changes in the *Chlamydomonas* genome, special care must be taken to investigate the potential occurrence of second-site hits in these transformed strains.

5.1.3 DyNAPs in *Chlamydomonas*

In Chapter 4, I use immunofluorescence analysis to show that ODA8 may have biochemical or genetic interactions with WDR92. I also show that ODA8 abundance and localization appears unaffected by mutations in *PF22*, *PF13*, and *PF23*. ODA8 also does not appear to be affected by loss of ODAs. However, there may be a slight reduction in ODA8 expression in the background of the *oda5* and *oda10* maturation factor mutants. Additionally, ODA8 is not affected by changes in the actin cytoskeleton in *Chlamydomonas*. Preliminary immunofluorescence data shows co-localization between HA-tagged *PF23* protein and dynein arm

intermediate chain IC69. This suggests that there may be DyNAPs or DNAAF assembly factors in *Chlamydomonas* cytoplasm. Further experiments will be necessary to confirm this data.

5.2 Discussion of Findings and Future work

5.2.1 Models of SSNC in *Chlamydomonas reinhardtii*

In Chapter 2 of this dissertation, I utilized *Chlamydomonas reinhardtii*, a well-characterized model organism for motile cilia studies, to investigate whether SSNC occurs among dynein structural, transport, and assembly genes. There are three models of SSNC: the poison model requires allele-specificity at both loci, the sequestration model requires a specific allele at one locus only, and the combined haploinsufficiency model does not require allele specificity at either locus. Another mechanism, dominant enhancement, occurs when the phenotype observed in a heterozygote is worsened by the presence of a heterozygous mutation in another gene.⁸⁷

Previously, SSNC has been observed in *Chlamydomonas* among IFT genes with mutations that create temperature-sensitive IFT proteins. The cells can swim at the permissive temperature, but the cilia contain large bulbs at the end that contain IFT particles. This suggests that the mutation is not fully recessive. At the restrictive temperature, the cells completely lack cilia. When two of the temperature-sensitive IFT alleles are heterozygous in diploids, the cells fail to assemble cilia at both the permissive and restrictive temperatures.¹⁰⁵ This behavior suggests that the temperature-sensitive IFT mutants in *Chlamydomonas* exhibit dominant enhancement in heterozygous diploids.

Many of the strains that I utilized for the SSNC screen described in this work contain null alleles, or predicted null alleles based on the location of the mutation. Thus, in my screen, the predominant SSNC mechanism is likely to be combined haploinsufficiency. Indeed, SSNC

between strains *pf23-4* and *wdr92* occurs in the presence of null and predicted null alleles, respectively. I also observed SSNC in double heterozygous strains with *pf13* and *oda6* or *oda9*, though this combination was not examined further. Extensive analysis of the interactions between these three proteins is already described. However, these are the only two combinations I obtained where one of the heterozygous alleles is a dynein arm assembly factor and the other is a structural gene. ODA6 and ODA9 are highly interdependent on each other for stability. I hypothesize that SSNC in this instance may be due to the reduction of all three factors, PF13, ODA6, and ODA9. For example, in the *pf13/PF13; oda6;ODA6* diploid, a reduction of PF13 and ODA6 could lead to the concurrent reduction of ODA9. This will be an interesting hypothesis to test in future studies.

One additional question to consider is the limiting factor that contributes to the cilia regeneration phenotypes that I observe. Cycloheximide affects global protein synthesis including tubulin, the core building block of the axoneme. Therefore, the question arises of whether it is a limitation of the tubulin pool that affects cilia regeneration in my SSNC strains, or if the phenotype arises because of reductions in dynein arm assembly factor and dynein structural protein pools. Work by Baker *et. al.* shows that the tubulin pool is rapidly upregulated after deciliation.³⁴⁴ Therefore, it is highly possible that restricting tubulin synthesis with cycloheximide can impair cilia regeneration. However, since all the strains in my screen are subjected to the same conditions, I argue that the phenotypes I observe are a direct result of reduction of the genes in question – these phenotypes may be additive to any other phenotypes caused by reduced tubulin availability.

In my work, I demonstrate that PF23 exhibits a dosage-dependent phenotype. In the single heterozygous strain, PF23 is reduced by half, and is further reduced in the *pf23-4/PF23; wdr92-1/WDR92* double heterozygote in steady-state cells. Immunoblot analysis of dynein arm components IC138, IC69 and axonemal component RIB43a did not reveal consistent significant

differences of these proteins in the heterozygotes compared to wild-type. Due to the unavailability of reagents, I was unable to test other assembly factors with their corresponding antibodies to ask whether they show similar dosage effects. These experiments would provide additional insight into the mechanism of SSNC occurring among DNAAFs. Furthermore, because the dosage-dependent reduction in PF23 that I observe is in steady-state cells, I hypothesize that this phenotype will be exacerbated in strains that are subjected to the sensitized deciliation assay where protein synthesis is restricted. It is also possible that there will be a change in the abundance of dynein structural components, or in the stability of assembled dyneins.

5.2.2 SSNC among the *Chlamydomonas* mutants selected is gene-specific

It is interesting to note that I did not observe SSNC among steady state heterozygous diploids, or among motile cilia mutants in dynein structural genes like dynein heavy and intermediate chains, ODA maturation factors and docking complex, or radial spoke component *pf14* under the sensitized condition of cycloheximide treatment. One DNAAF, PF22, did not show SSNC with other assembly factors or dynein structural proteins. Notably, PF22 did not appear to interact with other dynein arm assembly factors by co-immunoprecipitation.¹³⁵ It is possible PF22 functions separately from other DNAAFs, or that the interactions are very transient.

Work by Rosenbaum *et. al.* shows that the pool of proteins in the cytoplasm is sufficient to rebuild half-length cilia without additional protein synthesis.¹¹³ We also know that the expression of motile cilia genes is massively upregulated after deciliation.¹⁹¹ This novel protein synthesis must provide the additional components needed for complete cilia regeneration that are lacking due to limiting factors in the presence of cycloheximide. It is possible that the size of the

pool of proteins that is maintained in double heterozygous strains is sufficient for normal ciliogenesis and function under steady-state conditions.

The total protein complement in double heterozygotes in the motile cilia gene categories mentioned above appears to be sufficient for normal cilia regeneration in cycloheximide. Perhaps there is a minimum threshold of structural protein products needed for normal dynein assembly, and I was unable to generate the conditions needed to reduce the threshold significantly enough to produce a phenotype. It may be important to test other conditions like changes in temperature or pH to see if this affects the phenotypes that I observed. Another interesting approach will be to attempt this screen using motile cilia mutants that have been crossed into a strain with a sensitized background. For example, the actin mutant *ida5* exhibits slow regeneration after deciliation, even though the cilia eventually reach wild-type length.³⁴⁵

5.2.3 The Mechanism Behind Short Cilia Phenotypes in *Chlamydomonas*

The SSNC phenotypes I observe in my screen are based on cilia length regeneration in a sensitized environment.¹¹³ In *Chlamydomonas*, dynein arm assembly factor mutants, and *ccdc39* and *ccdc40* mutants have short cilia,¹⁸⁶ but strains with mutations in dynein arm proteins do not. Assembly factor mutants in *Chlamydomonas* show loss of ODAs and IDAs in the cilia to varying degrees. In most cases, both ODAs and IDAs are severely affected.

Previous analysis of the *pf23-1* allele causes mostly loss of IDAs with a moderate reduction in ODAs. The *pf23-4* null allele I generated completely lacks the PF23 protein, and all the ODAs and IDAs are missing from the cilia. This raises two important points. Firstly, it is important to know the characteristics of the mutant allele under question before any deductions about SSNC mechanisms can be made. There are clear differences between the *pf23-1*

hypomorphic allele and the *pf23-4* null allele. Analysis of the new *pf23-4* allele overturns a longstanding belief that PF23 is primarily responsible for the assembly of IDAs. Secondly, the cilia of the *pf23-4* strains are significantly shorter than the *pf23-1* strain under gametic conditions. Although the difference is not large, it suggests that there is a relationship between the severity of simultaneous loss ODAs and IDAs and cilia length. Other work shows that *oda*; *ida* double mutants have short cilia and are paralyzed.^{173,346,347} In contrast, strains with only *oda* or *ida* mutations have normal length cilia.

These data imply that a normal complement of both ODAs and IDAs are needed to maintain full-length cilia in *Chlamydomonas*. When ODAs and IDAs are lost, it is probable that the 9+2 axonemal doublet becomes unstable and depolymerizes (or fails to grow). Work by Lin *et. al.* shows that mutants in *cnk11* (a NIMA-related kinase) and *tpg1* suppress the length phenotypes of *ccdc39* and/or *ccdc40* mutants that lack several axonemal components.¹⁸⁶ The *tpg1* mutation (a tubulin polyglutamylase) also partially suppresses the short cilia phenotype in the *wdr92-1* mutant strain.¹³⁷ In my work, the *cnk11* mutation fully rescued the cilia length phenotype in the *pf23-4* strain. However, I noticed that this cilia length rescue was not stable. If the cells were left in media lacking nitrogen for longer than 3-5 hours, the cilia began to resorb or depolymerize. Exposing these strains to fixation and other experimental measures for immunofluorescence also caused the cilia to fall apart. I am curious about other conditions that lead to axonemal instability in the *pf23*; *cnk11* strains, and what conditions may stabilize the length rescue we observe.

Together, these results suggest that cilia length stability in *Chlamydomonas* may depend on the presence of certain combinations of axonemal components that include both ODAs and IDAs, as well as various tubulin post-translational modifications. It will be interesting to explore

the mechanism by which the cilia length suppression occurs, as well as possibly discover other suppressors that may have an important role in cilia assembly/maintenance in relation to DNAAFs.

5.2.4 A Consideration of DyNAPs in *Chlamydomonas*

There are many unanswered questions with regards to how dynein arm assembly occurs, and which factors co-operate with each other during the process. Because there are many overlaps between the phenotypes seen across different DNAAFs, it is difficult to fully distinguish where each DNAAF acts in the assembly pathway, although several models have been presented.^{207,348,349} The concept of DyNAPs was proposed by Wallingford's group using overexpression constructs in *Xenopus*. They show that DNAAFs co-localize with dynein structural proteins and with each other, and that stress granule proteins are also present in these biomolecular condensates. Furthermore, they show that there is sub-compartmentalization of ODA and IDA assembly within these DyNAPs.^{350,351} Another model proposes that the aggregation of DNAAFs is not related to the formation of biomolecular condensates, but rather that there are multiple instances of translation of large dyneins occurring simultaneously that generate assembly 'factories'.³²⁴

In Chapter 4, I began to explore the question of whether DyNAPs exist in *Chlamydomonas reinhardtii*. I also wanted to learn more about the relationship between ODA8 and other DNAAFs, since several hits in my SSNC screen involved ODA8 and dynein arm assembly factors, although no interaction has been shown between those two groups thus far. Analysis of an HA-tagged ODA8 strain shows that ODA8 appears reduced in the *wdr92* mutant, but not other assembly factors. This will be an interesting discovery to perform further studies

on, since the *oda8/ODA8; wdr92/WDR92* diploid shows the most severe phenotype out of all the SSNC hits. It is possible that there is a genetic or biochemical interaction between ODA8 and WDR92. A second experiment shows that HA-tagged PF23 co-localizes with IC69. Although these results are preliminary, it presents the exciting possibility that DNAAFs and dynein arm components may form DyNAPs in *Chlamydomonas*, like that observed in Huizar's studies. Importantly, these HA-tagged strains are expressed under their endogenous promoters. This gives the opportunity to observe localization under native conditions and reduces the possibility of false positive aggregation due to excessive proteins in the cell.

I have begun to generate c-terminal fluorescently tagged strains of other DNAAFs with their endogenous promoters to ask whether I can observe co-localization between dynein assembly factors in addition to localization of DNAAFs with dynein structural components. This work will be important to shed further light on the dynein assembly process in *Chlamydomonas*, and perhaps have broader implications for dynein assembly.

5.3 Conclusions

In the work discussed in this dissertation, I show that SSNC occurs among dynein arm assembly factors in *Chlamydomonas reinhardtii*. The dynein arm assembly factor PF23 shows SSNC in the *pf23-4/PF23; wdr92-1/WDR92* double heterozygote. The mechanism for this appears to be a combined haploinsufficiency. To date, there are no reported cases of SSNC in human PCD patients. Given that approximately 30 percent of clinical PCD diagnoses remain without genetic etiology, it is important to consider the possibility that some patients may have double heterozygous hits in motile cilia genes. The phenotypes I observed manifested when the cells were placed under very specific stress conditions. It may be important to examine patients

who have mild PCD phenotypes or a subset of PCD-related symptoms for the possibility of double heterozygous mutations. Additionally, patients who are double heterozygotes for motile cilia mutations may have difficulty recovering from insults to their motile cilia due to illness or injury. Although this is an unfounded hypothesis, it is certainly an interesting idea worth consideration.

Many examples of SSNC exhibit the poison or dominant enhancement mechanisms of action. I was unable to test these models using the mutant strains that were available. The inability to detect additional SSNC combinations in my screen may be because I did not have the right alleles to generate a phenotype in the combinations tested. Furthermore, I only tested a limited subset of genes and there are more than 20 other genes that I was unable to test, including some additional assembly factors.

Finally, given that the number of known PCD genes has increased from 35 to over 50 in less than 10 years, I am convinced that there are many more PCD genes that are yet undiscovered. Therefore, the possibility of SSNC among motile cilia genes in humans may still exist.

References

1. Leeuwenhoek, A. van. Observations, communicated to the publisher by Mr. Antony van Leewenhoek, in a dutch letter of the 9th Octob. 1676. here English'd: concerning little animals by him observed in rain-well-sea- and snow water; as also in water wherein pepper had lain infused. *Philos Trans R Soc Lond* **12**, 821–831 (1677).
2. Purkinje, J. & Valentin, G. Entdeckung continuerlicher durch Wimperhaare erzeugter Flimmerbewegungen. *Arch Anat Physiol Wiss Med* **3**, 391–400 (1834).
3. Gray, J. The mechanism of ciliary movement. *Proceedings of the Royal Society of London. Series B, Containing Papers of a Biological Character* **93**, 104–121 (1922).
4. Gray, J. The mechanism of ciliary movement.—VI. Photographic and stroboscopic analysis of ciliary movement. *Proceedings of the Royal Society of London. Series B, Containing Papers of a Biological Character* *93(650) 104-121* **93**, 104–121 (1930).
5. Afzelius, B. Electron Microscopy of the Sperm Tail Results Obtained with a New Fixative. *J Biophys Biochem Cytol* **5**, 269–278 (1959).
6. Gibbons, I. R. THE RELATIONSHIP BETWEEN THE FINE STRUCTURE AND DIRECTION OF BEAT IN GILL CILIA OF A LAMELLIBRANCH MOLLUSC. *J Biophys Biochem Cytol* **11**, 179–205 (1961).
7. Gibbons, I. R. & Grimstone, A. v. On Flagellar Structure in Certain Flagellates. *J Biophys Biochem Cytol* **7**, 697–716 (1960).
8. Gibbons, I. R. & Rowe, A. J. Dynein: A Protein with Adenosine Triphosphatase Activity from Cilia. *Science (1979)* **149**, 424–426 (1965).
9. Summers, K. E. & Gibbons, I. R. Adenosine Triphosphate-Induced Sliding of Tubules in Trypsin-Treated Flagella of Sea-Urchin Sperm. *Proceedings of the National Academy of Sciences* **68**, 3092–3096 (1971).
10. Gibbons, B. H. & Gibbons, I. R. The Effect of Partial Extraction of Dynein Arms on the Movement of Reactivated Sea-Urchin Sperm. *J Cell Sci* **13**, 337–357 (1973).
11. Niziolek, M. *et al.* PCD Genes—From Patients to Model Organisms and Back to Humans. *International Journal of Molecular Sciences* *2022, Vol. 23, Page 1749* **23**, 1749 (2022).
12. Lee, L. & Ostrowski, L. E. Motile cilia genetics and cell biology: big results from little mice. *Cellular and Molecular Life Sciences* *2020 78:3* **78**, 769–797 (2020).

13. Becker-Heck, A. *et al.* The coiled-coil domain containing protein CCDC40 is essential for motile cilia function and left-right axis formation. *Nature Genetics* 2010 43:1 **43**, 79–84 (2010).
14. Pinto, A. L. *et al.* Zebrafish Motile Cilia as a Model for Primary Ciliary Dyskinesia. *International Journal of Molecular Sciences* 2021, Vol. 22, Page 8361 **22**, 8361 (2021).
15. Austin-Tse, C. *et al.* Zebrafish Ciliopathy Screen Plus Human Mutational Analysis Identifies C21orf59 and CCDC65 Defects as Causing Primary Ciliary Dyskinesia. *The American Journal of Human Genetics* **93**, 672–686 (2013).
16. Werner, M. E. & Mitchell, B. J. Understanding ciliated epithelia: The power of *Xenopus*. *genesis* **50**, 176–185 (2012).
17. Stubbs, J. L., Oishi, I., Izpisua Belmonte, J. C. & Kintner, C. The forkhead protein Foxj1 specifies node-like cilia in *Xenopus* and zebrafish embryos. *Nature Genetics* 2008 40:12 **40**, 1454–1460 (2008).
18. Omran, H. *et al.* Ktu/PF13 is required for cytoplasmic pre-assembly of axonemal dyneins. *Nature* 2008 456:7222 **456**, 611–616 (2008).
19. Hojo, M. *et al.* Right-elevated expression of charon is regulated by fluid flow in medaka Kupffer's vesicle. *Wiley Online Library* **49**, 395–405 (2007).
20. Rompolas, P., Patel-King, R. S. & King, S. M. *Schmidtea mediterranea*: A Model System for Analysis of Motile Cilia. *Methods Cell Biol* **93**, 81–98 (2009).
21. Patel-King, R. S. & King, S. M. A prefoldin-associated WD-repeat protein (WDR92) is required for the correct architectural assembly of motile cilia. *Mol Biol Cell* **27**, 1204–1209 (2016).
22. Morga, B. & Bastin, P. Getting to the heart of intraflagellar transport using *Trypanosoma* and *Chlamydomonas* models: The strength is in their differences. *Cilia* **2**, 1–16 (2013).
23. Gadelha, C. *et al.* Basal body and flagellum mutants reveal a rotational constraint of the central pair microtubules in the axonemes of trypanosomes. *J Cell Sci* **119**, 2405–13 (2006).
24. Bonnefoy, S. *et al.* Biallelic Mutations in LRRC56, Encoding a Protein Associated with Intraflagellar Transport, Cause Mucociliary Clearance and Laterality Defects. *The American Journal of Human Genetics* **103**, 727–739 (2018).
25. Valentine, M. & Van Houten, J. Using *Paramecium* as a Model for Ciliopathies. *Genes* 2021, Vol. 12, Page 1493 **12**, 1493 (2021).

26. Loges, N. T. *et al.* Recessive DNAH9 Loss-of-Function Mutations Cause Laterality Defects and Subtle Respiratory Ciliary-Beating Defects. *Am J Hum Genet* **103**, 995–1008 (2018).
27. Stoddard, D. *et al.* Tetrahymena RIB72A and RIB72B are microtubule inner proteins in the ciliary doublet microtubules. *Mol Biol Cell* **29**, 2566–2577 (2018).
28. Brown, J. M., Marsala, C., Kosoy, R. & Gaertig, J. Kinesin-II is preferentially targeted to assembling cilia and is required for ciliogenesis and normal cytokinesis in Tetrahymena. *Mol Biol Cell* **10**, 3081–3096 (1999).
29. Sale, W. S. & Satir, P. Direction of active sliding of microtubules in Tetrahymena cilia. *Proc Natl Acad Sci U S A* **74**, 2045–2049 (1977).
30. Coggin, S. J. & Kochert, G. FLAGELLAR DEVELOPMENT AND REGENERATION IN VOLVOX CARTERI (CHLOROPHYTA)1. *J Phycol* **22**, 370–381 (1986).
31. Brumley, D. R., Polin, M., Pedley, T. J. & Goldstein, R. E. Metachronal waves in the flagellar beating of Volvox and their hydrodynamic origin. *J R Soc Interface* **12**, (2015).
32. Harris, E. *The Chlamydomonas sourcebook: introduction to Chlamydomonas and its laboratory use.* (2009).
33. Zivert, A. Über einen Fall von Bronchiectasie bei einem Patienten mit situs inversus viscerum. *Berliner klinische Wochenschrift* **41**, 3–3 (1904).
34. Kartagener M. Zur. Pathogenese der Bronchiectasien. Bronchiectasien bei Situs inversus viscerum. *Beitr Klin Tuberk* **83**, 489–501 (1933).
35. Afzelius, B. A. A human syndrome caused by immotile cilia. *Science (1979)* **193**, 317–319 (1976).
36. Rossman, C. M., Forrest, J. B., Lee, R. M. K. W. & Newhouse, M. T. The Dyskinetic Cilia Syndrome: Ciliary Motility in Immotile Cilia Syndrome. *Chest* **78**, 580–582 (1980).
37. Bartoloni, L. *et al.* Mutations in the DNAH11 (axonemal heavy chain dynein type 11) gene cause one form of situs inversus totalis and most likely primary ciliary dyskinesia. *Proc Natl Acad Sci U S A* **99**, 10282–10286 (2002).
38. Guichard, C. *et al.* Axonemal Dynein Intermediate-Chain Gene (DNAI1) Mutations Result in Situs Inversus and Primary Ciliary Dyskinesia (Kartagener Syndrome). *The American Journal of Human Genetics* **68**, 1030–1035 (2001).
39. Nakhleh, N. *et al.* High prevalence of respiratory ciliary dysfunction in congenital heart disease patients with heterotaxy. *Circulation* **125**, 2232–2242 (2012).

40. Kennedy, M. P. *et al.* Congenital Heart Disease and Other Heterotaxic Defects in a Large Cohort of Patients With Primary Ciliary Dyskinesia. *Circulation* **115**, 2814–2821 (2007).
41. Li, Y. *et al.* DNAH6 and Its Interactions with PCD Genes in Heterotaxy and Primary Ciliary Dyskinesia. *PLoS Genet* **12**, e1005821 (2016).
42. Essner, J. J. *et al.* Conserved function for embryonic nodal cilia. *Nature* **418**, 37–38 (2002).
43. Okada, Y., Takeda, S., Tanaka, Y., Belmonte, J. C. I. & Hirokawa, N. Mechanism of Nodal Flow: A Conserved Symmetry Breaking Event in Left-Right Axis Determination. *Cell* **121**, 633–644 (2005).
44. Sironen, A., Shoemark, A., Patel, M., Loebinger, M. R. & Mitchison, H. M. Sperm defects in primary ciliary dyskinesia and related causes of male infertility. *Cellular and Molecular Life Sciences* **77**, 2029–2048 (2019).
45. Horani, A., Ferkol, T. W., Dutcher, S. K. & Brody, S. L. Genetics and biology of primary ciliary dyskinesia. *Paediatric Respiratory Reviews* vol. 18 18–24 Preprint at <https://doi.org/10.1016/j.prrv.2015.09.001> (2016).
46. Leigh, M. W. *et al.* Primary ciliary dyskinesia (PCD): A genetic disorder of motile cilia. *Transl Sci Rare Dis* **4**, 51–75 (2019).
47. Davis, S. D. *et al.* Clinical features of childhood primary ciliary dyskinesia by genotype and ultrastructural phenotype. *Am J Respir Crit Care Med* **191**, 316–324 (2015).
48. Zariwala, M. A., Knowles, M. R. & Leigh, M. W. Primary Ciliary Dyskinesia. *GeneReviews*® (2019).
49. Goutaki, M. & Shoemark, A. Diagnosis of Primary Ciliary Dyskinesia. *Clin Chest Med* **43**, 127–140 (2022).
50. Hannah, W. B. *et al.* The global prevalence and ethnic heterogeneity of primary ciliary dyskinesia gene variants: a genetic database analysis. *Lancet Respir Med* **10**, 459–468 (2022).
51. Henriques, A. R. *et al.* Primary ciliary dyskinesia due to CCNO mutations—A genotype-phenotype correlation contribution. *Pediatr Pulmonol* **56**, 2776–2779 (2021).
52. Wang, L. na, Gao, L. wei, Liu, X. yun & Xu, B. ping. Mutations in CCNO Result in Primary Ciliary Dyskinesia Complicated with Diffuse Bronchiolitis. *Indian J Pediatr* (2023) doi:10.1007/S12098-023-04543-7.

53. Xu, X. *et al.* Establishment of an induced pluripotent stem cell line from a patient with primary ciliary dyskinesia carrying biallelic mutations in CCNO. *Elsevier*.
54. Ma, C. *et al.* Bi-allelic mutations in MCIDAS and CCNO cause human infertility associated with abnormal gamete transport. *Wiley Online Library* **100**, 731–742 (2021).
55. Horani, A. & Ferkol, T. W. Advances in the Genetics of Primary Ciliary Dyskinesia: Clinical Implications. *Chest* **154**, 645–652 (2018).
56. Al Mutairi, F. *et al.* Homozygous truncating NEK10 mutation, associated with primary ciliary dyskinesia: a case report. *BMC Pulm Med* **20**, 141 (2020).
57. Shapiro, A. J. *et al.* Autosomal dominant variants in FOXJ1 causing primary ciliary dyskinesia in two patients with obstructive hydrocephalus. *Wiley Online Library* **9**, 1726 (2021).
58. Wallmeier, J., Frank, D., ... A. S.-T. A. J. of & 2019, undefined. De novo mutations in FOXJ1 result in a motile ciliopathy with hydrocephalus and randomization of left/right body asymmetry. *Elsevier*.
59. Becker-Heck, A. *et al.* The coiled-coil domain containing protein CCDC40 is essential for motile cilia function and left-right axis formation. *Nat Genet* **43**, 79–84 (2011).
60. Antony, D. *et al.* Mutations in CCDC39 and CCDC40 are the Major Cause of Primary Ciliary Dyskinesia with Axonemal Disorganization and Absent Inner Dynein Arms. *Hum Mutat* **34**, 462–472 (2013).
61. Merveille, A. C. *et al.* CCDC39 is required for assembly of inner dynein arms and the dynein regulatory complex and for normal ciliary motility in humans and dogs. *Nat Genet* **43**, 72–78 (2011).
62. Loges, N. T. *et al.* Deletions and Point Mutations of LRRC50 Cause Primary Ciliary Dyskinesia Due to Dynein Arm Defects. *The American Journal of Human Genetics* **85**, 883–889 (2009).
63. Duquesnoy, P. *et al.* Loss-of-Function Mutations in the Human Ortholog of *Chlamydomonas reinhardtii* ODA7 Disrupt Dynein Arm Assembly and Cause Primary Ciliary Dyskinesia. *The American Journal of Human Genetics* **85**, 890–896 (2009).
64. Tarkar, A. *et al.* DYX1C1 is required for axonemal dynein assembly and ciliary motility. *Nat Genet* **45**, 995–1003 (2013).
65. Tarkar, A. *et al.* DYX1C1 is required for axonemal dynein assembly and ciliary motility. *Nat Genet* **45**, 995–1003 (2013).

66. Knowles, M. R. *et al.* Mutations in SPAG1 Cause Primary Ciliary Dyskinesia Associated with Defective Outer and Inner Dynein Arms. *The American Journal of Human Genetics* **93**, 711–720 (2013).
67. Vos, R. *et al.* New DNAH11 mutations in primary ciliary dyskinesia with normal axonemal ultrastructure. *Eur Respiratory Soc* doi:10.1183/09031936.00183509.
68. Knowles, M. R. *et al.* Mutations of DNAH11 in patients with primary ciliary dyskinesia with normal ciliary ultrastructure. *thorax.bmj.com* doi:10.1136/thoraxjnl-2011-200301.
69. Wheway, G. *et al.* Whole genome sequencing in the diagnosis of primary ciliary dyskinesia. *BMC Med Genomics* **14**, 1–21 (2021).
70. Shapiro, A. J. *et al.* Diagnosis, monitoring, and treatment of primary ciliary dyskinesia: PCD foundation consensus recommendations based on state of the art review. *Pediatr Pulmonol* **51**, 115–132 (2016).
71. Onoufriadis, A. *et al.* Combined exome and whole-genome sequencing identifies mutations in ARMC4 as a cause of primary ciliary dyskinesia with defects in the outer dynein arm. *J Med Genet* **51**, 61–67 (2014).
72. Marshall, C. R. *et al.* Whole-exome sequencing and targeted copy number analysis in primary ciliary dyskinesia. *G3: Genes, Genomes, Genetics* **5**, 1775–1781 (2015).
73. Reiter, J. F. & Leroux, M. R. Genes and molecular pathways underpinning ciliopathies. *Nature Reviews Molecular Cell Biology* vol. 18 533–547 Preprint at <https://doi.org/10.1038/nrm.2017.60> (2017).
74. Pazour, G. J., Agrin, N., Leszyk, J. & Witman, G. B. Proteomic analysis of a eukaryotic cilium. *Journal of Cell Biology* **170**, 103–113 (2005).
75. Li, J. B. *et al.* Comparative Genomics Identifies a Flagellar and Basal Body Proteome that Includes the BBS5 Human Disease Gene. *Cell* **117**, 541–552 (2004).
76. Gherman, A., Davis, E. E. & Katsanis, N. The ciliary proteome database: an integrated community resource for the genetic and functional dissection of cilia. *Nature Genetics* **2006 38:9 38**, 961–962 (2006).
77. Ishikawa, T. Axoneme Structure from Motile Cilia. *Cold Spring Harb Perspect Biol* **9**, a028076 (2017).
78. Nogales, E., Whittaker, M., Milligan, R. A. & Downing, K. H. High-resolution model of the microtubule. *Cell* **96**, 79–88 (1999).

79. Bhabha, G., Johnson, G. T., Schroeder, C. M. & Vale, R. D. How Dynein Moves Along Microtubules. *Trends in Biochemical Sciences* vol. 41 94–105 Preprint at <https://doi.org/10.1016/j.tibs.2015.11.004> (2016).
80. Brokaw, C. J. & Kamiya, R. Bending patterns of Chlamydomonas flagella: IV. Mutants with defects in inner and outer dynein arms indicate differences in dynein arm function. *Cell Motil Cytoskeleton* **8**, 68–75 (1987).
81. Porter, M. E., Power, J. & Dutcher, S. K. Extragenic suppressors of paralyzed flagellar mutations in Chlamydomonas reinhardtii identify loci that alter the inner dynein arms. *Journal of Cell Biology* **118**, 1163–1176 (1992).
82. King, S. M. Composition and assembly of axonemal dyneins. in *Dyneins: The Biology of Dynein Motors: Second Edition* 163–201 (Elsevier Inc., 2017). doi:10.1016/B978-0-12-809471-6.00005-X.
83. Viswanadha, R., Sale, W. S. & Porter, M. E. Ciliary motility: Regulation of axonemal dynein motors. *Cold Spring Harb Perspect Biol* **9**, a018325 (2017).
84. Desai, P. B., Dean, A. B. & Mitchell, D. R. Cytoplasmic preassembly and trafficking of axonemal dyneins. in *Dyneins: The Biology of Dynein Motors: Second Edition* 141–161 (Elsevier Inc., 2017). doi:10.1016/B978-0-12-809471-6.00004-8.
85. Qiu, T. & Roy, S. Ciliary dynein arms: Cytoplasmic preassembly, intraflagellar transport, and axonemal docking. *J Cell Physiol* **237**, 2644–2653 (2022).
86. Zschocke, J., Byers, P. H. & Wilkie, A. O. M. Mendelian inheritance revisited: dominance and recessiveness in medical genetics. *Nature Reviews Genetics* **2023** 1–22 (2023) doi:10.1038/s41576-023-00574-0.
87. Hawley, R. S. & Gilliland, W. D. Sometimes the Result Is Not the Answer: The Truths and the Lies That Come From Using the Complementation Test. *Genetics* **174**, 5–15 (2006).
88. Fincham, J. R. S. & Coddington, A. The mechanism of complementation between am mutants of Neurospora crassa. *Cold Spr. Harb. Symp. quant. Biol.* **28**, 517–527 (1963).
89. Fincham, J. R. S. & Stadler, D. R. Complementation relationships of Neurospora am mutants in relation to their formation of abnormal varieties of glutamate dehydrogenase. *Genet Res (Camb)* **6**, 121–129 (1965).
90. Fincham, J. R. S. Genetically determined multiple forms of glutamic dehydrogenase in Neurospora crassa. *J. Mol. Biol.* **4**, 257–274 (1962).

91. FINCHAM, J. R. On the nature of the glutamic dehydrogenase produced by interallelic complementation at the am locus of *Neurospora crassa*. *J. gen. Microbiol.* **21**, 600–611 (1958).
92. Nashed, N., Jabbur, G. & Zimmermann, F. K. Negative complementation among ad2mutants of yeast. *MGG Molecular & General Genetics* **99**, 69–75 (1967).
93. Zariwala, M. A. *et al.* Mutations of DNAI1 in Primary Ciliary Dyskinesia. <https://doi.org/10.1164/rccm.200603-370OC> **174**, 858–866 (2012).
94. Austin-Tse, C. *et al.* Zebrafish Ciliopathy Screen Plus Human Mutational Analysis Identifies C21orf59 and CCDC65 Defects as Causing Primary Ciliary Dyskinesia. *The American Journal of Human Genetics* **93**, 672–686 (2013).
95. Knowles, M. R. *et al.* Mutations of DNAH11 in patients with primary ciliary dyskinesia with normal ciliary ultrastructure. *Thorax* **67**, 433–441 (2012).
96. Thiel, C. *et al.* NEK1 Mutations Cause Short-Rib Polydactyly Syndrome Type Majewski. *The American Journal of Human Genetics* **88**, 106–114 (2011).
97. Loewen, C. J. R., Moritz, O. L. & Molday, R. S. Molecular Characterization of Peripherin-2 and Rom-1 Mutants Responsible for Digenic Retinitis Pigmentosa. *Journal of Biological Chemistry* **276**, 22388–22396 (2001).
98. Kajiwara, K., Berson, E. L. & Dryja, T. P. Digenic Retinitis Pigmentosa Due to Mutations at the Unlinked Peripherin/RDS and ROM1 Loci. *Science (1979)* **264**, 1604–1608 (1994).
99. Stearns, T. & Botstein, D. Unlinked noncomplementation: isolation of new conditional-lethal mutations in each of the tubulin genes of *Saccharomyces cerevisiae*. *Genetics* **119**, 249–260 (1988).
100. Hays, T. S., Deuring, R., Robertson, B., Prout, M. & Fuller, M. T. Interacting proteins identified by genetic interactions: a missense mutation in alpha-tubulin fails to complement alleles of the testis-specific beta-tubulin gene of *Drosophila melanogaster*. *Mol Cell Biol* **9**, 875–884 (1989).
101. Rancourt, D. E., Tsuzuki, T. & Capecchi, M. R. Genetic interaction between *hoxb-5* and *hoxb-6* is revealed by nonallelic noncomplementation. *Genes Dev* **9**, 108–122 (1995).
102. Davis, A. P. & Capecchi, M. R. A mutational analysis of the 5' *HoxD* genes: Dissection of genetic interactions during limb development in the mouse. *Development* **122**, (1996).
103. Debeer, P., Bacchelli, C., Scambler, P. J., De Smet, L. & Fryns, J.-P. Severe digital abnormalities in a patient heterozygous for both a novel missense mutation in *HOXD13*

- and a polyalanine tract expansion in HOXA13. *jmg.bmj.com* (2002)
doi:10.1136/jmg.39.11.852.
104. Yook, K. J., Proulx, S. R. & Jorgensen, E. M. Rules of Nonallelic Noncomplementation at the Synapse in *Caenorhabditis elegans*. *Genetics* **158**, 209–220 (2001).
 105. Iomini, C., Li, L., Esparza, J. M. & Dutcher, S. K. Retrograde Intraflagellar Transport Mutants Identify Complex A Proteins With Multiple Genetic Interactions in *Chlamydomonas reinhardtii*. *Genetics* **183**, 885–896 (2009).
 106. Dutcher, S. K., Gibbons, W. & Inwood, W. B. A genetic analysis of suppressors of the PF10 mutation in *Chlamydomonas reinhardtii*. *Genetics* **120**, 965–976 (1988).
 107. Lamb, M., Dutcher, S., Worley, C., Genetics, C. D.- & 1999, undefined. Eyespot-assembly mutants in *Chlamydomonas reinhardtii*. *academic.oup.com*.
 108. Phytologist, J. H.-T. N. & 1953, undefined. The function of the eyespot in *Chlamydomonas*. *JSTOR*.
 109. Roberts, D., Lamb, M., Genetics, C. D.- & 2001, undefined. Characterization of the EYE2 Gene Required for Eyespot Assembly in *Chlamydomonas reinhardtii*. *academic.oup.com*.
 110. Matsuura, K., Lefebvre, P. A., Kamiya, R. & Hirono, M. Bld10p, a novel protein essential for basal body assembly in *Chlamydomonas* localization to the cartwheel, the first ninefold symmetrical structure appearing during assembly. *Journal of Cell Biology* **165**, 663–671 (2004).
 111. Nakazawa, Y., Hiraki, M., Kamiya, R. & Hirono, M. SAS-6 is a Cartwheel Protein that Establishes the 9-Fold Symmetry of the Centriole. *Current Biology* **17**, 2169–2174 (2007).
 112. Foster, K. W. Analysis of the Ciliary/Flagellar Beating of *Chlamydomonas*. *Methods Cell Biol* **91**, 173–239 (2009).
 113. Rosenbaum, J. L., Moulder, J. E. & Ringo, D. L. Flagellar elongation and shortening in *Chlamydomonas*. The use of cycloheximide and colchicine to study the synthesis and assembly of flagellar proteins. *J Cell Biol* **41**, 600–19 (1969).
 114. Blaby, I. K. *et al.* The *Chlamydomonas* genome project: a decade on. *Trends Plant Sci* **19**, 672–680 (2014).
 115. Craig, R. J. *et al.* The *Chlamydomonas* Genome Project, version 6: reference assemblies for mating type plus and minus strains reveal extensive structural mutation in the laboratory. (2022) doi:10.1101/2022.06.16.496473.

116. Gallaher, S. D. *et al.* High-throughput sequencing of the chloroplast and mitochondrion of *Chlamydomonas reinhardtii* to generate improved de novo assemblies, analyze expression patterns and transcript speciation, and evaluate diversity among laboratory strains and wild isolates. *The Plant Journal* **93**, 545–565 (2018).
117. Merchant, S. S. *et al.* The *Chlamydomonas* Genome Reveals the Evolution of Key Animal and Plant Functions. *Science* **318**, 245–250 (2007).
118. Payne, Z. L., Penny, G. M., Turner, T. N. & Dutcher, S. K. A gap-free genome assembly of *Chlamydomonas reinhardtii* and detection of translocations induced by CRISPR-mediated mutagenesis. *Plant Commun* **4**, 100493 (2023).
119. Silflow, C. D. & Lefebvre, P. A. Assembly and Motility of Eukaryotic Cilia and Flagella. Lessons from *Chlamydomonas reinhardtii*. *Plant Physiol* **127**, 1500–1507 (2001).
120. Lefebvre, P. A., Laudon, M. & Silflow, C. The *chlamydomonas* resource center. *The Biological Resources of Model Organisms* 95–111 (2019) doi:10.1201/9781315100999-6/CHLAMYDOMONAS-RESOURCE-CENTER-PAUL-LEFEBVRE-MATTHEW-LAUDON-CAROLYN-SILFLOW.
121. Li, X. *et al.* A genome-wide algal mutant library and functional screen identifies genes required for eukaryotic photosynthesis. *Nature Genetics* 2019 51:4 **51**, 627–635 (2019).
122. Kamiya, R. Mutations at twelve independent loci result in absence of outer dynein arms in *Chlamydomonas reinhardtii*. *Journal of Cell Biology* **107**, 2253–2258 (1988).
123. Sakakibara, H., Mitchell, D. R. & Kamiya, R. A *Chlamydomonas* outer arm dynein mutant missing the alpha heavy chain. *Journal of Cell Biology* **113**, 615–622 (1991).
124. Wilkerson, C. G., King, S. M. & Witman, G. B. Molecular analysis of the gamma heavy chain of *Chlamydomonas* flagellar outer-arm dynein. *J Cell Sci* **107**, 497–506 (1994).
125. Porter, M. E., Knott, J. A., Gardner, L. C., Mitchell, D. R. & Dutcher, S. K. Mutations in the SUP-PF-1 locus of *Chlamydomonas reinhardtii* identify a regulatory domain in the beta-dynein heavy chain. *Journal of Cell Biology* **126**, 1495–1507 (1994).
126. Huang, B., Ramanis, Z. & Luck, D. J. L. Suppressor mutations in *chlamydomonas* reveal a regulatory mechanism for flagellar function. *Cell* **28**, 115–124 (1982).
127. Mitchell, D. R. & Kang, Y. Identification of *oda6* as a *Chlamydomonas* dynein mutant by rescue with the wild-type gene. *Journal of Cell Biology* **113**, 835–842 (1991).
128. Wilkerson, C. G., King, S. M., Koutoulis, A., Pazour, G. J. & Witman, G. B. The 78,000 M(r) intermediate chain of *Chlamydomonas* outer arm dynein is a WD-repeat protein required for arm assembly. *Journal of Cell Biology* **129**, 169–178 (1995).

129. Pazour, G. J. *et al.* LC2, the Chlamydomonas homologue of the t complex-encoded protein Tctex2, is essential for outer dynein arm assembly. *Mol Biol Cell* **10**, 3507–3520 (1999).
130. Oda, T., Abe, T., Yanagisawa, H. & Kikkawa, M. Docking-complex-independent alignment of Chlamydomonas outer dynein arms with 24-nm periodicity in vitro. *J Cell Sci* **129**, 1547–1551 (2016).
131. Ide, T., Owa, M., King, S. M., Kamiya, R. & Wakabayashi, K. I. Protein–protein interactions between intermediate chains and the docking complex of Chlamydomonas flagellar outer arm dynein. *FEBS Lett* **587**, 2143–2149 (2013).
132. Takada, S., Wilkerson, C. G., Wakabayashi, K. I., Kamiya, R. & Witman, G. B. The outer dynein arm-docking complex: Composition and characterization of a subunit (Oda1) necessary for outer arm assembly. *Mol Biol Cell* **13**, 1015–1029 (2002).
133. Koutoulis, A. *et al.* The Chlamydomonas reinhardtii ODA3 Gene Encodes a Protein of the Outer Dynein Arm Docking Complex. *Journal of Cell Biology* **137**, 1069–1080 (1997).
134. Casey, D. M. *et al.* DC3, the 21-kDa subunit of the outer dynein arm-docking complex (ODA-DC), is a novel EF-hand protein important for assembly of both the outer arm and the ODA-DC. *Mol Biol Cell* **14**, 3650–3663 (2003).
135. Schmidts, M. *et al.* Mutations in the dynein assembly factor PF22 (DNAAF3) cause primary ciliary dyskinesia with absent dynein arms. *Cilia* **2012 1:1** 1, 1–1 (2012).
136. Yamamoto, R. *et al.* Chlamydomonas DYX1C1/PF23 is essential for axonemal assembly and proper morphology of inner dynein arms. *PLoS Genet* **13**, e1006996 (2017).
137. Patel-King, R. S., Sakato-Antoku, M., Yankova, M. & King, S. M. WDR92 is required for axonemal dynein heavy chain stability in cytoplasm. *Mol Biol Cell* **30**, 1834–1845 (2019).
138. Liu, G., Wang, L., Pan, J. & Yao, X. Chlamydomonas WDR92 in association with R2TP-like complex and multiple DNAAFs to regulate ciliary dynein preassembly. *J Mol Cell Biol* **11**, 770–780 (2019).
139. Freshour, J., Yokoyama, R. & Mitchell, D. R. Chlamydomonas flagellar outer row dynein assembly protein Oda7 interacts with both outer row and I1 inner row dyneins. *Journal of Biological Chemistry* **282**, 5404–5412 (2007).
140. Wirschell, M. *et al.* Oda5p, a novel axonemal protein required for assembly of the outer dynein arm and an associated adenylate kinase. *Mol Biol Cell* **15**, 2729–2741 (2004).

141. Dean, A. B. & Mitchell, D. R. Late steps in cytoplasmic maturation of assembly-competent axonemal outer arm dynein in *Chlamydomonas* require interaction of ODA5 and ODA10 in a complex. *Mol Biol Cell* **26**, 3596–3605 (2015).
142. Dean, A., cell, D. M.-M. biology of the & 2013, undefined. *Chlamydomonas* ODA10 is a conserved axonemal protein that plays a unique role in outer dynein arm assembly. *Am Soc Cell Biol* **24**, 3689–3696 (2013).
143. Desai, P. B., Freshour, J. R. & Mitchell, D. R. *Chlamydomonas* axonemal dynein assembly locus ODA8 encodes a conserved flagellar protein needed for cytoplasmic maturation of outer dynein arm complexes. *Cytoskeleton* **72**, 16–28 (2015).
144. Ahmed, N. T. & Mitchell, D. R. ODA16p, a *chlamydomonas* flagellar protein needed for dynein assembly. *Mol Biol Cell* **16**, 5004–5012 (2005).
145. Ahmed, N. T., Gao, C., Lucker, B. F., Cole, D. G. & Mitchell, D. R. ODA16 aids axonemal outer row dynein assembly through an interaction with the intraflagellar transport machinery. *Journal of Cell Biology* **183**, 313–322 (2008).
146. Hunter, E. L. *et al.* The IDA3 adapter, required for intraflagellar transport of I1 dynein, is regulated by ciliary length. *Mol Biol Cell* **29**, 886–896 (2018).
147. Gui, M. *et al.* Structures of radial spokes and associated complexes important for ciliary motility. *Nature Structural & Molecular Biology* 2020 28:1 **28**, 29–37 (2020).
148. Williams, B. D., Velleca, M. A., Curry, A. M. & Rosenbaum, J. L. Molecular cloning and sequence analysis of the *Chlamydomonas* gene coding for radial spoke protein 3: flagellar mutation pf-14 is an ochre allele. *Journal of Cell Biology* **109**, 235–245 (1989).
149. Craige, B., Brown, J. M. & Witman, G. B. Isolation of *Chlamydomonas* Flagella. *Curr Protoc Cell Biol* **59**, 3.41.1-3.41.9 (2013).
150. Nicastro, D. *et al.* Cryo-electron tomography reveals conserved features of doublet microtubules in flagella. *Proceedings of the National Academy of Sciences* **108**, E845–E853 (2011).
151. Starling, D., Research, J. R.-G. & 1971, undefined. The flagella of temporary dikaryons of *Chlamydomonas reinhardtii*. *cambridge.org* **18**, 107–113 (1971).
152. Dutcher, S. K. The awesome power of dikaryons for studying flagella and basal bodies in *Chlamydomonas reinhardtii*. *Cytoskeleton* **71**, 79–94 (2014).
153. Ebersold, W. T. *Chlamydomonas reinhardtii*: Heterozygous Diploid Strains. *New Series* **157**, 447–449 (1967).

154. Ferris, P. J. & Goodenough, U. W. Mating Type in Chlamydomonas Is Specified by mid, the Minus-Dominance Gene. *Genetics* **146**, (1997).
155. Dutcher, S. K. Nuclear fusion-defective phenocopies in Chlamydomonas reinhardtii: mating-type functions for meiosis can act through the cytoplasm. *Proc Natl Acad Sci U S A* **85**, 3946–3950 (1988).
156. Wetherell, D. F. & Krauss, R. W. Colchicine-induced polyploidy in chlamydomonas. *Science (1979)* **124**, 25–26 (1956).
157. Joo, S. *et al.* Gene Regulatory Networks for the Haploid-to-Diploid Transition of Chlamydomonas reinhardtii [OPEN]. *Plant Physiol* **175**, 314–332 (2017).
158. Zamora, I., Feldman, J. L. & Marshall, W. F. PCR-based assay for mating type and diploidy in Chlamydomonas. *Biotechniques* **37**, 534–536 (2004).
159. Matagne, R. F., Remacle, C. & Dinant, M. Cytofusion in Chlamydomonas reinhardtii. *Proceedings of the National Academy of Sciences* **88**, 7447–7450 (1991).
160. Matagne, R., Deltour, R., Nature, L. L.- & 1979, undefined. Somatic fusion between cell wall mutants of Chlamydomonas reinhardtii. *Springer*.
161. Galloway, R. E. & Goodenough, U. W. GENETIC ANALYSIS OF MATING LOCUS LINKED MUTATIONS IN CHLAMYDOMONAS REINHARDTII. *Genetics* **111**, 447–461 (1985).
162. Lacey, S. E., Foster, H. E. & Pigino, G. The molecular structure of IFT-A and IFT-B in anterograde intraflagellar transport trains. *Nature Structural & Molecular Biology* **2023** 1–10 (2023) doi:10.1038/s41594-022-00905-5.
163. IFT-A structure reveals carriages for membrane protein transport into cilia. *Elsevier*.
164. Lin, H., Miller, M. L., Granas, D. M. & Dutcher, S. K. Whole Genome Sequencing Identifies a Deletion in Protein Phosphatase 2A That Affects Its Stability and Localization in Chlamydomonas reinhardtii. *PLoS Genet* **9**, e1003841 (2013).
165. Omran, H. *et al.* Ktu/PF13 is required for cytoplasmic pre-assembly of axonemal dyneins. *Nature* **2008** 456:7222 **456**, 611–616 (2008).
166. Koutoulis, A. *et al.* The Chlamydomonas reinhardtii ODA3 Gene Encodes a Protein of the Outer Dynein Arm Docking Complex. *J Cell Biol* **137**, (1997).
167. Published, ; *et al.* DC3, the Smallest Subunit of the Chlamydomonas Flagellar Outer Dynein Arm-docking Complex, Is a Redox-sensitive Calcium-binding Protein*. *Mol. Biol. Cell* **14**, 3650–3663 (2003).

168. Mitchell, D. R. & Kang, Y. Reversion analysis of dynein intermediate chain function. *J Cell Sci* **105**, 1069–1078 (1993).
169. Fowkes, M. E. & Mitchell, D. R. The role of preassembled cytoplasmic complexes in assembly of flagellar dynein subunits. *Mol Biol Cell* **9**, 2337–2347 (1998).
170. Sakakibara, H., Mitchell, D. R. & Kamiya, R. A Chlamydomonas outer arm dynein mutant missing the α heavy chain. *Journal of Cell Biology* **113**, 615–622 (1991).
171. Li, X. *et al.* A genome-wide algal mutant library and functional screen identifies genes required for eukaryotic photosynthesis. *Nature Genetics* **2019 51:4 51**, 627–635 (2019).
172. Ahmed, N. T. & Mitchell, D. R. ODA16p, a chlamydomonas flagellar protein needed for dynein assembly. *Mol Biol Cell* **16**, 5004–5012 (2005).
173. Hunter, E. L. *et al.* The IDA3 adapter, required for intraflagellar transport of II dynein, is regulated by ciliary length. *Mol Biol Cell* **29**, 886–896 (2018).
174. Kyuji, A., Patel-King, R. S., Hisabori, T., King, S. M. & Wakabayashi, K. I. Cilia loss and dynein assembly defects in planaria lacking an outer arm dynein docking complex subunit. *Zoolog Sci* **37**, 7 (2020).
175. Mosley, A. *et al.* Characterization of a new oda3 allele, oda3-6, defective in assembly of the outer dynein arm-docking complex in Chlamydomonas reinhardtii. *PLoS One* **12**, (2017).
176. Casey, D., Inaba, K., Pazour, G., ... S. T.-M. biology of & 2003, undefined. DC3, the 21-kDa subunit of the outer dynein arm-docking complex (ODA-DC), is a novel EF-hand protein important for assembly of both the outer arm and the ODA. *Am Soc Cell Biol*.
177. Pazour, G. J. *et al.* LC2, the Chlamydomonas homologue of the t complex-encoded protein Tctex2, is essential for outer dynein arm assembly. *Mol Biol Cell* **10**, 3507–3520 (1999).
178. Kamiya, R. & Okamoto, M. A mutant of Chlamydomonas reinhardtii that lacks the flagellar outer dynein arm but can swim. *J Cell Sci* **VOL. 74**, 181–191 (1985).
179. Kamiya, R. Mutations at twelve independent loci result in absence of outer dynein arms in Chlamydomonas reinhardtii. *Journal of Cell Biology* **107**, 2253–2258 (1988).
180. Lin, H., Cliften, P. F. & Dutcher, S. K. MAPINS, a Highly Efficient Detection Method That Identifies Insertional Mutations and Complex DNA Rearrangements. *Plant Physiol* **178**, 1436–1447 (2018).

181. Dent, R. M. *et al.* Large-scale insertional mutagenesis of *Chlamydomonas* supports phylogenomic functional prediction of photosynthetic genes and analysis of classical acetate-requiring mutants. *The Plant Journal* **82**, 337–351 (2015).
182. Walton, T., Wu, H. & Brown, A. Structure of a microtubule-bound axonemal dynein. *Nature Communications* 2021 12:1 **12**, 1–9 (2021).
183. Hendrickson, T. W. *et al.* IC138 is a WD-repeat dynein intermediate chain required for light chain assembly and regulation of flagellar bending. *Mol Biol Cell* **15**, 5431–5442 (2004).
184. Habermacher, G. & Sale, W. S. Regulation of Flagellar Dynein by Phosphorylation of a 138-kD Inner Arm Dynein Intermediate Chain. *Journal of Cell Biology* **136**, 167–176 (1997).
185. Yang, P. & Sale, W. S. Casein kinase I is anchored on axonemal doublet microtubules and regulates flagellar dynein phosphorylation and activity. *Journal of Biological Chemistry* **275**, 18905–18912 (2000).
186. Lin, H. *et al.* A NIMA-Related Kinase Suppresses the Flagellar Instability Associated with the Loss of Multiple Axonemal Structures. *PLoS Genet* **11**, e1005508 (2015).
187. Patel-King, R. S., Sakato-Antoku, M., Yankova, M. & King, S. M. WDR92 is required for axonemal dynein heavy chain stability in cytoplasm. *Mol Biol Cell* **30**, 1834–1845 (2019).
188. Terhorst, A. *et al.* The environmental stress response causes ribosome loss in aneuploid yeast cells. *Proc Natl Acad Sci U S A* **117**, 17031–17040 (2020).
189. Schloss, J. A., Silflow, C. D. & Rosenbaum, J. L. mRNA abundance changes during flagellar regeneration in *Chlamydomonas reinhardtii*. *Mol Cell Biol* **4**, 424–434 (1984).
190. Baker, E. J., Schloss, J. A. & Rosenbaum, J. L. Rapid changes in tubulin RNA synthesis and stability induced by deflagellation in *Chlamydomonas*. *Journal of Cell Biology* **99**, 2074–2081 (1984).
191. Albee, A. J. *et al.* Identification of Cilia Genes That Affect Cell-Cycle Progression Using Whole-Genome Transcriptome Analysis in *Chlamydomonas reinhardtii*. *G3: Genes|Genomes|Genetics* **3**, 979–991 (2013).
192. Lefebvre, P. A. Genetic control of cilia length in *Chlamydomonas*. *The Chlamydomonas Sourcebook* 337–355 (2023) doi:10.1016/B978-0-12-822508-0.00006-X.
193. Tam, L. W., Wilson, N. F. & Lefebvre, P. A. A CDK-related kinase regulates the length and assembly of flagella in *Chlamydomonas*. *Journal of Cell Biology* **176**, 819–829 (2007).

194. Tam, L. W., Ranum, P. T. & Lefebvre, P. A. CDKL5 regulates flagellar length and localizes to the base of the flagella in *Chlamydomonas*. *Mol Biol Cell* **24**, 588–600 (2013).
195. Nguyen, R. L., Tam, L. W. & Lefebvre, P. A. The LF1 Gene of *Chlamydomonas reinhardtii* Encodes a Novel Protein Required for Flagellar Length Control. *Genetics* **169**, 1415–1424 (2005).
196. JARVIK, J. W., REINHART, F. D., KUCHKA, M. R. & ADLER, S. A. Altered Flagellar Size-Control in shf-1 Short-Flagella Mutants of *Chlamydomonas reinhardtii*. *J Protozool* **31**, 199–204 (1984).
197. Perlaza, K., Mirvis, M., Ishikawa, H. & Marshall, W. The short flagella 1 (SHF1) gene in *Chlamydomonas* encodes a Crescerin TOG-domain protein required for late stages of flagellar growth. *Mol Biol Cell* **33**, (2022).
198. Bradley, B. A. & Quarmby, L. M. A NIMA-related kinase, Cnk2p, regulates both flagellar length and cell size in *Chlamydomonas*. *J Cell Sci* **118**, 3317–3326 (2005).
199. Tarkar, A. *et al.* DYX1C1 is required for axonemal dynein assembly and ciliary motility. *Nature Genetics* *2013* **45**:9 **45**, 995–1003 (2013).
200. Chandrasekar, G., Vesterlund, L., Hultenby, K., Tapia-Páez, I. & Kere, J. The Zebrafish Orthologue of the Dyslexia Candidate Gene DYX1C1 Is Essential for Cilia Growth and Function. *PLoS One* **8**, e63123 (2013).
201. Takada, S. & Kamiya, R. Functional reconstitution of *Chlamydomonas* outer dynein arms from alpha-beta and gamma subunits: requirement of a third factor. *J Cell Biol* **126**, 737–745 (1994).
202. Lin, J. *et al.* FAP57/WDR65 targets assembly of a subset of inner arm dyneins and connects to regulatory hubs in cilia. *Mol Biol Cell* **30**, 2659–2680 (2019).
203. Bustamante-Marin, X. M. *et al.* Mutation of CFAP57, a protein required for the asymmetric targeting of a subset of inner dynein arms in *Chlamydomonas*, causes primary ciliary dyskinesia. *PLoS Genet* **16**, e1008691 (2020).
204. King, S. J. & Dutcher, S. K. Phosphoregulation of an Inner Dynein Arm Complex in *Chlamydomonas reinhardtii* Is Altered in Phototactic Mutant Strains. *Journal of Cell Biology* **136**, 177–191 (1997).
205. VanderWaal, K. E. *et al.* bop5 mutations reveal new roles for the IC138 phosphoprotein in the regulation of flagellar motility and asymmetric waveforms. *Mol Biol Cell* **22**, 2862–2874 (2011).

206. Habermacher, G. & Sale, W. S. Regulation of Flagellar Dynein by Phosphorylation of a 138-kD Inner Arm Dynein Intermediate Chain. *Journal of Cell Biology* **136**, 167–176 (1997).
207. Mitchison, H. M. *et al.* Mutations in axonemal dynein assembly factor DNAAF3 cause primary ciliary dyskinesia. *Nature Genetics* *2012 44:4* **44**, 381–389 (2012).
208. Boaretto, F. *et al.* Diagnosis of Primary Ciliary Dyskinesia by a Targeted Next-Generation Sequencing Panel: Molecular and Clinical Findings in Italian Patients. *The Journal of Molecular Diagnostics* **18**, 912–922 (2016).
209. Berg, J. S. *et al.* Next generation massively parallel sequencing of targeted exomes to identify genetic mutations in primary ciliary dyskinesia: Implications for application to clinical testing. *Genetics in Medicine* *2011 13:3* **13**, 218–229 (2011).
210. Sager, R. & Granick, S. Nutritional studies with *Chlamydomonas reinhardi*. *Ann N Y Acad Sci* **56**, 831–838 (1953).
211. SAGER, R. & GRANICK, S. NUTRITIONAL CONTROL OF SEXUALITY IN *CHLAMYDOMONAS REINHARDI*. *J Gen Physiol* **37**, 729 (1954).
212. Soto-Sierra, L., Wilken, L. R. & Dixon, C. K. Aqueous enzymatic protein and lipid release from the microalgae *Chlamydomonas reinhardtii*. *Bioresour Bioprocess* **7**, 1–14 (2020).
213. Emrich-Mills, T. Z. *et al.* A recombineering pipeline to clone large and complex genes in *Chlamydomonas*. *Plant Cell* **33**, 1161–1181 (2021).
214. Cingolani, P. *et al.* A program for annotating and predicting the effects of single nucleotide polymorphisms, SnpEff: SNPs in the genome of *Drosophila melanogaster* strain w1118; iso-2; iso-3. *Fly (Austin)* **6**, 80–92 (2012).
215. Cingolani, P. Variant Annotation and Functional Prediction: SnpEff. *Methods in Molecular Biology* **2493**, 289–314 (2022).
216. Gaudet, M., Fara, A. G., Beritognolo, I. & Sabatti, M. Allele-specific PCR in SNP genotyping. *Methods Mol Biol* **578**, 415–424 (2009).
217. Merchant, S. S. *et al.* The *Chlamydomonas* Genome Reveals the Evolution of Key Animal and Plant Functions. *Science* **318**, 245–250 (2007).
218. Meng, D. & Pan, J. *Chlamydomonas*: Cilia and Ciliopathies. in *Chlamydomonas: Biotechnology and Biomedicine* (eds. Hippler, M. & Hippler, M.) 73–97 (2017).

219. Rochaix, J.-D. Assembly, Function, and Dynamics of the Photosynthetic Machinery in *Chlamydomonas reinhardtii*. *Plant Physiol* **127**, 1394–1398 (2001).
220. Scranton, M. A., Ostrand, J. T., Fields, F. J. & Mayfield, S. P. *Chlamydomonas* as a model for biofuels and bio-products production. *Plant J* **82**, 523–531 (2015).
221. Goodenough, U., Lin, H. & Lee, J. H. Sex determination in *Chlamydomonas*. *Semin Cell Dev Biol* **18**, 350–361 (2007).
222. Mussgnug, J. H. Genetic tools and techniques for *Chlamydomonas reinhardtii*. *Appl Microbiol Biotechnol* **99**, 5407–5418 (2015).
223. Crozet, P. *et al.* Birth of a Photosynthetic Chassis: A MoClo Toolkit Enabling Synthetic Biology in the Microalga *Chlamydomonas reinhardtii*. *ACS Synth Biol* **7**, 2074–2086 (2018).
224. Ferenczi, A., Pyott, D. E., Xipnitou, A. & Molnar, A. Efficient targeted DNA editing and replacement in *Chlamydomonas reinhardtii* using Cpf1 ribonucleoproteins and single-stranded DNA. *Proceedings of the National Academy of Sciences* **114**, 13567–13572 (2017).
225. Akella, S. *et al.* Co-targeting strategy for precise, scarless gene editing with CRISPR/Cas9 and donor ssODNs in *Chlamydomonas*. *Plant Physiol* **187**, 2637–2655 (2021).
226. Mahmoud, M. *et al.* Structural variant calling: the long and the short of it. *Genome Biol* **20**, 246 (2019).
227. Wang, P., Meng, F., Moore, B. M. & Shiu, S.-H. Impact of short-read sequencing on the misassembly of a plant genome. *BMC Genomics* **22**, 99 (2021).
228. Miga, K. H. *et al.* Telomere-to-telomere assembly of a complete human X chromosome. *Nature* **585**, 79–84 (2020).
229. Logsdon, G. A. *et al.* The structure, function and evolution of a complete human chromosome 8. *Nature* **593**, 101–107 (2021).
230. Neale, D. B. *et al.* Assembled and annotated 26.5 Gbp coast redwood genome: a resource for estimating evolutionary adaptive potential and investigating hexaploid origin. *G3 Genes|Genomes|Genetics* **12**, jkab380 (2022).
231. Cretu Stancu, M. *et al.* Mapping and phasing of structural variation in patient genomes using nanopore sequencing. *Nat Commun* **8**, 1326 (2017).
232. Sedlazeck, F. J. *et al.* Accurate detection of complex structural variations using single-molecule sequencing. *Nat Methods* **15**, 461–468 (2018).

233. Hiatt, S. M. *et al.* Long-read genome sequencing for the molecular diagnosis of neurodevelopmental disorders. *Human Genetics and Genomics Advances* **2**, 100023 (2021).
234. Zhang, J.-Y. *et al.* Using de novo assembly to identify structural variation of eight complex immune system gene regions. *PLoS Comput Biol* **17**, e1009254 (2021).
235. Craig, R. J., Hasan, A. R., Ness, R. W. & Keightley, P. D. Comparative genomics of *Chlamydomonas*. *Plant Cell* **33**, 1016–1041 (2021).
236. Kim, B. Y. *et al.* Highly contiguous assemblies of 101 drosophilid genomes. *Elife* **10**, e66405 (2021).
237. Payne, A., Holmes, N., Rakyan, V. & Loose, M. BulkVis: a graphical viewer for Oxford nanopore bulk FAST5 files. *Bioinformatics* **35**, 2193–2198 (2019).
238. Logsdon, G. A., Vollger, M. R. & Eichler, E. E. Long-read human genome sequencing and its applications. *Nat Rev Genet* **21**, 597–614 (2020).
239. Miga, K. H. *et al.* Telomere-to-telomere assembly of a complete human X chromosome. *Nature* **585**, 79–84 (2020).
240. Nurk, S. *et al.* The complete sequence of a human genome. *Science (1979)* **376**, 44–53 (2022).
241. Deng, Y. *et al.* A telomere-to-telomere gap-free reference genome of watermelon and its mutation library provide important resources for gene discovery and breeding. *Mol Plant* **15**, 1268–1284 (2022).
242. Li, G. *et al.* A high-quality genome assembly highlights rye genomic characteristics and agronomically important genes. *Nat Genet* **53**, 574–584 (2021).
243. Song, J.-M. *et al.* Two gap-free reference genomes and a global view of the centromere architecture in rice. *Mol Plant* **14**, 1757–1767 (2021).
244. Wang, B. *et al.* High-quality *Arabidopsis thaliana* Genome Assembly with Nanopore and HiFi Long Reads. *Genomics Proteomics Bioinformatics* (2021) doi:10.1016/j.gpb.2021.08.003.
245. Chakraborty, M., Baldwin-Brown, J. G., Long, A. D. & Emerson, J. J. Contiguous and accurate de novo assembly of metazoan genomes with modest long read coverage. *Nucleic Acids Res* **44**, e147 (2016).
246. Koren, S. *et al.* Canu: scalable and accurate long-read assembly via adaptive k-mer weighting and repeat separation. *Genome Res* **27**, 722–736 (2017).

247. Xu, M. *et al.* TGS-GapCloser: A fast and accurate gap closer for large genomes with low coverage of error-prone long reads. *Gigascience* **9**, giaa094 (2020).
248. Dohm, J. C., Lottaz, C., Borodina, T. & Himmelbauer, H. Substantial biases in ultra-short read data sets from high-throughput DNA sequencing. *Nucleic Acids Res* **36**, e105 (2008).
249. Hyams, J. & Davies, D. R. The induction and characterisation of cell wall mutants of *Chlamydomonas reinhardi*. *Mutation Research/Fundamental and Molecular Mechanisms of Mutagenesis* **14**, 381–389 (1972).
250. Cheng, H., Concepcion, G. T., Feng, X., Zhang, H. & Li, H. Haplotype-resolved de novo assembly using phased assembly graphs with hifiasm. *Nat Methods* **18**, 170–175 (2021).
251. Nurk, S. *et al.* HiCanu: accurate assembly of segmental duplications, satellites, and allelic variants from high-fidelity long reads. *Genome Res* gr.263566.120 (2020)
doi:10.1101/gr.263566.120.
252. O’Donnell, S., Chau, F. & Fischer, G. Highly Contiguous Nanopore Genome Assembly of *Chlamydomonas reinhardtii* CC-1690. *Microbiol Resour Announc* **9**, (2020).
253. Pröschold, T., Harris, E. H. & Coleman, A. W. Portrait of a Species. *Genetics* **170**, 1601–1610 (2005).
254. Benson, G. Tandem repeats finder: a program to analyze DNA sequences. *Nucleic Acids Res* **27**, 573–580 (1999).
255. Smit, A. F. A., Hubley, R. & Green, P. RepeatMasker Open-4.0. Preprint at <https://www.repeatmasker.org/> (2013).
256. Chau, F., Jukic, F. *et al.* Architecture and evolution of subtelomeres in the unicellular green alga *Chlamydomonas reinhardtii*. *bioRxiv* 2021.01.29.428817 (2021)
doi:10.1101/2021.01.29.428817.
257. Manni, M., Berkeley, M. R., Seppey, M., Simão, F. A. & Zdobnov, E. M. BUSCO Update: Novel and Streamlined Workflows along with Broader and Deeper Phylogenetic Coverage for Scoring of Eukaryotic, Prokaryotic, and Viral Genomes. *Mol Biol Evol* **38**, 4647–4654 (2021).
258. Stanke, M. & Morgenstern, B. AUGUSTUS: a web server for gene prediction in eukaryotes that allows user-defined constraints. *Nucleic Acids Res* **33**, W465–W467 (2005).
259. Rhie, A., Walenz, B. P., Koren, S. & Phillippy, A. M. Merqury: reference-free quality, completeness, and phasing assessment for genome assemblies. *Genome Biol* **21**, 245 (2020).

260. Kolmogorov, M., Yuan, J., Lin, Y. & Pevzner, P. A. Assembly of long, error-prone reads using repeat graphs. *Nat Biotechnol* **37**, 540–546 (2019).
261. Chen, Y. *et al.* Efficient assembly of nanopore reads via highly accurate and intact error correction. *Nat Commun* **12**, 60 (2021).
262. Solares, E. A. *et al.* Rapid Low-Cost Assembly of the *Drosophila melanogaster* Reference Genome Using Low-Coverage, Long-Read Sequencing. *G3: Genes, Genomes, Genetics* **8**, 3143–3154 (2018).
263. Chen, Y., Zhang, Y., Wang, A. Y., Gao, M. & Chong, Z. Accurate long-read de novo assembly evaluation with Inspector. *Genome Biol* **22**, 312 (2021).
264. Levy Karin, E., Mirdita, M. & Söding, J. MetaEuk—sensitive, high-throughput gene discovery, and annotation for large-scale eukaryotic metagenomics. *Microbiome* **8**, 48 (2020).
265. Simpson, J. T. *et al.* Detecting DNA cytosine methylation using nanopore sequencing. *Nat Methods* **14**, 407–410 (2017).
266. Yuen, Z. W.-S. *et al.* Systematic benchmarking of tools for CpG methylation detection from nanopore sequencing. *Nat Commun* **12**, 3438 (2021).
267. Liu, Y. *et al.* DNA methylation-calling tools for Oxford Nanopore sequencing: a survey and human epigenome-wide evaluation. *Genome Biol* **22**, 295 (2021).
268. Lopez, D. *et al.* Dynamic Changes in the Transcriptome and Methylome of *Chlamydomonas reinhardtii* throughout Its Life Cycle. *Plant Physiol* **169**, 2730–2743 (2015).
269. Feng, S. *et al.* Conservation and divergence of methylation patterning in plants and animals. *Proceedings of the National Academy of Sciences* **107**, 8689–8694 (2010).
270. Tang, Y., Gao, X.-D., Wang, Y., Yuan, B.-F. & Feng, Y.-Q. Widespread Existence of Cytosine Methylation in Yeast DNA Measured by Gas Chromatography/Mass Spectrometry. *Anal Chem* **84**, 7249–7255 (2012).
271. Lin, H., Cliften, P. F. & Dutcher, S. K. MAPINS, a Highly Efficient Detection Method That Identifies Insertional Mutations and Complex DNA Rearrangements. *Plant Physiol* **178**, 1436–1447 (2018).
272. Craig, R. J., Hasan, A. R., Ness, R. W. & Keightley, P. D. Comparative genomics of *Chlamydomonas*. *Plant Cell* **33**, 1016–1041 (2021).

273. Gallaher, S. D. *et al.* Widespread polycistronic gene expression in green algae. *Proceedings of the National Academy of Sciences* **118**, e2017714118 (2021).
274. Feng, T. Y. & Chiang, K. S. The persistence of maternal inheritance in *Chlamydomonas* despite hypomethylation of chloroplast DNA induced by inhibitors. *Proc Natl Acad Sci U S A* **81**, 3438–3442 (1984).
275. Beckers, M.-C., Munaut, C., Minet, A. & Matagne, R. F. The fate of mitochondrial DNAs of mt⁺ and mt⁻ origin in gametes and zygotes of *Chlamydomonas*. *Curr Genet* **20**, 239–243 (1991).
276. Tardaguila, M. *et al.* SQANTI: extensive characterization of long-read transcript sequences for quality control in full-length transcriptome identification and quantification. *Genome Res* **28**, 396–411 (2018).
277. Martin, W. & Herrmann, R. G. Gene Transfer from Organelles to the Nucleus: How Much, What Happens, and Why? *Plant Physiol* **118**, 9–17 (1998).
278. Wei, W. *et al.* Nuclear-embedded mitochondrial DNA sequences in 66,083 human genomes. *Nature* 1–10 (2022) doi:10.1038/s41586-022-05288-7.
279. Huang, C. Y., Ayliffe, M. A. & Timmis, J. N. Direct measurement of the transfer rate of chloroplast DNA into the nucleus. *Nature* **422**, 72–76 (2003).
280. Stegemann, S., Hartmann, S., Ruf, S. & Bock, R. High-frequency gene transfer from the chloroplast genome to the nucleus. *Proc Natl Acad Sci U S A* **100**, 8828–8833 (2003).
281. Thorsness, P. E. & Fox, T. D. Escape of DNA from mitochondria to the nucleus in *Saccharomyces cerevisiae*. *Nature* **346**, 376–379 (1990).
282. Thorsness, P. E. & Fox, T. D. Nuclear Mutations in *Saccharomyces Cerevisiae* That Affect the Escape of DNA from Mitochondria to the Nucleus. *Genetics* **134**, 21–28 (1993).
283. Lister, D. L., Bateman, J. M., Purton, S. & Howe, C. J. DNA transfer from chloroplast to nucleus is much rarer in *Chlamydomonas* than in tobacco. *Gene* **316**, 33–38 (2003).
284. Richly, E. & Leister, D. NUPTs in Sequenced Eukaryotes and Their Genomic Organization in Relation to NUMTs. *Mol Biol Evol* **21**, 1972–1980 (2004).
285. Smith, D. R., Crosby, K. & Lee, R. W. Correlation between Nuclear Plastid DNA Abundance and Plastid Number Supports the Limited Transfer Window Hypothesis. *Genome Biol Evol* **3**, 365–371 (2011).

286. Yoshida, T., Furihata, H. Y., To, T. K., Kakutani, T. & Kawabe, A. Genome defense against integrated organellar DNA fragments from plastids into plant nuclear genomes through DNA methylation. *Sci Rep* **9**, 2060 (2019).
287. Fields, P. D. *et al.* Complete Sequence of a 641-kb Insertion of Mitochondrial DNA in the *Arabidopsis thaliana* Nuclear Genome. *Genome Biol Evol* **14**, evac059 (2022).
288. Novikova, O. & Belfort, M. Mobile group II introns as ancestral eukaryotic elements. *Trends Genet* **33**, 773–783 (2017).
289. Picariello, T. *et al.* TIM, a targeted insertional mutagenesis method utilizing CRISPR/Cas9 in *Chlamydomonas reinhardtii*. *PLoS One* **15**, e0232594 (2020).
290. Perkins, D. D. The manifestation of chromosome rearrangements in unordered asci of *Neurospora*. *Genetics* **77**, 459–489 (1974).
291. Loidl, J., Jin, Q. W. & Jantsch, M. Meiotic pairing and segregation of translocation quadrivalents in yeast. *Chromosoma* **107**, 247–254 (1998).
292. Greiner, A. *et al.* Targeting of Photoreceptor Genes in *Chlamydomonas reinhardtii* via Zinc-Finger Nucleases and CRISPR/Cas9. *Plant Cell* **29**, 2498–2518 (2017).
293. Jinek, M. *et al.* RNA-programmed genome editing in human cells. *Elife* **2**, e00471 (2013).
294. Cong, L. *et al.* Multiplex Genome Engineering Using CRISPR/Cas Systems. *Science (1979)* **339**, 819–823 (2013).
295. Zones, J. M., Blaby, I. K., Merchant, S. S. & Umen, J. G. High-Resolution Profiling of a Synchronized Diurnal Transcriptome from *Chlamydomonas reinhardtii* Reveals Continuous Cell and Metabolic Differentiation[OPEN]. *Plant Cell* **27**, 2743–2769 (2015).
296. Joo, S. *et al.* Gene Regulatory Networks for the Haploid-to-Diploid Transition of *Chlamydomonas reinhardtii*[OPEN]. *Plant Physiol* **175**, 314–332 (2017).
297. Shin, S.-E. *et al.* CRISPR/Cas9-induced knockout and knock-in mutations in *Chlamydomonas reinhardtii*. *Sci Rep* **6**, 27810 (2016).
298. Gui, M., Wang, X., Dutcher, S. K., Brown, A. & Zhang, R. Ciliary central apparatus structure reveals mechanisms of microtubule patterning. *Nat Struct Mol Biol* **29**, 483–492 (2022).
299. Howell, S. H. The Differential Synthesis and Degradation of Ribosomal DNA during the Vegetative Cell Cycle in *Chlamydomonas reinhardtii*. *Nat New Biol* **240**, 264–267 (1972).

300. Marco, Y. & Rochaix, J.-D. Organization of the nuclear ribosomal DNA of *Chlamydomonas reinhardtii*. *Mol Gen Genet* **177**, 715–723 (1980).
301. Flynn, J. M., Lower, S. E., Barbash, D. A. & Clark, A. G. Rates and Patterns of Mutation in Tandem Repetitive DNA in Six Independent Lineages of *Chlamydomonas reinhardtii*. *Genome Biol Evol* **10**, 1673–1686 (2018).
302. Baubec, T. & Schübeler, D. Genomic patterns and context specific interpretation of DNA methylation. *Curr Opin Genet Dev* **25**, 85–92 (2014).
303. Nasrullah, Hussain, A., Ahmed, S., Rasool, M. & Shah, A. J. DNA methylation across the tree of life, from micro to macro-organism. *Bioengineered* **13**, 1666–1685 (2022).
304. Fachinetti, D. *et al.* DNA Sequence-Specific Binding of CENP-B Enhances the Fidelity of Human Centromere Function. *Dev Cell* **33**, 314–327 (2015).
305. Naish, M. *et al.* The genetic and epigenetic landscape of the Arabidopsis centromeres. *Science* **374**, eabi7489 (2021).
306. Miller, M. S. *et al.* Mutant Kinesin-2 Motor Subunits Increase Chromosome Loss. *Mol Biol Cell* **16**, 3810–3820 (2005).
307. Davidson, M. K., Young, N. P., Glick, G. G. & Wahls, W. P. Meiotic chromosome segregation mutants identified by insertional mutagenesis of fission yeast *Schizosaccharomyces pombe*; tandem-repeat, single-site integrations. *Nucleic Acids Res* **32**, 4400–4410 (2004).
308. Betts, M. F. *et al.* Development of a high throughput transformation system for insertional mutagenesis in *Magnaporthe oryzae*. *Fungal Genetics and Biology* **44**, 1035–1049 (2007).
309. Nelson, J. A. & Lefebvre, P. A. Targeted disruption of the NIT8 gene in *Chlamydomonas reinhardtii*. *Mol Cell Biol* **15**, 5762–5769 (1995).
310. Dent, R. M., Haglund, C. M., Chin, B. L., Kobayashi, M. C. & Niyogi, K. K. Functional Genomics of Eukaryotic Photosynthesis Using Insertional Mutagenesis of *Chlamydomonas reinhardtii*. *Plant Physiol* **137**, 545–556 (2005).
311. Creighton, H. B. & McClintock, B. A Correlation of Cytological and Genetical Crossing-Over in *Zea Mays*. *Proc Natl Acad Sci U S A* **17**, 492–497 (1931).
312. Stern, C. & Ogura, S. Neue Untersuchungen über Aberrationen des Y-Chromosoms von *Drosophila melanogaster*. *Z Indukt Abstamm Vererbungs* **58**, 81–121 (1931).
313. Cleland, R. *Oenothera: cytogenetics and evolution*. (1972).

314. Kraft, K. *et al.* Deletions, Inversions, Duplications: Engineering of Structural Variants using CRISPR/Cas in Mice. *Cell Rep* **10**, 833–839 (2015).
315. Adikusuma, F. *et al.* Large deletions induced by Cas9 cleavage. *Nature* **560**, E8–E9 (2018).
316. Kosicki, M., Tomberg, K. & Bradley, A. Repair of double-strand breaks induced by CRISPR–Cas9 leads to large deletions and complex rearrangements. *Nat Biotechnol* **36**, 765–771 (2018).
317. Cullot, G. *et al.* CRISPR-Cas9 genome editing induces megabase-scale chromosomal truncations. *Nature Communications* 2019 10:1 **10**, 1–14 (2019).
318. Rayner, E. *et al.* CRISPR-Cas9 Causes Chromosomal Instability and Rearrangements in Cancer Cell Lines, Detectable by Cytogenetic Methods. *CRISPR J* **2**, 406–416 (2019).
319. Rönspies, M., Schindele, P., Wetzels, R. & Puchta, H. CRISPR–Cas9-mediated chromosome engineering in *Arabidopsis thaliana*. *Nat Protoc* **17**, 1332–1358 (2022).
320. Eleveld, T. F. *et al.* Engineering large-scale chromosomal deletions by CRISPR-Cas9. *Nucleic Acids Res* **49**, 12007–12016 (2021).
321. Jiang, J. *et al.* Induction of site-specific chromosomal translocations in embryonic stem cells by CRISPR/Cas9. *Scientific Reports* 2016 6:1 **6**, 1–9 (2016).
322. Vanoli, F. *et al.* CRISPR-Cas9–guided oncogenic chromosomal translocations with conditional fusion protein expression in human mesenchymal cells. *Proceedings of the National Academy of Sciences* **114**, 3696–3701 (2017).
323. Jeong, J. *et al.* High-efficiency CRISPR induction of t(9;11) chromosomal translocations and acute leukemias in human blood stem cells. *Blood Adv* **3**, 2825–2835 (2019).
324. King, S. M. Cytoplasmic factories for axonemal dynein assembly. *J Cell Sci* **134**, (2021).
325. Desai, P. B., Freshour, J. R. & Mitchell, D. R. *Chlamydomonas* axonemal dynein assembly locus ODA8 encodes a conserved flagellar protein needed for cytoplasmic maturation of outer dynein arm complexes. *Cytoskeleton* **72**, 16–28 (2015).
326. Dai, J., Barbieri, F., Mitchell, D. R. & Lehtreck, K. F. In vivo analysis of outer arm dynein transport reveals cargo-specific intraflagellar transport properties. *Mol Biol Cell* **29**, 2553–2565 (2018).
327. Bates, T. C. *et al.* Dyslexia and DYX1C1: Deficits in reading and spelling associated with a missense mutation. *Mol Psychiatry* **15**, (2010).

328. Scerri, T. S. *et al.* Putative functional alleles of DYX1C1 are not associated with dyslexia susceptibility in a large sample of sibling pairs from the UK. *jmg.bmj.com* **41**, 853–857 (2004).
329. Paff, T. *et al.* Mutations in PIH1D3 Cause X-Linked Primary Ciliary Dyskinesia with Outer and Inner Dynein Arm Defects. *The American Journal of Human Genetics* **100**, 160–168 (2017).
330. Yamamoto, R. *et al.* Chlamydomonas DYX1C1/PF23 is essential for axonemal assembly and proper morphology of inner dynein arms. *PLoS Genet* **13**, e1006996 (2017).
331. Zhang, N. *et al.* Comparative Phenotyping of Two Commonly Used Chlamydomonas reinhardtii Background Strains: CC-1690 (21gr) and CC-5325 (The CLiP Mutant Library Background). *Plants* **11**, 585 (2022).
332. Van den Hoek, H. *et al.* In situ architecture of the ciliary base reveals the stepwise assembly of intraflagellar transport trains. *Science (1979)* **377**, 543–548 (2022).
333. Deane, J. A., Cole, D. G., Seeley, E. S., Diener, D. R. & Rosenbaum, J. L. Localization of intraflagellar transport protein IFT52 identifies basal body transitional fibers as the docking site for IFT particles. *Current Biology* **11**, 1586–1590 (2001).
334. Hamel, V. *et al.* Identification of Chlamydomonas Central Core Centriolar Proteins Reveals a Role for Human WDR90 in Ciliogenesis. *Current Biology* **27**, 2486–2498.e6 (2017).
335. Lv, B. *et al.* Intraflagellar transport protein IFT52 recruits IFT46 to the basal body and flagella. *J Cell Sci* **130**, 1662–1674 (2017).
336. Bigge, B. M., Rosenthal, N. E. & Avasthi, P. Initial ciliary assembly in Chlamydomonas requires Arp2/3 complex-dependent endocytosis. *Mol Biol Cell* **34**, ar24 (2023).
337. Belzile, O., Hernandez-Lara, C. I., Wang, Q. & Snell, W. J. Regulated Membrane Protein Entry into Flagella Is Facilitated by Cytoplasmic Microtubules and Does Not Require IFT. *Current Biology* **23**, 1460–1465 (2013).
338. Yamamoto, R. *et al.* Chlamydomonas DYX1C1/PF23 is essential for axonemal assembly and proper morphology of inner dynein arms. *PLoS Genet* **13**, e1006996 (2017).
339. Dutcher, S. K. Chapter 76 Mating and Tetrad Analysis in Chlamydomonas reinhardtii. in *Methods in Cell Biology* (eds. Dentler, W., Witman, G., Dentler, W. & Witman, G.) vol. 47 531–540 (1995).
340. Yamano, T., Iguchi, H. & Fukuzawa, H. Rapid transformation of Chlamydomonas reinhardtii without cell-wall removal. *J Biosci Bioeng* **115**, 691–694 (2013).

341. Bottier, M., Thomas, K. A., Dutcher, S. K. & Bayly, P. V. How Does Cilium Length Affect Beating? *Biophys J* **116**, 1292–1304 (2019).
342. Hamel, V. *et al.* Identification of Chlamydomonas Central Core Centriolar Proteins Reveals a Role for Human WDR90 in Ciliogenesis. *Current Biology* **27**, 2486–2498.e6 (2017).
343. Picariello, T. *et al.* TIM, a targeted insertional mutagenesis method utilizing CRISPR/Cas9 in Chlamydomonas reinhardtii. *PLoS One* **15**, (2020).
344. Baker, E. J., Schloss, J. A. & Rosenbaum, J. L. Rapid changes in tubulin RNA synthesis and stability induced by deflagellation in Chlamydomonas. *Journal of Cell Biology* **99**, 2074–2081 (1984).
345. Avasthi, P. *et al.* Actin Is Required for IFT Regulation in Chlamydomonas reinhardtii. *Current Biology* **24**, 2025–2032 (2014).
346. Brokaw, C. J. & Kamiya, R. Bending Patterns of Chlamydomonas Flagella: IV. Mutants With Defects in Inner and Outer Dynein Arms Indicate Differences in Dynein Arm Function. *Cell Motil Cytoskeleton* **8**, 68–75 (1987).
347. Kamiya, R. Exploring the Function of Inner and Outer Dynein Arms With Chlamydomonas Mutants. *Cell Motil Cytoskeleton* **32**, 9–102 (1995).
348. Horani, A. *et al.* Establishment of the early cilia preassembly protein complex during motile ciliogenesis. *Proc Natl Acad Sci U S A* **115**, E1221–E1228 (2018).
349. Omran, H. *et al.* Ktu/PF13 is required for cytoplasmic pre-assembly of axonemal dyneins. *Nature* **456**, 611–616 (2008).
350. Huizar, R. L. *et al.* A liquid-like organelle at the root of motile ciliopathy. *Elife* **7**, (2018).
351. Lee, C. *et al.* Functional partitioning of a liquid-like organelle during assembly of axonemal dyneins. *Elife* **9**, 1–23 (2020).

Appendix: BioRender Publication Licenses for Figures Used in This Dissertation



49 Spadina Ave. Suite 200
Toronto ON M5V 2J1 Canada
www.biorender.com

Confirmation of Publication and Licensing Rights

April 24th, 2023
Science Suite Inc.

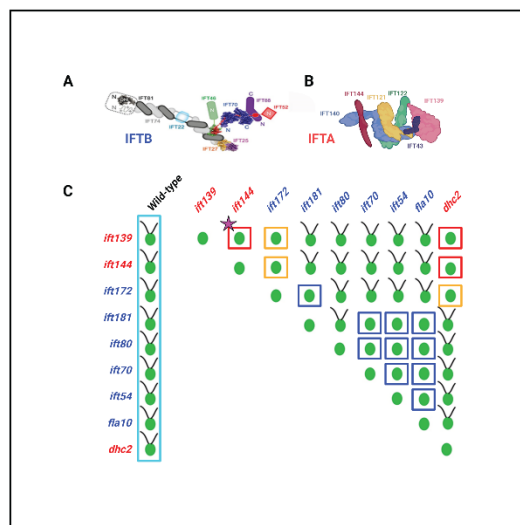
Subscription: Student Plan
Agreement number: VS25AB2SDK
Journal name: Dissertation

To whom this may concern,

This document is to confirm that Gervette Penny has been granted a license to use the BioRender content, including icons, templates and other original artwork, appearing in the attached completed graphic pursuant to BioRender's [Academic License Terms](#). This license permits BioRender content to be sublicensed for use in journal publications.

All rights and ownership of BioRender content are reserved by BioRender. All completed graphics must be accompanied by the following citation: "Created with BioRender.com".

BioRender content included in the completed graphic is not licensed for any commercial uses beyond publication in a journal. For any commercial use of this figure, users may, if allowed, recreate it in BioRender under an Industry BioRender Plan.



For any questions regarding this document, or other questions about publishing with BioRender refer to our [BioRender Publication Guide](#), or contact BioRender Support at support@biorender.com.

Confirmation of Publication and Licensing Rights

April 24th, 2023
 Science Suite Inc.

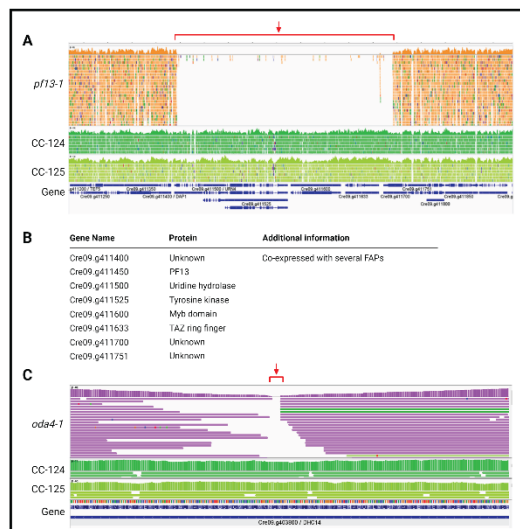
Subscription: Student Plan
Agreement number: DL25AB3X9R
Journal name: Dissertation

To whom this may concern,

This document is to confirm that Gervette Penny has been granted a license to use the BioRender content, including icons, templates and other original artwork, appearing in the attached completed graphic pursuant to BioRender's [Academic License Terms](#). This license permits BioRender content to be sublicensed for use in journal publications.

All rights and ownership of BioRender content are reserved by BioRender. All completed graphics must be accompanied by the following citation: "Created with BioRender.com".

BioRender content included in the completed graphic is not licensed for any commercial uses beyond publication in a journal. For any commercial use of this figure, users may, if allowed, recreate it in BioRender under an Industry BioRender Plan.



For any questions regarding this document, or other questions about publishing with BioRender refer to our [BioRender Publication Guide](#), or contact BioRender Support at support@biorender.com.

Confirmation of Publication and Licensing Rights

April 24th, 2023
 Science Suite Inc.

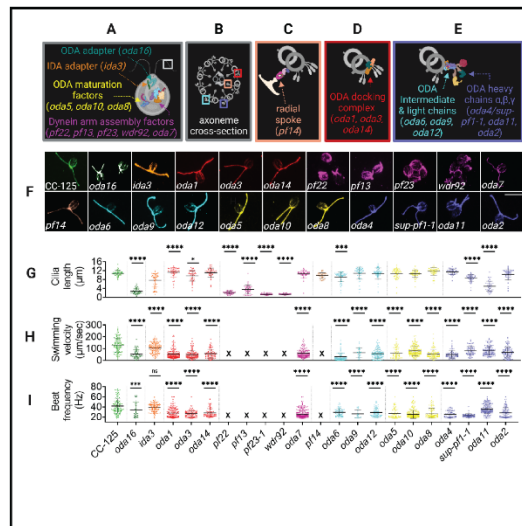
Subscription: Student Plan
Agreement number: GN25AB6V74
Journal name: Dissertation

To whom this may concern,

This document is to confirm that Gervette Penny has been granted a license to use the BioRender content, including icons, templates and other original artwork, appearing in the attached completed graphic pursuant to BioRender's Academic License Terms. This license permits BioRender content to be sublicensed for use in journal publications.

All rights and ownership of BioRender content are reserved by BioRender. All completed graphics must be accompanied by the following citation: "Created with BioRender.com".

BioRender content included in the completed graphic is not licensed for any commercial uses beyond publication in a journal. For any commercial use of this figure, users may, if allowed, recreate it in BioRender under an Industry BioRender Plan.



For any questions regarding this document, or other questions about publishing with BioRender refer to our BioRender Publication Guide, or contact BioRender Support at support@biorender.com.

Confirmation of Publication and Licensing Rights

April 24th, 2023
 Science Suite Inc.

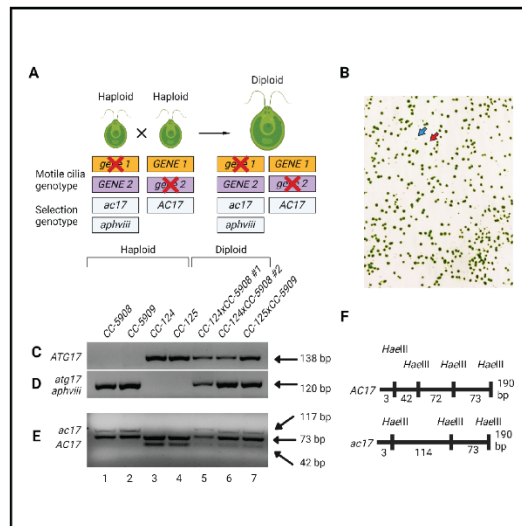
Subscription: Student Plan
Agreement number: JL25AB7CRX
Journal name: Dissertation

To whom this may concern,

This document is to confirm that Gervette Penny has been granted a license to use the BioRender content, including icons, templates and other original artwork, appearing in the attached completed graphic pursuant to BioRender's [Academic License Terms](#). This license permits BioRender content to be sublicensed for use in journal publications.

All rights and ownership of BioRender content are reserved by BioRender. All completed graphics must be accompanied by the following citation: "Created with BioRender.com".

BioRender content included in the completed graphic is not licensed for any commercial uses beyond publication in a journal. For any commercial use of this figure, users may, if allowed, recreate it in BioRender under an Industry BioRender Plan.



For any questions regarding this document, or other questions about publishing with BioRender refer to our [BioRender Publication Guide](#), or contact BioRender Support at support@biorender.com.

Confirmation of Publication and Licensing Rights

April 24th, 2023
 Science Suite Inc.

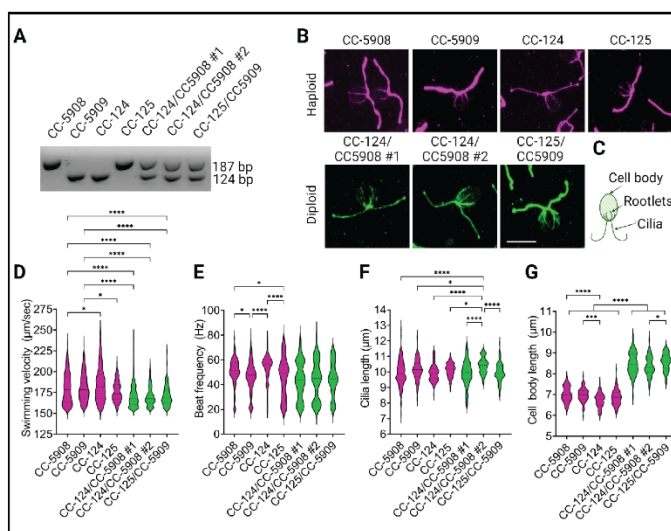
Subscription: Student Plan
Agreement number: KL25AB7SW6
Journal name: Dissertation

To whom this may concern,

This document is to confirm that Gervette Penny has been granted a license to use the BioRender content, including icons, templates and other original artwork, appearing in the attached completed graphic pursuant to BioRender's Academic License Terms. This license permits BioRender content to be sublicensed for use in journal publications.

All rights and ownership of BioRender content are reserved by BioRender. All completed graphics must be accompanied by the following citation: "Created with BioRender.com".

BioRender content included in the completed graphic is not licensed for any commercial uses beyond publication in a journal. For any commercial use of this figure, users may, if allowed, recreate it in BioRender under an Industry BioRender Plan.



For any questions regarding this document, or other questions about publishing with BioRender refer to our BioRender Publication Guide, or contact BioRender Support at support@biorender.com.

Confirmation of Publication and Licensing Rights

April 24th, 2023
 Science Suite Inc.

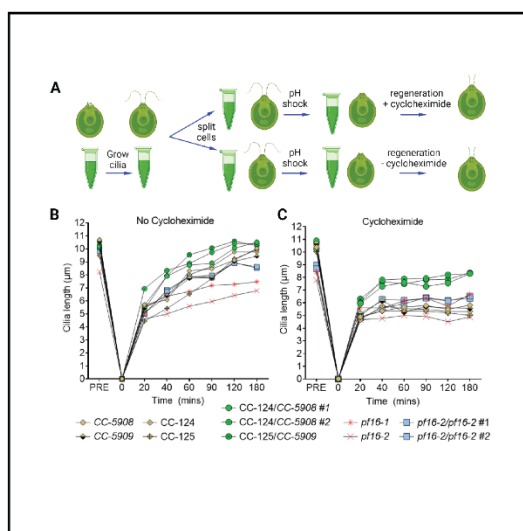
Subscription: Student Plan
Agreement number: SQ25AB8M66
Journal name: Dissertation

To whom this may concern,

This document is to confirm that Gervette Penny has been granted a license to use the BioRender content, including icons, templates and other original artwork, appearing in the attached completed graphic pursuant to BioRender's [Academic License Terms](#). This license permits BioRender content to be sublicensed for use in journal publications.

All rights and ownership of BioRender content are reserved by BioRender. All completed graphics must be accompanied by the following citation: "Created with BioRender.com".

BioRender content included in the completed graphic is not licensed for any commercial uses beyond publication in a journal. For any commercial use of this figure, users may, if allowed, recreate it in BioRender under an Industry BioRender Plan.



For any questions regarding this document, or other questions about publishing with BioRender refer to our [BioRender Publication Guide](#), or contact BioRender Support at support@biorender.com.

Confirmation of Publication and Licensing Rights

April 24th, 2023
 Science Suite Inc.

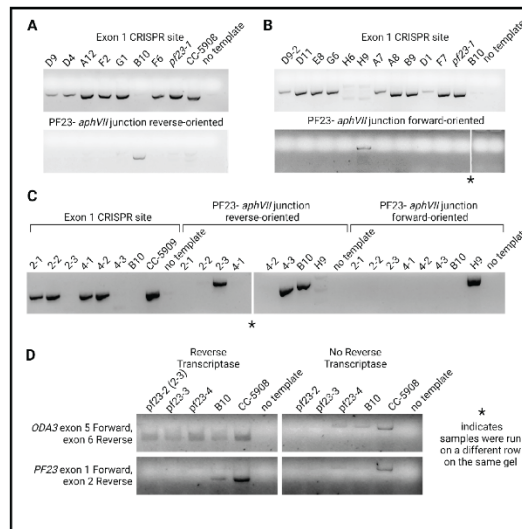
Subscription: Student Plan
Agreement number: AE25AB8XUF
Journal name: Dissertation

To whom this may concern,

This document is to confirm that Gervette Penny has been granted a license to use the BioRender content, including icons, templates and other original artwork, appearing in the attached completed graphic pursuant to BioRender's Academic License Terms. This license permits BioRender content to be sublicensed for use in journal publications.

All rights and ownership of BioRender content are reserved by BioRender. All completed graphics must be accompanied by the following citation: "Created with BioRender.com".

BioRender content included in the completed graphic is not licensed for any commercial uses beyond publication in a journal. For any commercial use of this figure, users may, if allowed, recreate it in BioRender under an Industry BioRender Plan.



For any questions regarding this document, or other questions about publishing with BioRender refer to our BioRender Publication Guide, or contact BioRender Support at support@biorender.com.

Confirmation of Publication and Licensing Rights

April 24th, 2023
 Science Suite Inc.

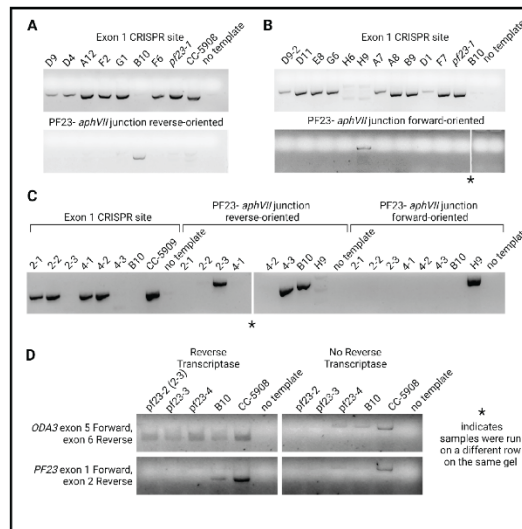
Subscription: Student Plan
Agreement number: PV25AB9781
Journal name: Dissertation

To whom this may concern,

This document is to confirm that Gervette Penny has been granted a license to use the BioRender content, including icons, templates and other original artwork, appearing in the attached completed graphic pursuant to BioRender's Academic License Terms. This license permits BioRender content to be sublicensed for use in journal publications.

All rights and ownership of BioRender content are reserved by BioRender. All completed graphics must be accompanied by the following citation: "Created with BioRender.com".

BioRender content included in the completed graphic is not licensed for any commercial uses beyond publication in a journal. For any commercial use of this figure, users may, if allowed, recreate it in BioRender under an Industry BioRender Plan.



For any questions regarding this document, or other questions about publishing with BioRender refer to our BioRender Publication Guide, or contact BioRender Support at support@biorender.com.

Confirmation of Publication and Licensing Rights

April 24th, 2023
 Science Suite Inc.

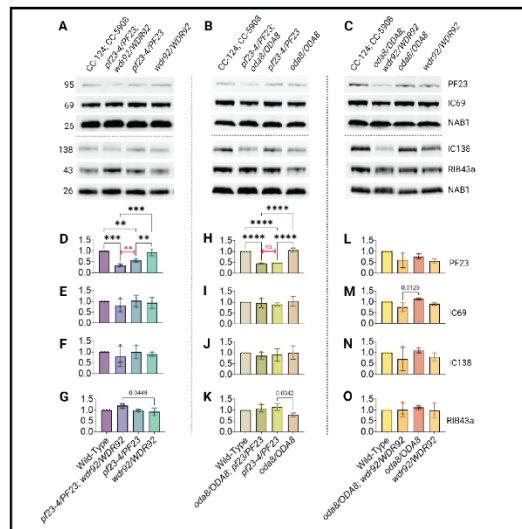
Subscription: Student Plan
Agreement number: YG25AB9UYY
Journal name: Dissertation

To whom this may concern,

This document is to confirm that Gervette Penny has been granted a license to use the BioRender content, including icons, templates and other original artwork, appearing in the attached completed graphic pursuant to BioRender's Academic License Terms. This license permits BioRender content to be sublicensed for use in journal publications.

All rights and ownership of BioRender content are reserved by BioRender. All completed graphics must be accompanied by the following citation: "Created with BioRender.com".

BioRender content included in the completed graphic is not licensed for any commercial uses beyond publication in a journal. For any commercial use of this figure, users may, if allowed, recreate it in BioRender under an Industry BioRender Plan.



For any questions regarding this document, or other questions about publishing with BioRender refer to our BioRender Publication Guide, or contact BioRender Support at support@biorender.com.

Confirmation of Publication and Licensing Rights

April 24th, 2023
Science Suite Inc.

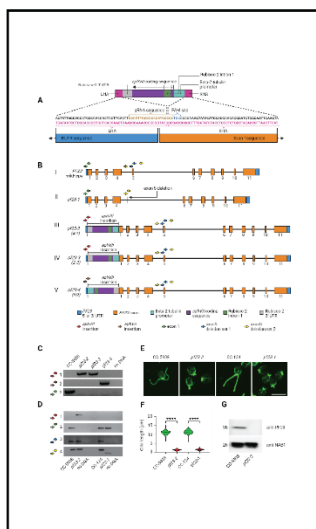
Subscription: Student Plan
Agreement number: VX25ABAT18
Journal name: Dissertation

To whom this may concern,

This document is to confirm that Gervette Penny has been granted a license to use the BioRender content, including icons, templates and other original artwork, appearing in the attached completed graphic pursuant to BioRender's [Academic License Terms](#). This license permits BioRender content to be sublicensed for use in journal publications.

All rights and ownership of BioRender content are reserved by BioRender. All completed graphics must be accompanied by the following citation: "Created with BioRender.com".

BioRender content included in the completed graphic is not licensed for any commercial uses beyond publication in a journal. For any commercial use of this figure, users may, if allowed, recreate it in BioRender under an Industry BioRender Plan.



For any questions regarding this document, or other questions about publishing with BioRender refer to our [BioRender Publication Guide](#), or contact BioRender Support at support@biorender.com.

Confirmation of Publication and Licensing Rights

April 24th, 2023
 Science Suite Inc.

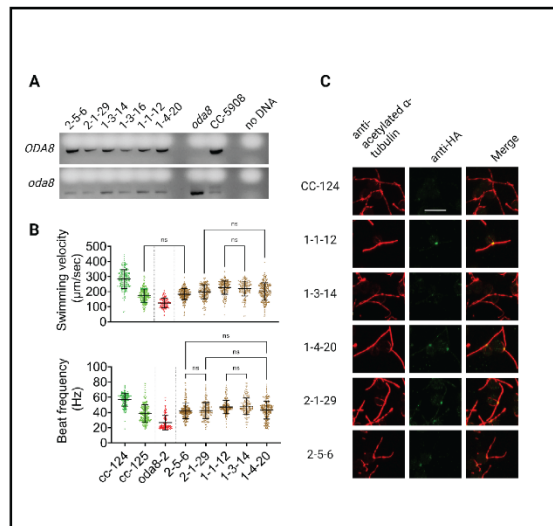
Subscription: Student Plan
Agreement number: NX25ABB5WS
Journal name: Dissertation

To whom this may concern,

This document is to confirm that Gervette Penny has been granted a license to use the BioRender content, including icons, templates and other original artwork, appearing in the attached completed graphic pursuant to BioRender's [Academic License Terms](#). This license permits BioRender content to be sublicensed for use in journal publications.

All rights and ownership of BioRender content are reserved by BioRender. All completed graphics must be accompanied by the following citation: "Created with BioRender.com".

BioRender content included in the completed graphic is not licensed for any commercial uses beyond publication in a journal. For any commercial use of this figure, users may, if allowed, recreate it in BioRender under an Industry BioRender Plan.



For any questions regarding this document, or other questions about publishing with BioRender refer to our [BioRender Publication Guide](#), or contact BioRender Support at support@biorender.com.